Fakultät für
Mathematik, Informatik
und Naturwissenschaften

RWTH AACHEN UNIVERSITY

Reusing Monte Carlo Events for Parameter Scans at the LHC

Von der Fakultät für Mathematik, Informatik und Naturwissenschaften der RWTH Aachen University zur Erlangung des akademischen Grades eines Doktors der Naturwissenschaften genehmigte Dissertation

vorgelegt von

Frederic Alexander Poncza M. Sc.

aus

Moers

Berichter: Univ.-Prof. Dr. rer. nat. Michael Krämer
Dr. rer. nat. Jamie Tattersall

Tag der mündlichen Prüfung: 18.09.2020

Diese Dissertation ist auf den Internetseiten der Universitätsbibliothek verfügbar.

Zusammenfassung

Es wird eine neue Methode zur Wiederverwendung von Monte Carlo Events für Parameter-Scans am LHC, die auf einer Kombination von Impuls-Transformationen und Event-bezogenen Neugewichtungen basiert, vorgestellt. Eine solche Wiederverwendung von Monte Carlo Events wurde bereits in der Literatur diskutiert. Die dortigen Ansätze beschränken sich jedoch auf die bloße Neugewichtung der Events und sind daher nicht in der Lage, kinematische Verteilungen für Parameterpunkte mit unterschiedlichen Massen vorherzusagen. Durch die Transformation der Impulse der ursprünglichen Events so, dass die Energieskalen der neuen Impulse nahe an der Zielpunkt-Energieskala liegen, wird ein Wiederverwendung der Events auch für Massenänderungen möglich. Nach der Transformation verbleibende Differenzen können dann durch Neugewichtung der beteiligten Events mit ihren differentiellen Wirkungsquerschnitten aufgelöst werden. Diese neue Methode kann verwendet werden, um die Abtastzeiten für Parameter-Scans zu reduzieren. Diese Scans werden typischerweise durchgeführt, wenn theoretische Vorhersagen von Modellen für Physik jenseits des Standardmodells mit experimentellen Daten verglichen werden.
Im Vergleich zu anderen Algorithmen, die den Berechnungsaufwand von Parameter-Scans reduzieren können, ist dieser neue Ansatz prinzipiell unabhängig vom betrachteten physikalischen Modell und kann, je nach Vorgabe, ohne die Kenntnis der jeweiligen Matrixelemente verwendet werden.

Abstract

A new method is presented for reusing Monte Carlo events in parameter scans at the LHC, which is based on the combination of momentum transformations and event-by-event reweighting. While reusing Monte Carlo events was already proposed in the literature, these approaches were limited to reweighting events and therefore are inadequate when predicting kinematical distributions for parameter points with different mass configurations. By transforming momenta of the original events in a way that the energy scales of the new momenta are close to the target point energy scale, then a reweighting approach can also be applied for mass changes. Any remaining mismatch after the transformation can then be resolved by reweighting the involved events with their differential cross sections. This new method can be used to decrease sampling times for parameter scans that are typically performed when comparing theoretical predictions of models for beyond the Standard Model physics against experimental data.
In contrast to other algorithms that can reduce computational efforts for parameter scans, this new approach is in principal independent of the physics model. Depending on individual requirements, a combinations of momentum transformations and reweighting can also be used without explicit knowledge of the involved matrix elements.

Contents

Chapter 1

Motivation

More than 10 years ago experiments at the world's largest particle accelerator to date, the Large Hadron Collider (LHC) at CERN in Geneva, began their search for previously undiscovered particles [1]. Already in the first phase of measurements from 2010 to 2013 (run 1) [2], the two largest particle detectors at the LHC, ATLAS [3] and CMS [4], succeeded in discovering the Higgs boson, which was theoretically predicted in the 1960s [5, 6, 7]. Thus, the Standard Model of particle physics could finally be completed about 40 years after its theoretical formulation. To this day, the Standard Model (SM) represents one of the most closely examined and most rigorously tested models in all of physics. It combines three of the (currently known) four fundamental forces in a unified gauge theory with symmetry group

$$SU(3) \times SU(2) \times U(1). \tag{1.1}$$

The individual terms in Eq. (1.1) describe, from left to right, the strong, weak and electromagnetic interactions. Each of these interactions is mediated by one or more gauge bosons. Gluons, the gauge bosons of $SU(3)$, are responsible for the coupling of color-charged particles, for instance quarks and gluons themselves. The coupling constant of the interaction α_s is, with a value of $\alpha_s(M_Z) \approx 0.118$, roughly two orders of magnitude larger than the electromagnetic coupling constant, also called fine-structure constant, $\alpha \approx 0.0073$. It is also 13 orders of magnitude larger than the couplings of the weak interaction, explaining the origin of the "strong" and "weak" force terminology [8]. The weak interaction is carried by the charged $W^{\pm}$ and the neutral Z bosons, while the electromagnetic force is mediated by the photon. The $SU(2) \times U(1)$ term of the full symmetry group describes the unification of the weak and electromagnetic interactions to

the so-called electroweak force. Only gravity, which is weak in relation to the other forces, still refuses (and might possibly even permanently refuse) the quantum field theory formulation that is the basis of the SM. Conceptualizing the importance of searching for physics beyond the Standard Model (BSM) through such methods as the one described in the present work, requires an understanding of both the achievements and failures of the Standard Model.

The development of the SM can be seen as one of the great success stories of physics. When the formulation of the Standard Model was finalized at the end of the 1960s, it implied the existence of various, at that point in time, unknown particles. All of which could be experimentally detected over the years. The discovery of quarks, especially the bottom quark [9], the $W^{\pm}$ [10] and Z [11] bosons, the top quark [12] as well as the τ neutrino [13] and finally the Higgs boson [3, 4] have strikingly and repeatedly confirmed the predictions of the Standard Model. To this day and after the end of run 2, which increased the integrated luminosity of the LHC to $139\,\mathrm{fb}^{-1}$, neither ATLAS nor CMS have measured any significant deviations from the Standard Model (see Fig. 1.1) [14, 15, 16]. One does, however, not even have to consider the absence of gravity in the SM to realize that essential, particularly astrophysical and cosmological discoveries cannot be explained within its scope.
It is well known, for example, that ordinary matter, whose interactions are described by the SM, makes up only $\approx 5\%$ of the total energy density of the universe. The remaining $\approx 95\%$ is made up of dark matter and dark energy [17], which are both still subject to intensive study (e.g. [18, 19, 20]). Dark energy, for instance, is implemented in the standard model of cosmology (or ΛCDM model) as a cosmological constant whose value cannot be directly derived within the SM [21]. But even within the realm of ordinary matter, the Standard Model of particles physics has shortcomings. Prominent examples include the existence of neutrino masses or baryon asymmetry. Neutrino masses are, on the one hand, not part of the SM, but could, on the other hand, clearly be demonstrated experimentally by measurements of neutrino oscillations [22, 23]. The Baryon asymmetry problem describes the fact that the amount of CP violation, that enters the SM through the CKM matrix, is not strong enough to explain the observed matter-antimatter asymmetry in the universe [24, 25]. From a theoretical point of view, the SM is additionally unsatisfactory with regard to various naturalness considerations. In this context, for example, the much discussed strong CP problem (SCPP) comes into play. While the electromagnetic interaction, due to the abelian nature of its underlying symmetry group, is invariant under parity (P) transformations,

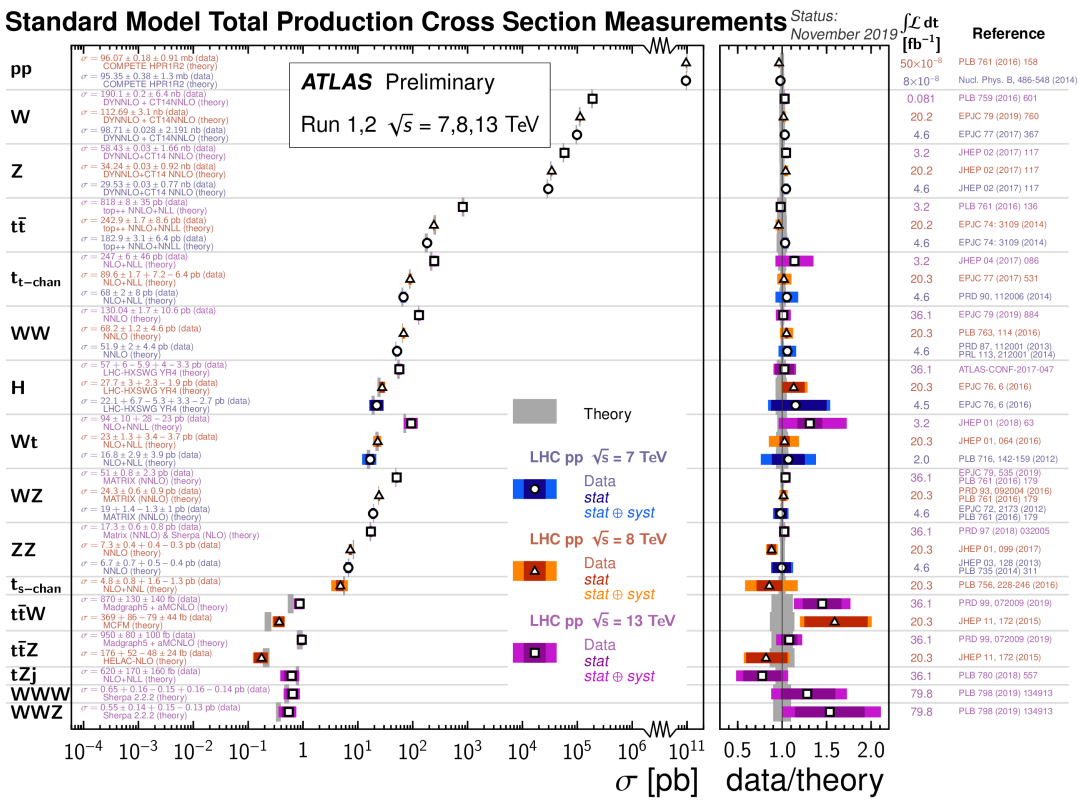

Figure 1.1: Overview of different cross section measurements by ATLAS at the LHC. The measured cross sections (blue, red and purple) are compared to the theoretical predictions of the Standard Model. All predictions are compatible with the experimental measurements within 2-3 σ. Note that even if the total pp cross section is left out, the SM cross sections agree with the experiment across seven orders of magnitude. [14]

charge conjugation (C) and time reversal (T), the weak and strong interactions do not show this behavior. In fact only the violation of the combination of all three symmetries (CPT) is forbidden in the full SM [26]. However, while violations of all pairwise combinations of C, P and T could be observed for the weak force, no detection of CP violation has ever been made for the strong force. This apparent absence of strong CP violation contradicts, what is usually referred to as, the *Totalitarian Principle*, namely that

> "what is not forbidden [by the laws of physics] is compulsory" [27].

The Totalitarian Principle suggests that, insofar as the strong interaction actually conserves CP, this would be accompanied by a corresponding theoretical justification. Already in the 1970s the so-called *Peccei-Quinn mechanism*, was proposed, which predicts a new pseudo-scalar particle, called *Axion* [28, 29]. Although the original formulation of this mechanism has already been empirically ruled out (e.g.

[30]), modifications and further developments are still part of current research. The Axion is particularly interesting because it would not only solve the strong CP problem, but also represents a suitable dark matter candidate [31, 32, 33]. All attempts to discover the Axion, however, have, so far, failed. An explanation for the smallness of the CP violating terms of QCD and thus a solution of the strong CP problem is still pending. In addition to the SCPP, other phenomena that contradict the notion of naturalness, which physicists have developed over decades and centuries, are frequently discussed in the literature. One of these phenomena is the electroweak hierarchy problem, i.e. the question why the observed mass of the Higgs boson is small compared to the Planck mass. If the SM is considered an effective theory at relatively low scales, quantum corrections in the calculation of the Higgs mass are quadratic in the cutoff scale of the Standard Model [34]:

$$\Delta m_H^2 = -\frac{|\lambda_f|^2}{8\pi^2}\Lambda_{\text{cutoff}} + \dots . \tag{1.2}$$

Thus, assuming that the Standard Model is an effective theory and that gravitational effects become relevant at the Planck scale, the magnitude of the correction is of the order of the Planck scale itself. One way to eliminate this issue is to assume that higher order corrections cancel the quadratic term and also each other out. Such a fine tuning however would be equally unsettling to a physicists' mind. If the corrections individually take on values 16 orders of magnitude [34] above the mass of the Higgs, one would not expect that just adding up these large terms would lead to a finite result that then accidentally matches the scale of the electroweak sector of the SM. The striking size of fine tuning, that would be required, is equivalent to balancing a pencil as large as solar system on its tip, when the tip is merely a millimeter wide [35]. However, the type of quadratic corrections, that enter into the Higgs mass calculation, have even more far-reaching consequences. One of which is an increased sensitivity of the Higgs mass to the masses of heavy new particles that are predicted in extensions of the SM [34].

Requesting some degree of naturalness has long been a guiding principle in theoretical physics. The discovery of "unnatural" terms or parameters has always been followed by the search for a deeper reason, which may go beyond the scope of the SM. The apparent absence of empirical evidence for BSM physics, however, feeds the criticism and new arguments are made that nature may simply be fine-tuned (e.g. [36]). Whether naturalness and beauty play a role in the search for new physics or whether one takes a completely different approach, both from

an experimental and a theoretical point of view, it is clear that the SM is not the full story. The search for BSM physics remains a central occupation of modern physics.
One of the approaches, that is often applied, is extending the symmetry group of the SM. A relatively simple example, on the face of it, is the extension of the SM gauge group by an additional local $U(1)$ symmetry, so that the total gauge group takes the form

$$SU(3)_C \times SU(2)_L \times U(1)_Y \times U'(1). \tag{1.3}$$

The phenomenology of such a model strongly depends on the concrete implementation of the additional $U'(1)$. In many cases, so-called Z' bosons, which embody heavy siblings of the Z bosons of SM, are studied in this context [37]. From an experimental point of view, there are already significant limitations of such models, which will be discussed in more detail in Ch. 4.1. In contrast to the extension of the gauge group of the SM, a new space-time symmetry is postulated in the context of supersymmetry (SUSY). Specifically, SUSY connects fermions and bosons through its (spinor) generator Q (and its hermitian conjugate $Q^\dagger$), that transforms a fermionic state into a bosonic state and vice versa

$$Q\,|\text{Fermion}\rangle = |\text{Boson}\rangle \tag{1.4}$$

$$Q\,|\text{Boson}\rangle = |\text{Fermion}\rangle\,. \tag{1.5}$$

Since Q is a spinor, SUSY is an extension of the Poincare group, i.e. of the symmetry of spacetime [38]. However, this also means that this additional symmetry multiplies the number of particles that could, in principle, be observed. For each boson of the SM, there would be a new fermion and for each fermion of the SM there would be a corresponding new boson. If the symmetry is unbroken the masses of the SM particles and their supersymmetric partners are exactly equal [34]. However, since none of the SUSY partners have experimentally been detected, if SUSY was to exist, it must be a broken symmetry. Different supersymmetric models are distinguished, among other things, by the exact mechanism of the symmetry breaking. For a long time, supersymmetric theories were the most promising candidates for BSM physics at the TeV scale; a discovery by the LHC was only a matter of time. However, so far the LHC has not only failed to find any evidence for superpartners of SM particles, it has even ruled out, or at least killed softly, some supersymmetric models like the CMSSM [39]. The parameter space of the most widespread supersymmetric theory, the Minimal

Supersymmetric Standard Model (MSSM), has already been severely restricted for many of its implementations by many searches at the LHC, without any solid indication of its existence [40].

A major reason for the success of supersymmetry in theoretical physics lies in its potential to solve many of the problems mentioned above. By introducing new particles (the sfermions), for example, a cancellation of the quadratic corrections to the Higgs mass can be achieved in a natural way, as long as the masses of the new SUSY particles do not become too large [34]. Also, the lightest stable (and electrically neutral) particle of the MSSM, the neutralino, the lightest of the partners of the Z boson, photon and Higgs, is a candidate for the explanation of dark matter in the form of weakly interacting massive particles (WIMPs) (e.g. [41]). A simple supersymmetric model is also considered in Ch. 4.3. At this point, however, the theoretical shortcomings of SUSY, apart from the lack of evidence, should not be omitted. Due to the introduction of new particles and thus new masses and couplings as well as a mechanism for breaking SUSY, the number of free parameters increases significantly compared to the SM. The MSSM, for example, introduces 105 new free parameters [42]. Adding such a large amount of new free parameters of course counteracts the desire of many theoretical physicists to reduce the number of free parameters by studying more fundamental theories.
Also, the solution of the hierarchy problem through SUSY depends on the fact that the difference in the masses of the fermions and sfermions is manageable, in order to ensure a sufficient cancellation of the correction terms in the Higgs mass [34]. Considering the excluded parameter spaces of popular supersymmetric theories, it becomes more and more unlikely that SUSY provides a satisfactory explanation without introducing new fine-tuning problems. It is therefore important to consider alternatives to supersymmetric models; among other things in the search for an answer to one of the biggest questions of modern physics: the nature of dark matter.
Already in the 1930s, rotational speeds of outer stars in galaxies [43] and kinetic energies of galaxies in galaxy clusters [44, 45] were measured and both deviated from the theoretical expectations. In both cases, the astrophysical objects, i.e. stars and galaxies, behaved as if there was more mass acting through Newton's theory of gravity than could be observed. Therefore, additional, dark, i.e. non-luminous, mass would be necessary to explain the measurements. Also more recent measurements confirm that the observable mass in the universe is not sufficient to explain all gravitational phenomena. For instance, the power spectrum of

the cosmic microwave background (CMB) radiation is strongly dependent on how much of the energy present in the universe is made up of baryonic, i.e. ordinary, and dark mass. The most recent measurements by Planck set the baryonic matter density at $\Omega_b = 0.0493(6)$ and the cold dark matter density at $\Omega_c = 0.265(7)$ [46]. Furthermore, measurements of gravitational lensing, similar to the already mentioned observations, have found stronger effects than could be explained by ordinary matter alone [47].

Broadly speaking, the search for dark matter can be divided into two categories. On the one hand, the assumption is made that dark matter is actually made of matter, that then either consists of yet unknown elementary particles or known matter in unusual compositions ("particle dark matter"). On the other hand, there is the hypothesis that on very large scales gravity behaves differently than predicted by general relativity ("modified gravity"). In the field of particle dark matter, theories can be distinguished in which astrophysical objects that are difficult or impossible to observe serve as the cause of the additional gravitation, from those in which new elementary particles provide the necessary mass. Especially the search for weakly interacting massive particles (WIMPs) has received much attention both in direct and indirect detection experiments. WIMPs are predicted by a variety of theories and models. Under certain conditions (e.g. R-Parity conservation) this includes the above mentioned MSSM. At the LHC the range of models studied goes from simplified models, where the dark matter is effectively coupled to SM particles, to complete models, where the full particle content of the model and its dynamics is studied [48]. So far, however, all of these searches have been unsuccessful. The same is true for other candidates of particle dark matter like the Axion. Only recently however a new kind of dark matter candidate in the form of Bose-Einstein condensates formed by $d^*(2380)$ hexaquarks briefly after the big bang was proposed. Further study on this is however needed [49]. On the other hand, there are even some experimental findings that are difficult to reconcile with a particle nature of dark matter. Such a case is presented by the collision of two clusters of galaxies, the so-called *bullet cluster*. The observation of the bullet cluster implied that the mass determined by gravitational lensing was separated from the radiating visible mass after the collision [50]. At first glance, this result seems to confirm the hypothesis that dark matter is actually made of matter and not explained by changing the laws of gravity. On closer inspection, however, difficulties with this interpretation arise. Simulations of the collision speeds of galaxy clusters differ from those of the observed galaxy clusters, making an explanation in the context of particle dark matter difficult.

The observed collision speed of about 3000 $\frac{\text{km}}{\text{s}}$ [51] is so high that only few of the simulated collisions can keep up. The probability of observing an event like the bullet cluster in the framework of the models used for the simulations is in the order of $6.4 \cdot 10^{-6}$ [52] to $4.6 \cdot 10^{-4}$ [53]. This, in turn, indicates that the particle dark matter model is challenged by the bullet cluster observation [54]. For these reasons, an adjustment of the laws of gravity, also called *modified gravity* or *modified newtonian dynamics (MOND)*, is still part of active research.

Either way, the search for new physics waiting beyond the Standard Model, in whichever form, is one of the most important activities of modern physics research in general and the accelerator physics community in particular. Ever since the LHC has started its run 1, a large number of searches for extensions of the SM have been performed. However, none of the searches were able to identify a persistent signal that would indicate a deviation from the SM. Instead, the parameter spaces of many models have been successfully restricted [55]. For example, many of the allowed masses of particles in the most studied supersymmetric models are now at or above the TeV limit (see Fig. 1.2). Other models, such as Technicolor [57] or the CMSSM [39], could be excluded. Higgs [58] and top quark [59] studies have repeatedly shown how accurate the predictions of the Standard Model actually are (see Fig. 1.3 and Fig. 1.4). But despite, or perhaps because of, the missing indications of BSM physics, the LHC has changed the expectations of many about what physics beyond the Standard Model looks like. As a reaction theoretical studies have been moving away from focusing on specific models and instead increasingly embrace model-independent approaches. In SUSY studies, for example, phenomenological models like the pMSSM-11 or the pMSSM-19 are preferred over models with specific soft breaking terms [60, 61, 62, 63]. However, the challenge then lies in the fact that the parameter spaces of these phenomenological models are large. Thus fitting the models in order to find the one that is best described by the experimental data, particularly from LHC direct searches, is computationally very demanding. For the comparison of theory and experiment, generating Monte Carlo events and performing detector simulations is required, which can collectively take up to one or more hours of CPU time per parameter point. This means that in order to sample merely two points per dimension in models like the pMSSM-19 with 19 free parameters, more than half a million CPU hours would be required. An additional complication comes from the fact that in most cases there is no unique minimum in the parameter space. Instead several different combinations of parameter points can simultaneously explain a given set of data and therefore have to be sampled. For this reason much

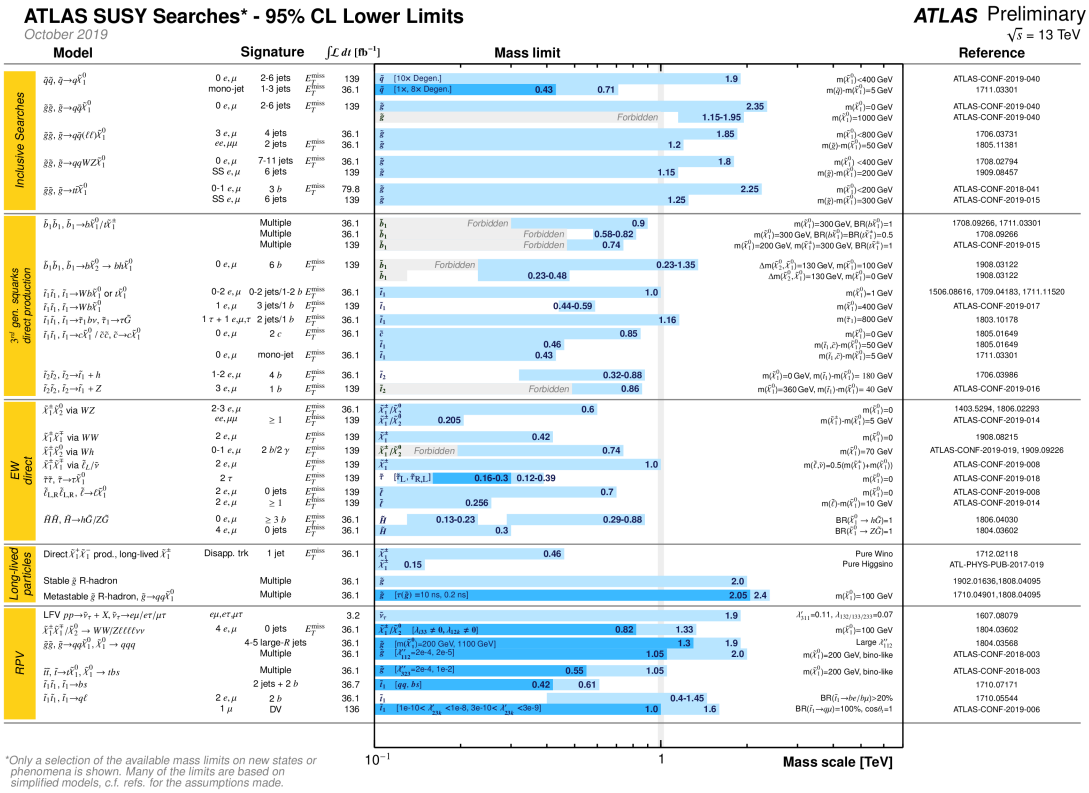

Figure 1.2: 95% CL lower limits on sparticle masses for different models and searches as reported by ATLAS. In many cases the lower limit now exceeds the 1 TeV threshold. If the masses are too large, many of the motivations for SUSY like solving the electroweak hierarchy problem, are no longer sustainable to the same extend. [56]

effort has gone into reducing the sampling time by for example parameterizing the LHC results (e.g. [64]), using simplified models (e.g. [65]) or applying machine learning methods (e.g. [66]). All of these approaches can however, depending on the studied model, lead to flawed results. While parameterizing LHC results by the most relevant masses of the model, for example, works well for the purpose of giving a first approximation to the LHC likelihood, it is not appropriate to fit or understand regions in parameter space with unusual decay topologies, which is, for most applications, the intend of performing the fit in the first place. Consequently refinements of this method, like simplified models, that add additional information, e.g. branching ratios, to the fit, promise better performance. Various tools, that allow fast limit setting in SUSY or vector-like quark models (e.g. sModelS [65, 67], FastLim [68] or XQCUT [69]) are built around this idea. The disadvantage of using simplified models is the fact that one needs to include all possible decay chains in order to rigorously perform fits. This can however be a challenging endeavour for realistic models with very large numbers of decay

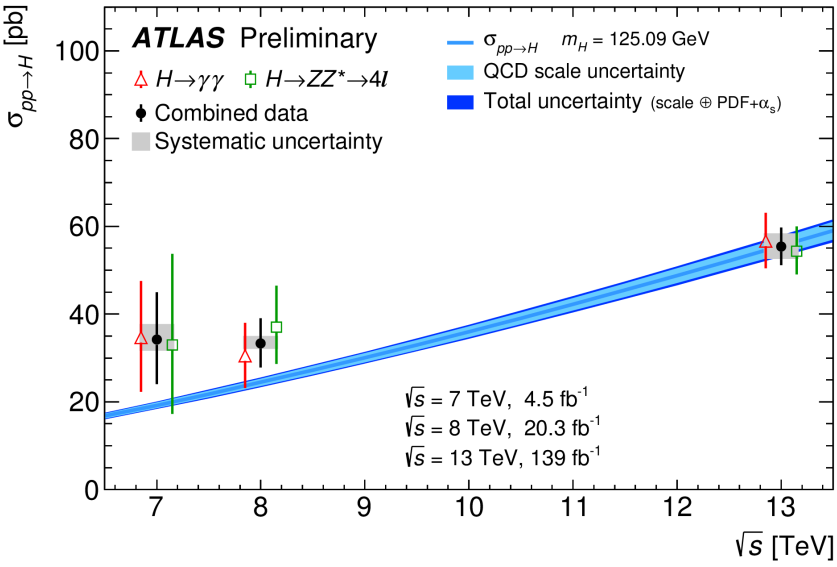

Figure 1.3: ATLAS cross section measurements of $H \to \gamma\gamma$ (red) and $H \to ZZ^* \to 4l$ (green) for center-of-mass energies $\sqrt{s} = 7$ TeV, 8 TeV, 13 TeV. Black bars denote the combination of the measured production cross sections. The blue curve corresponds to the theoretical SM expectation including QCD scale and PDF uncertainties. Theory and experiment agree within 1-2σ for low center-of-mass energies and match perfectly for $\sqrt{s} = 13$ TeV. [58]

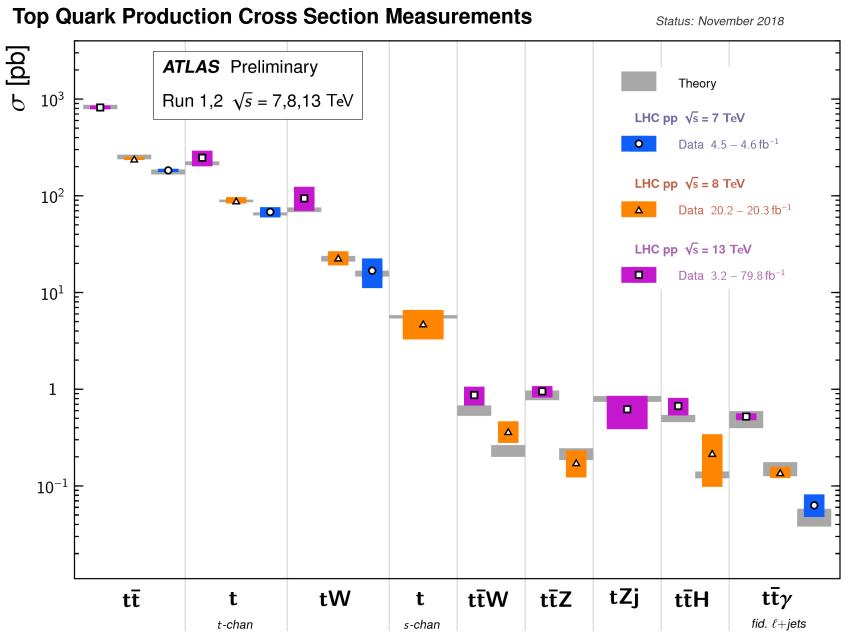

Figure 1.4: Production cross sections for top quarks with and without an associated boson. All measured cross sections agree with the SM predictions. [59]

chains.

Finally machine learning methods have been applied in the literature to predict the LHC likelihood and event counts, that can be used to classify parameter points as "excluded" or "allowed" using tools like CheckMATE2 [70, 71, 72]. Similar algorithms like e.g. SCYNet are able to predict the global χ^2 of a set of LHC analyses for certain models [66]. These machine learning approaches have the advantage that once the model is trained, the execution, i.e. prediction only take at about the order of milliseconds. This however comes in many cases at the cost of accuracy specifically in regions that the models was not trained on or show unexpected behaviour from the point of view of the training data.

In this work a new approach is proposed, that is based on the combination of kinematic transformations and reweighting of existing Monte Carlo events. Once events are generated for one parameter point, corresponding events for new parameters points are generated by the algorithm in a two step process. First kinematical transformations are applied to the involved momenta, then the Monte Carlo weights of the events are readjusted. This approach can be seen as an extension of the idea described in [73] where reweighting was employed to reuse Monte Carlo events between different BSM models. The technique outlined in this work presents an extension of this approach that additionally allows for changes of particle masses from one set of Monte Carlo events to another. This is achieved by introducing kinematical transformations that modify the momenta of the relevant particles such that regions that were kinematically excluded for the original masses become available. The advantage of this method is that expensive Monte Carlo simulations for large parts of the parameter space can be bypassed, therefore allowing for a reduction of sampling time by a factor of ≈10-100, at the same time maintaining high accuracy.

In Ch. 2 a summary of the Monte Carlo method and the mechanics of Monte Carlo event generation in high energy particles physics is given. Ch. 3 then presents the description of the algorithm proposed here, including a discussion of kinematical transformations and required reweighting factors. In Ch. 4 finally the algorithm is applied to different processes and its results are compared to the results of an ATLAS search at the LHC.

Chapter 2

Monte Carlo Methods

2.1 Monte Carlo Basics

Calculations in most areas of modern physics in general and in theoretical particle physics in particular involve complicated multidimensional integrals that cannot be solved analytically and instead require sophisticated numerical methods. Most of these methods rely on what is called the *Monte Carlo method*, that is based on the idea of employing the generation of pseudorandom numbers and the law of large numbers to evaluate definite integrals.
Consider the simple case of a one-dimensional integral of a real-valued function $f : D \subseteq \mathbb{R} \to \mathbb{R}$ over an interval $(a, b) \subset D$. From the mean value theorem for definite integrals it follows that the value of the integral can be written as

$$I = \int_a^b \mathrm{d}x \; f(x) = (b - a) \langle f(x) \rangle \,, \tag{2.1}$$

where

$$\langle f(x) \rangle \equiv E[f(x)|a < x < b] \tag{2.2}$$

is the mean or expected value of f on (a, b). Monte Carlo integration now describes the process of estimating this expected value by generating a finite set of N uniformly distributed pseudorandom points

$$S = \{x_1, \ldots, x_N\} \tag{2.3}$$

in order to calculate the average value μ_N of f on S:

$$\mu_N = \frac{1}{N} \sum_{i=1}^{N} f(x_i). \tag{2.4}$$

In the literature S is often called a Monte Carlo sample and x_i are called Monte Carlo events. The (weak) law of large numbers then implies that the average value converges to the expected value if N becomes large, i.e.

$$\lim_{N\to\infty} \Pr\left(|\mu_N - \langle f(x)\rangle \,| > \epsilon\right) = 0, \quad \text{for all } \epsilon > 0. \tag{2.5}$$

One can therefore define an estimator $\hat{I}$ for the integral in Eq. (2.1) as

$$I = \int_a^b \mathrm{d}x \; f(x) \tag{2.6}$$

$$= (b-a) \left\langle f(x)\right\rangle \tag{2.7}$$

$$\overset{N\gg 1}{\approx} \frac{b-a}{N} \sum_{i=1}^{N} f(x_i) =: \hat{I}. \tag{2.8}$$

The estimator can be identified as the usual estimator of the expectation value and be interpreted as the weighted average of the sample points with the weights given by the value of the integrand at that point, i.e.

$$\hat{I} = \frac{1}{N} \sum_{i=1}^{N} w_i, \quad w_i = (b-a) f(x_i). \tag{2.9}$$

In most applications however it is computationally inefficient or even unfeasible to sample the integration region uniformly, since the same amount of time is spent sampling regions that contribute comparatively little to the overall value of the integral as sampling dominant regions. A more sophisticated approach, that is typically referred to as *importance sampling*, is to generate S from a probability density p with

$$\int_a^b \mathrm{d}x \; p(x) = 1 \quad \text{and} \quad p(x) > 0 \; \forall x \in (a,b), \tag{2.10}$$

that replicates the overall behavior of the integrand. Then S contains many points in regions with larger values of f and fewer points in regions where f is

small.[1] Using importance sampling one can write Eq. (2.1) as

$$I = \int_a^b \mathrm{d}x \; f(x) \tag{2.11}$$

$$= \int_a^b \mathrm{d}x \; \frac{f(x)}{p(x)} \, p(x) \tag{2.12}$$

$$= E_p \left[\frac{f(x)}{p(x)} \middle| \, a < x < b \right] \tag{2.13}$$

$$\overset{N \gg 1}{\approx} \frac{1}{N} \sum_{i=1}^{N} \frac{f(x_i)}{p(x_i)}, \quad x_i \sim p \tag{2.14}$$

where $E_p[\cdot]$ is the expected value given probability density p. Eq. (2.9) similarly becomes

$$\hat{I} = \frac{1}{N} \sum_{i=1}^{N} w_i, \quad w_i = \frac{f(x_i)}{p(x_i)}. \tag{2.15}$$

One can see this equation as the general Monte Carlo integration formula in one dimension.[2] The generalization to d dimensions is straightforward and given by the following substitutions:

$$f, p : D \subset \mathbb{R} \to \mathbb{R} \quad \to \quad f, p : D \subset \mathbb{R}^d \to \mathbb{R}, \tag{2.16}$$

$$(a, b) \subset D \quad \to \quad \Omega \subset D, \tag{2.17}$$

$$\mathrm{d}x \quad \to \quad \mathrm{d}^d x. \tag{2.18}$$

Then

$$I = \int_\Omega \mathrm{d}^d x \; f(\vec{x}) \tag{2.19}$$

$$= \int_\Omega \mathrm{d}^d x \; \frac{f(\vec{x})}{p(\vec{x})} \, p(\vec{x}) \tag{2.20}$$

$$= E_p \left[\frac{f(\vec{x})}{p(\vec{x})} \middle| \, a < x < b \right] \tag{2.21}$$

[1] Generally, if arbitrary integrands are allowed, p should behave similar to the absolute value of f, since the contribution of a given region $\mathrm{d}x \subset (a, b)$ to the integral is independent of sign of the function in that region and $p(x) > 0$ on (a, b) by construction.

[2] Note that Eq. (2.7) and (2.9) are just the special cases of Eq. (2.13) and (2.15) with p being a normalized uniform distribution, i.e. $p(x) = u(x) = \frac{1}{b-a}$.

$$\overset{N\gg 1}{\approx} \frac{1}{N}\sum_{i=1}^{N} w_i =: \hat{I}_d, \quad w_i = \frac{f(\vec{x}_i)}{p(\vec{x}_i)},\ \vec{x}_i \sim p. \tag{2.22}$$

This equation will be the basis for the approach introduced in this work.
An important property of Monte Carlo integration is that one can estimate the error of the approximation, that is introduced by using a finite sample size. Eq. (2.21) describes the reduction of the integral I to an expectation value of $f(\vec{x})/p(\vec{x})$. Therefore the variance of the integral can be written as

$$\sigma_I^2 = \frac{1}{N}\,\mathrm{Var}\left[\frac{f(\vec{x})}{p(\vec{x})}\right] \tag{2.23}$$

$$= \frac{1}{N}\,E\left[\left(\frac{f(\vec{x})}{p(\vec{x})} - I\right)^2\right] \tag{2.24}$$

$$= \frac{1}{N}\left(E\left[\left(\frac{f(\vec{x})}{p(\vec{x})}\right)^2\right] - I^2\right). \tag{2.25}$$

The corresponding estimator reads

$$\hat{\sigma}_I^2 = \frac{1}{N-1}\left(\frac{1}{N}\sum_{i=1}^{N} w_i^2 - \left(\frac{1}{N}\sum_{i=1}^{N} w_i\right)^2\right), \quad w_i = \frac{f(\vec{x}_i)}{p(\vec{x}_i)}. \tag{2.26}$$

It should be noted that if f is strictly positive on (a, b) the choice $p(x) = f(x)$ or $w_i = 1$ leads to a vanishing variance. In practice however this choice cannot easily be made, since upon being able to generate random numbers from p in order to integrate f one has to effectively integrate p which was chosen to be equivalent to f. Finding a suitable probability density p is a non trivial problem. One of the most commonly applied algorithms in this context is *VEGAS*. VEGAS uses an iterative approach to reduce the difference between the target function f and a step function p by sampling the integration region and histogramming the result [74].
In many cases though, instead of trying to find the value of the intrgral, one is interested in a set of events that follows the same distribution as the integrand. This can only be achieved if

$$p(x_i) = \mathrm{const.} f(x_i) \tag{2.27}$$

or in other words

$$w_i = \mathrm{const.}, \tag{2.28}$$

which means that all events have the same weight. Such a sample is called an unweighted Monte Carlo sample and is usually constructed by first generating a weighted sample as described above and subsequently unweighting the sample.
Eq. (2.26) also explicitly shows that the error of the estimate is independent of the number of dimensions of the integral. This is the major argument for preferring Monte Carlo integration over other numerical integration algorithms like Simpson's rule that require an exponentially increasing number of sample points in multiple dimensions.

2.2 Monte Carlo Event Generation

The most relevant application of Monte Carlo integration to particle physics, for the purposes of this work, is the calculation of cross sections for scattering processes at the Large Hadron Collider (LHC). Therefore subsequently only proton-proton collisions will be considered although a generalization to other hadronic collisions is straightforward.
While the determination of cross sections themselves is often crucial, generating sets of Monte Carlo events that can be used to study differential distributions of the cross sections is often more interesting. The full event generation process for hadron-hadron collisions can roughly be divided into five steps [75]:

1. Hard Process
2. Parton Shower
3. Multi-parton Interactions
4. Hadronization
5. Detector Simulation

As the proposed algorithm in Ch. 3 makes direct use of the generation of the hard process and the parton shower, these steps will be discussed in detail. Further descriptions of steps 3. - 5. can be found, among others, in [75], [76] and [77].

Hard Process
Scattering processes at the LHC often involve large momentum transfers above the scale of Quantum Chromodynamics (QCD) $Q > \Lambda_{\mathrm{QCD}}$, which means that for these processes the collision of the protons can be described as the scattering of two asymptotically free partons (gluons, quarks or anti-quarks) [78, 79]. This in turn can then be treated perturbatively and the cross section for the production of a given final state X through the scattering of two protons in collinear

factorization can be written as [75]

$$\sigma_{pp\to X} = \sum_{a,b} \int_0^1 \mathrm{d}x_1 \int_0^1 \mathrm{d}x_2 \; f_a(x_1, \mu_F^2) f_b(x_2, \mu_F^2) \int \mathrm{d}\hat{\sigma}_{ab\to X} \; . \tag{2.29}$$

The sum runs over all possible subprocesses that include the production of the final state through the collision of the initial state partons a and b. The parton distribution functions (PDFs) $f_i(x_j, \mu_F^2)$ describe the probability of finding parton i inside proton j at a given momentum fraction x_j and factorization scale μ_F. The dependence of the PDFs on the factorization scale μ_F is determined by the *Dokshitser-Gribov-Lipatov-Alterelli-Parisi (DGLAP)* equations that govern the evolution of the PDFs from a base scale μ_0, usually chosen to be at the order of 1 GeV, to any scale μ_F [80, 81, 82]. The values of the PDFs at the base scale must then be determined experimentally [83]. There are several different parametrization of the PDFs that are based on partially different experimental data. Examples include the PDFs published by the collaborations CTEQ [84] and NNPDF [85], that were also used for the computations in Ch. 4.

The final component of Eq. (2.29) is the partonic cross section $\hat{\sigma}_{ab\to X}$ for the production of the final state X through the scattering of two partons a and b:

$$\hat{\sigma}_{ab\to X} = \frac{1}{2\hat{s}} \int \mathrm{d}\Phi_n \; \overline{|M_{ab\to X}|^2}. \tag{2.30}$$

Here $\frac{1}{2\hat{s}}$ is the parton flux with

$$\hat{s} = (p_a + p_b)^2 = x_1 x_2 s \tag{2.31}$$

being the center of mass energy squared of the initial state partons. The integration is performed over the Lorentz-invariant n-particle final state phase space given by

$$\mathrm{d}\Phi_n = \prod_{i=1}^{n} \frac{\mathrm{d}^3\vec{p}_i}{(2\pi)^3 2E_i} \; (2\pi)^4 \delta^{(4)} \left(P_{\mathrm{in}} - \sum_{i=1}^{n} p_i \right), \tag{2.32}$$

where $P_{\mathrm{in}} = p_a + p_b$ is the total partonic initial state momentum. Finally $\overline{|M_{ab\to X}|^2}$ is the process specific squared matrix element that can be calculated in perturbation theory by for example using Feynman diagrams.

The generation of Monte Carlo parton level events now generally follows the

ideas of Ch. 2.1 with the integral to be solved being the integral in Eq. (2.29). Software packages like MadGraph5_aMCNLO [86] offer the fully automated generation of (weighted and unweighted) Monte Carlo events for nearly all processes in the Standard Model of Particle Physics and processes for many models beyond the Standard Model at leading and next-to-leading order. The output is then typically provided in the Les Houches Event File (LHEF) format, that contains, among others, information about the flavors and momenta of all particles involved in the process [87].

Parton Shower

The simulation of the hard process is maximally inclusive and as such assumes for example that the experimentally measured momenta of jets can sufficiently well be described by the momenta of final state partons in the hard process. A natural next step on top of the simulation of the hard process is therefore the addition of information about the QCD radiation of colored initial or final state particles in order to better describe the structure of these jets. By the definition of the hard process the participating particles are strongly accelerated and therefore emit radiation [75]. In the case of (anti-)quarks and gluons the emitted particles also hold an $SU(3)$ charge and therefore emit new QCD radiation themselves. A cascade of gluons and (anti-)squarks is produced where at each emission the scale of the emitted partons decreases until non-perturbative effects become important [75, 88]. The final result then is a shower of (anti-)quarks and gluons, i.e. partons - hence the name *parton shower*.

Essentially parton showers can be seen as iterative branchings of partons or, as it is typically modelled in modern Monte Carlo event generators, color dipoles [89]. Common descriptions of parton showers start by discussing parton branchings in the collinear limit for which it can be shown that the cross section factorizes independently of the process producing the partons in the first place. If the process before the branching has n final state particles, the cross section after the branching in leading order can be written as [88]

$$\mathrm{d}\sigma_{n+1} = \mathrm{d}\sigma_n \, \frac{\alpha_s}{2\pi} \frac{\mathrm{d}\theta^2}{\theta^2} \, \mathrm{d}z \, \mathrm{d}\phi \; P_{ba}(z, \phi), \tag{2.33}$$

where θ is the angle between the partons b and c produced by the branching of parton a, ϕ is the azimuthal angle of the splitting plane and z is the fraction of energy that the emitted particle b takes from the initial particle a. The functions $P_{ba}(z, \phi)$ are called *splitting functions* and can be found in standard textbooks, e.g. [90]. The incorporation of soft gluon emissions is less straight forward since the

above factorization property of the cross section no longer holds. Instead merely the matrix element itself factorizes and therefore interference terms between diagrams of emissions from different partons become relevant when calculating the squared matrix element. Fortunately one can avoid these difficulties by ordering the parton shower branchings in some defined scale that describes the angular separation of the gluon and the emitting parton, e.g. the opening angle θ, the transverse momentum of the gluon $k_\perp$ or its virtuality q^2. This is due to the fact that gluon emissions from different partons in the non-collinear region are coherent and thus the gluons can only see the total $SU(3)$ charge of the process. This means that it is irrelevant which parton emitted the gluon and the branching can be described as if the gluon was emitted by a particle with the total mass and color of all partons [89]. Given this kind of ordering and Eq. (2.33), one can derive the branching probability between virtuality q^2 and $q^2 + \mathrm{d}q^2$ of a parton a into two partons b and c [75]:

$$dP_a = \frac{\alpha_s}{2\pi}\frac{\mathrm{d}q^2}{q^2}\int\limits_{Q_0^2/q^2}^{1-Q_0^2/q^2} \mathrm{d}z\ P_{ba}(z), \tag{2.34}$$

where Q_0 is the low energy cutoff of the parton shower at which further branchings are physically not resolvable and $P_{ba}(z)$ are the spin averaged splitting functions[3] that can be found for example in [89] or [90]. In order to be able to use the Monte Carlo method for the production of parton showers however, the probability density for a new branching at a given scale q^2 is needed. This probability density is the derivative of the probability $\Delta_a(Q^2, q^2)$ that parton a does not emit any QCD radiation above a given q^2. Here Q^2 is the highest possible branching scale for parton a. It can be shown that $\Delta_a(Q^2, q^2)$ follows a simple differential equation [75]:

$$\frac{\mathrm{d}\Delta_a(Q^2, q^2)}{\mathrm{d}q^2} = \Delta_a(Q^2, q^2)\frac{\mathrm{d}P_a}{\mathrm{d}q^2}. \tag{2.35}$$

Inserting Eq. (2.34) and solving the differential equation yields [75]

$$\Delta_a(Q^2, q^2) = \exp\left\{-\int\limits_{q^2}^{Q^2}\frac{\mathrm{d}k^2}{k^2}\frac{\alpha_s}{2\pi}\int\limits_{Q_0^2/k^2}^{1-Q_0^2/k^2}\mathrm{d}z\ P_{ba}(z)\right\}. \tag{2.36}$$

[3]Note that in this notation the regular and the spin averaged splitting function only differ in whether the azimuthal angle ϕ is given as an argument or not.

From this the desired probability distribution can be found by calculating the right-hand side of Eq. (2.35). By repeatedly sampling from this probability distribution, each time decreasing the scale of the branching, a cascade of partons is created.

Algorithms that are based on this idea or in modern cases the branching of color dipoles, are implemented in a variety of different software libraries [91, 92, 93]. Given the output of the simulation for the hard process these libraries can be used to add a parton shower "on top". The result can then be stored in the HEPMC file format [94]. Details about the contained information and structure of this format are highly relevant to the algorithm proposed in Ch. 3 and will be discussed there.

Chapter 3

Reusing Events in Parameter Scans

3.1 General Idea

The algorithm proposed in this work can be thought of as a generalization of the importance sampling method in general, as described in Ch. 2.1, and of the methods described in [73] in particular.
Importance sampling is useful in cases where the integrand can be evaluated efficiently and it is computationally not viable to generate the Monte Carlo sample from a uniform distribution. In essence importance sampling enables the utilization of a set of phase space points S that were generated from a function f to calculate the integral over a different function f'. A natural generalization of this idea would consider whether one can use a Monte Carlo sample S that was generated from some (unnormalized) function f on a phase space Ω in order to calculate the integral over a different (unnormalized) function f' on a different phase space Ω'. The question then is, given

$$x_i \sim f \quad \text{and} \quad \int_{\Omega} \mathrm{d}x \; f(x) = \sigma, \tag{3.1}$$

is it possible to determine the value of

$$\sigma' = \int_{\Omega'} \mathrm{d}x' \; g(x'), \tag{3.2}$$

where $g : \Omega' :\to \mathbb{R}$ is a given function that can be different from f? To answer this question one can proceed just as in the case of normal importance sampling

only introducing a differentiable transformation $t : \Omega \to \Omega'$ from the old phase space Ω to the new phase space Ω'. For a one-dimensional integral this means:

$$\sigma' = \int_{\Omega'} \mathrm{d}x' \; g(x') \tag{3.3}$$

$$= \int_{\Omega'} \mathrm{d}x' \; \frac{g(x')}{f(x)} f(x) \tag{3.4}$$

$$= \int_{\Omega} \mathrm{d}x \; J(x) \frac{g(t(x))}{f(x)} f(x), \quad J(x) = \frac{\mathrm{d}t(x)}{\mathrm{d}x} \tag{3.5}$$

$$= \int_{\Omega} \mathrm{d}x \; J(x) \frac{g(t(x))}{f(x)} \left(\sigma \hat{f}(x)\right), \quad \int_{\Omega} \mathrm{d}x \; \hat{f}(x) = 1 \tag{3.6}$$

$$= \sigma \int_{\Omega} \mathrm{d}x \; J(x) \frac{g(t(x))}{f(x)} \; \hat{f}(x) \tag{3.7}$$

$$= \sigma E_{\hat{f}} \left[J(x) \frac{g(t(x))}{f(x)} \middle| x \in \Omega \right] \tag{3.8}$$

$$\overset{N \gg 1}{\approx} \sigma \frac{1}{N} \sum_{i=1}^{N} J(x_i) \frac{g(t(x_i))}{f(x_i)}, \quad x_i \sim f. \tag{3.9}$$

Here the variable transformation

$$x' = t(x), \tag{3.10}$$

$$\mathrm{d}x' = \mathrm{d}x \, J(x) \tag{3.11}$$

$$\Omega' = t(\Omega) \tag{3.12}$$

with the Jacobian $J(x)$ was introduced in the third line. One can therefore use a set of (unweighted) phase space points that are distributed according to f and reweight each point with

$$w_i = J(x_i) \frac{g(t(x_i))}{f(x_i)} \tag{3.13}$$

such that

$$(t(x_i), w_i) \sim g. \tag{3.14}$$

Note that in order for the derivation to hold f is required to be strictly positive on Ω or else $\hat{f}$ cannot be a probability density.

The generalization to d dimensions is straightforward and given by

$$\sigma' = \int_{\Omega'} \mathrm{d}^d\vec{x}' \; g(\vec{x}') \tag{3.15}$$

$$= \sigma E_{\hat{f}} \left[J(\vec{x}) \frac{g(t(\vec{x}))}{f(\vec{x})} \middle| \vec{x} \in \Omega \right] \tag{3.16}$$

$$\overset{N\gg 1}{\approx} \sigma \frac{1}{N} \sum_{i=1}^{N} w_i, \; w_i = J(\vec{x}_i) \frac{g(t(\vec{x}_i))}{f(\vec{x}_i)}, \quad \vec{x}_i \sim f, \tag{3.17}$$

with the Jacobian of the transformation

$$J(\vec{x}) = \left| \frac{\partial \vec{x}'}{\partial \vec{x}} \right|. \tag{3.18}$$

If one was to apply the procedure outlined in the previous chapter to LHC scattering processes, one needs to determine what the underlying integral is that one wants to solve. That way it can be seen what the weights of the Monte Carlo events are. As the quantity of interest is the hadronic cross section σ one should start there:

$$\sigma = \sum_{a,b} \int_0^1 \mathrm{d}x_1 \int_0^1 \mathrm{d}x_2 \; f_a(x_1) f_b(x_2) \int \mathrm{d}\hat{\sigma}_{ab}, \tag{3.19}$$

where $\hat{\sigma}_{ab}$ is the partonic cross section of the respective subprocess with initial partons a and b:

$$\mathrm{d}\hat{\sigma}_{ab} = \frac{1}{2\hat{s}} \int \mathrm{d}\Phi_n \; \overline{|M_{ab}|^2}, \tag{3.20}$$

where $\mathrm{d}\Phi_n$ is the n particle Lorentz invariant phase space. One still has to show that the integrand is strictly positive in the entire phase space. The integrand can be written as

$$f_a(x_1) f_b(x_2) \frac{1}{2\hat{s}} \Phi \overline{|M_{ab}|^2}. \tag{3.21}$$

Since the PDFs, the flux and the squared matrix element are positive by construction, the only non-trivial piece is to show that the finite part of the phase space integral is positive. Consider the differential n particle phase space

$$\mathrm{d}\Phi_n = \prod_{i=1}^{n} \frac{\mathrm{d}^3\vec{p}_i}{(2\pi)^3 2E_i} \; (2\pi)^4 \delta^{(4)} \left(P_{\mathrm{in}} - p_1 - \ldots - p_n \right). \tag{3.22}$$

As this expression is Lorentz-invariant it can be evaluated in the center-of-mass frame of the initial state partons where

$$P_{\text{in}} = (\sqrt{\hat{s}}, \vec{0}). \tag{3.23}$$

Then the spacial part of the δ-function can be used to perform the integral over $\vec{p}_n$, i.e.

$$\begin{aligned} \mathrm{d}\Phi_n &= \prod_{i=1}^{n-1} \frac{\mathrm{d}^3\vec{p}_i}{(2\pi)^3 2E_i} \frac{1}{(2\pi)^3 2E_n} (2\pi)^4 \delta\left(\sqrt{\hat{s}} - E_1 - \ldots - E_n\right) && (3.24) \\ &= \prod_{i=1}^{n-1} \frac{|\vec{p}_i|\,\mathrm{d}|\vec{p}_i|\,\mathrm{d}\cos\theta_i\,\mathrm{d}\phi_i}{(2\pi)^3 2E_i} \frac{2\pi}{2E_n} \delta\left(\sqrt{\hat{s}} - E_1 - \ldots - E_n\right), && (3.25) \end{aligned}$$

where $E_i^2 = \sqrt{m_i^2 + |\vec{p}_i|^2}$ and

$$E_n = \sqrt{m_n^2 + |\vec{p}_n|^2} = \sqrt{m_n^2 + (\vec{p}_1 + \ldots + \vec{p}_{n-1})^2}. \tag{3.26}$$

Rewriting the integration measure in terms of the energies yields

$$\mathrm{d}\Phi_n = \prod_{i=1}^{n-1} \frac{\sqrt{E_i^2 - m_i^2}\,\mathrm{d}E_i\,\mathrm{d}\cos\theta_i\,\mathrm{d}\phi_i}{2(2\pi)^3} \frac{2\pi}{2E_n} \delta\left(\sqrt{\hat{s}} - E_1 - \ldots - E_n\right). \tag{3.27}$$

One can now execute the δ-function to remove the integration over E_1:

$$\delta\left(g(E_1)\right) = \sum_k \frac{\delta(E_1 - E_k)}{|g'(E_k)|},\ g(E_1) = \sqrt{\hat{s}} - E_1 - \ldots - E_n. \tag{3.28}$$

This is strictly positive as each term is strictly positive. For $2 \to 2$ processes one can explicitly calculate the phase space as

$$\begin{aligned} \mathrm{d}\Phi_2 &= \frac{\mathrm{d}\vec{p}_3}{(2\pi)^3 2E_3} \frac{\mathrm{d}\vec{p}_4}{(2\pi)^3 2E_4} (2\pi)^4 \delta^{(4)}\left(p_{\text{in}} - p_3 - p_4\right) && (3.29) \\ &= \frac{\mathrm{d}\vec{p}_3}{(2\pi)^2 2E_3 2E_4} \delta\left(\sqrt{\hat{s}} - E_3 - E_4\right) && (3.30) \\ &= \frac{r^2 \mathrm{d}r\,\mathrm{d}\cos\theta\,\mathrm{d}\phi}{(2\pi)^2 2E_3 2E_4} \delta\left(\sqrt{\hat{s}} - \sqrt{r^2 + m_3^2} - \sqrt{r^2 + m_4^2}\right) && (3.31) \\ &= \frac{r^2 \mathrm{d}r\,\mathrm{d}\cos\theta\,\mathrm{d}\phi}{(2\pi)^2 2E_3 2E_4} \frac{\delta\left(r - \frac{\lambda^{\frac{1}{2}}(\hat{s}, m_3^2, m_4^2)}{2\sqrt{\hat{s}}}\right)}{r\frac{\sqrt{\hat{s}}}{E_3 E_4}} && (3.32) \\ &= \frac{\mathrm{d}\cos\theta\,\mathrm{d}\phi}{16\pi^2} \frac{r}{\sqrt{\hat{s}}} && (3.33) \end{aligned}$$

$$= \frac{\mathrm{d}\cos\theta\,\mathrm{d}\phi}{16\pi^2}\ \frac{\lambda^{\frac{1}{2}}(\hat{s}, m_3^2, m_4^2)}{2\hat{s}}, \tag{3.34}$$

which demonstrates the positivity explicitly. Here λ is the so-called Källén function, given by

$$\lambda(a, b, c) = a^2 + b^2 + c^2 - 2ab - 2ac - 2bc. \tag{3.35}$$

For equal mass two particle final states with $m_3 = m_4 = m$ this can be further simplified to

$$\frac{\mathrm{d}\cos\theta\,\mathrm{d}\phi}{16\pi^2}\ \frac{\lambda^{\frac{1}{2}}(\hat{s}, m_3^2, m_4^2)}{2\hat{s}} = \frac{\mathrm{d}\cos\theta\,\mathrm{d}\phi}{32\pi^2}\ \sqrt{1 - \frac{4m^2}{\hat{s}}}. \tag{3.36}$$

The total weight is therefore in this case given by

$$w_{ab} = f_a(x_1) f_b(x_2) \frac{1}{2\hat{s}} \frac{\lambda^{\frac{1}{2}}(\hat{s}, m_3^2, m_4^2)}{2\hat{s}} \overline{|M_{ab}|^2}. \tag{3.37}$$

The challenge now is to find a transformation that keeps the statistical error in Eq. (2.23), i.e. the variation of the weights, small. That means the transformation minimizes the influence of the reweighting, while still fulfilling the conditions of the derivation particularly the condition that

$$\Omega' = t(\Omega). \tag{3.38}$$

If one could find a transformation that perfectly maps the old integrand onto the new integrand, the new sample would be distributed according the new integrand and the weights would be constant. In this case the error is minimized. It is therefore desirable to use a transformation that maps the old integrand to a function that is as close as possible to the new integrand. The solution proposed in this work is presented in Ch. 3.2.

The general idea, in summary, is to first transform the integration variables of the integral in Eq. (3.19), then apply momentum conservation, where feasible, to determine the final states of the hard process, the parton shower and possibly decays. Finally one has to reweight each event according to Eq. (3.13). Using this method it is possible to take Monte Carlo events for a given process in a given physics model and use these events to analyze a different parameter point of the same model. Unlike the method described in [73] though, this method allows for changes in particle masses and is therefore an interesting candidate for the usage within programs like CheckMATE2 [72].

3.2 Kinematical Transformations

The idea of using kinematical transformation along reweighting to generate events for a different model parameter point is at the heart of the algorithm introduced in the present work. Transforming the momenta of the involved particles in a Monte Carlo event allows to extend the available phase space beyond what the original event was generated for.
The kind of kinematical transformations proposed here, make use of both detailed knowledge of the physical processes underlying the generation of the hard event and momentum conservation beyond the hard event. Two concrete transformations are introduced in Ch. 3.2.1. One transformation, that is derived in Ch. 3.2.1.1, is physically particularly interesting, as it does not change the lab frame of the considered process. A second transformation is discussed in Ch. 3.2.1.2, that, in contrast to the first, is bijective and therefore always fulfills the requirements laid out in Ch. 3.1.
Once the transformation of the hard process is understood, Ch. 3.2.2 describes how to exploit momentum conservation to propagate the transformations from the hard process to decay products, parton showers and jets.

3.2.1 Hard Process

The integration variables for the hard process can be read from Eq. (3.19) and Eq. (3.20) and are given by the momentum fractions x_1 and x_2 of the initial state partons as well as the phase space variables, i.e. the angles and energies of the final state particles that are consistent with momentum conservation. In most hard processes, be it SM or BSM processes, the immediate final state, i.e. the direct products of the initial state parton scattering, consists of two particles. The discussion of finding a suitable transformation in this chapter will therefore be restricted to 2-particle final states. In this case the phase space only consists of the angles of one of the final state particles. A first assumption of the below transformations is that all angles in the center-of-mass frame are constant under mass changes (see also Ch. 3.2.2). This obviously leads to errors if for example spin correlations are present and will have to be accounted for when determining reweighting factors.

3.2.1.1 Boost Invariant Transformations

Since, as described above, all angles of the final state momenta are kept constant and one is ultimately interested in the transformed final state in the laboratory frame of reference ("lab frame"), a natural approach would be to require the transformation to leave the lab frame unchanged. This essentially means that the boost between center-of-mass frame and lab frame is the same in the old and the new event. The boost, as determined by the boost vector $\vec{b}$, shall therefore be invariant under the transformation. In general boosts between center-of-mass frames and lab frames play an important role. A brief overview of the relevant formulas is therefore given in Appendix A.
The total momentum in the lab frame before the parton shower is given by

$$q = (x_1 + x_2, 0, 0, x_1 - x_2)\,\frac{\sqrt{s}}{2} \tag{3.39}$$

and so the corresponding boost vector is given by

$$\vec{b} = \frac{1}{E_q}\vec{q} = \left(0, 0, \frac{x_1 - x_2}{x_1 + x_2}\right). \tag{3.40}$$

Note that this implies that the boost vector is uniquely determined by the polar angle of the corresponding point (x_1, x_2) in the x_1-x_2-plane. This will be important later.
In the two-dimensional subspace of the integration region that one gets by fixing the phase space angles, the general form of the transformation $t : (0,1)^2 \to (0,1)^2$ is given by

$$t : (x_1, x_2) \mapsto (x_1', x_2'). \tag{3.41}$$

Under the assumption that x_1 and x_2 can be transformed independently this reads

$$x_1' = t_1(x_1) \tag{3.42}$$

$$x_2' = t_2(x_2). \tag{3.43}$$

Thus invariance of the boost vector implies

$$\frac{t_1(x_1) - t_2(x_2)}{t_1(x_1) + t_2(x_2)} = \frac{x_1 - x_2}{x_1 + x_2} \tag{3.44}$$

$$\Leftrightarrow (t_1(x_1) - t_2(x_2))(x_1 + x_2) = (t_1(x_1) + t_2(x_2))(x_1 - x_2) \tag{3.45}$$

$$\Leftrightarrow 2x_2 t_1(x_1) = 2x_1 t_2(x_2) \tag{3.46}$$

$$\Leftrightarrow \frac{t_1(x_1)}{x_1} = \frac{t_2(x_2)}{x_2}. \tag{3.47}$$

As x_1 and x_2 are arbitrary and independent numbers in $(0, 1)$ the variation of e.g. x_2 and simultaneous fixing of x_1 cannot change the right-hand side (RHS) as x_1 is fixed and the left-hand side (LHS) is therefore constant. This means that both sides of the equation must be constant and thus

$$\frac{t_1(x_1)}{x_1} = \frac{t_2(x_2)}{x_2} = a, \tag{3.48}$$

where[1] $a \in \mathbb{R}$. It follows that

$$t_1(x_1) = ax_1, \quad t_2(x_2) = ax_2 \tag{3.49}$$

$$\Rightarrow t_1 = t_2 = t \quad \text{and} \quad t(x_i) = ax_i. \tag{3.50}$$

Hence the transformation must be linear if one assumes the decoupling of the transformation described in Eq. (3.43).
One can now look at what happens if the transformations are not independent. Then

$$x_1' = t_1(x_1, x_2), \tag{3.51}$$

$$x_2' = t_2(x_1, x_2). \tag{3.52}$$

The invariance of the boost vector again implies

$$\frac{t_1(x_1, x_2)}{t_2(x_1, x_2)} = \frac{x_1}{x_2}. \tag{3.53}$$

Eq. (3.53) can be rewritten in polar coordinates with

$$x_1 = r_x \cos(\phi_x), \tag{3.54}$$

$$x_2 = r_x \sin(\phi_x), \tag{3.55}$$

$$x_1' = t_1(x_1, x_2) = r_t(r_x, \phi_x)\, \cos(\phi_t(r_x, \phi_x)), \tag{3.56}$$

$$x_2' = t_2(x_1, x_2) = r_t(r_x, \phi_x)\, \sin(\phi_t(r_x, \phi_x)), \tag{3.57}$$

[1] A more specific restriction of the allowed values for a follows below.

to arrive at

$$\tan(\phi_t) = \tan(\phi_x) \tag{3.58}$$

$$\Rightarrow \phi_t = n\pi + \arctan(\tan(\phi_x)) = n'\pi + \phi_x, \tag{3.59}$$

where n and n' are arbitrary integers. Since x_1 and x_2 as well as x_1' and x_2' are between 0 and 1, the angle of the new vector $t(x_1, x_2)$ must be contained in the interval $(0, \frac{\pi}{2})$ and therefore be equal to the angle of the old vector (x_1, x_2). This means that one can write

$$t(x_1, x_2) = (r_t \cos(\phi_t), r_t \sin(\phi_t)) \tag{3.60}$$

$$= (r_t \cos(\phi_x), r_t \sin(\phi_x)) \tag{3.61}$$

$$= r_t(\cos(\phi_x), \sin(\phi_x)) \tag{3.62}$$

$$= r_t \frac{1}{r_x}(x_1, x_2) \tag{3.63}$$

$$= a\ (x_1, x_2), \quad a \in \mathbb{R}^+. \tag{3.64}$$

The last equality follows from the fact that r_x is a given number and r_t is not restricted by Eq. (3.53) and is therefore arbitrary on $\mathbb{R}^+$. The determination of the corresponding Jacobian J of the transformation is trivial and yields

$$J = a^2. \tag{3.65}$$

One can conclude at this point that the invariance of the boost vector implies a linear transformation of the inputs. This linearity can lead to problems when the final state masses are changed and the hard process is already strongly boosted (i.e. x_1 or x_2 is close to 1). In this case there might not be enough phase space left for the new masses. Since

$$x_1' = a x_1 \quad \text{and} \quad x_2' = a x_2, \tag{3.66}$$

there is an upper limit to a that is given by

$$a_{\max} = \min\left(\frac{1}{x_1}, \frac{1}{x_2}\right). \tag{3.67}$$

Note that $a_{\max}$ depends on x_1 and x_2 and is not a global constant but must be determined on an event by event basis.
Now for the transformation to yield physical results one has to guarantee that the

center-of-mass energy of the new initial state is above the production threshold of the new final state, i.e.

$$\sqrt{\hat{s}'} > m_1' + m_2' \tag{3.68}$$

or

$$a_{\max}\sqrt{\hat{s}} > m_1' + m_2'. \tag{3.69}$$

This is however not necessarily always the case. The available phase space for

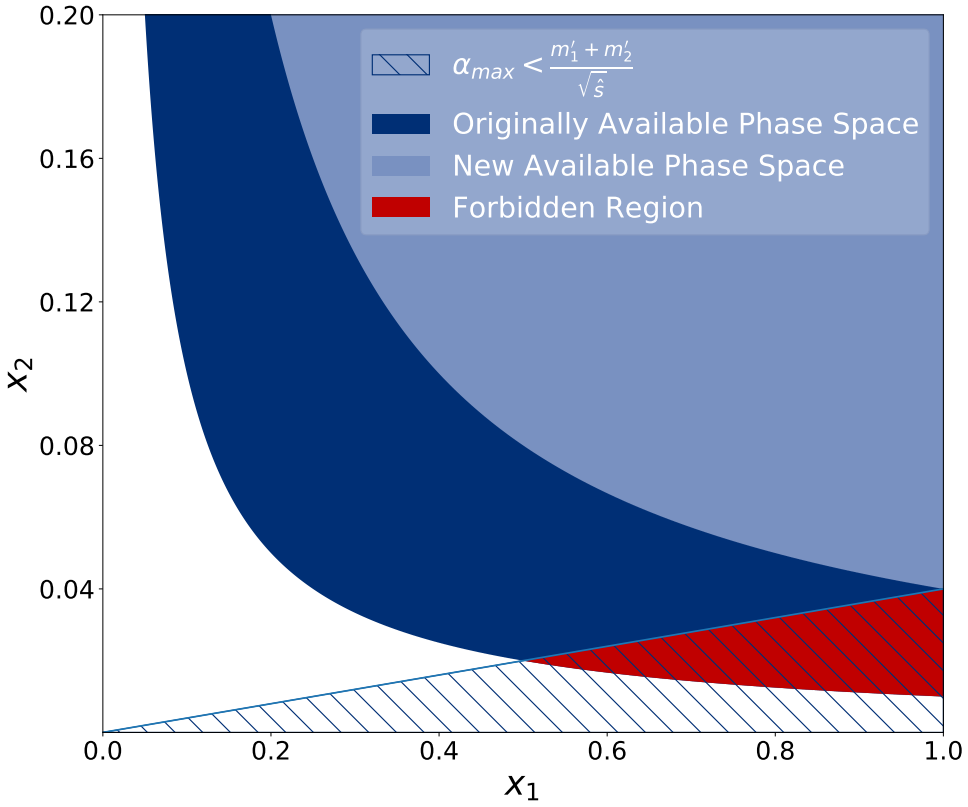

Figure 3.1: Sketch of the transformation of the kinematically allowed region in (x_1, x_2)-space for increasing final state masses. In order to produce larger final state masses, the kinematically allowed region shrinks and moves towards the top right corner (dark blue to light blue). The additional condition that $a_{\max}\sqrt{\hat{s}} < m_1' + m_2'$ implies that for the hatched region there is no corresponding point in the new allowed region (light blue), which means that these points must be transformed differently. Note that the plot is strongly compressed in the x_2 dimension in order to better display the effect. Consequently an analogous forbidden region also exists along the x_2-axis, that is not shown here.

the original parameter point with masses m_1 and m_2 is determined by Eq. (3.68):

$$\sqrt{\hat{s}} > m_1 + m_2 \tag{3.70}$$

$$\Rightarrow x_2(x_1) > \left(\frac{m_1 + m_2}{\sqrt{s}}\right)^2 \frac{1}{x_1}. \tag{3.71}$$

The same inequality holds for the primed quantities. In order to understand where the region in the x_1-x_2-plane lies, where Eq. (3.69) is not true one can, since Eq. (3.69) is symmetric under $x_1 \leftrightarrow x_2$, without loss of generality consider the case

$$x_1 > x_2. \tag{3.72}$$

Then

$$a_{\max} = \min\left(\frac{1}{x_1}, \frac{1}{x_2}\right) = \frac{1}{x_1}. \tag{3.73}$$

Inserting this into the inverse of Eq. (3.69) yields

$$a_{\max}\sqrt{\hat{s}} < m_1' + m_2' \tag{3.74}$$

$$\Leftrightarrow \quad \frac{1}{x_1}\sqrt{x_1 x_2} < \frac{m_1' + m_2'}{\sqrt{s}} \tag{3.75}$$

$$\Leftrightarrow \quad \frac{x_2}{x_1} < \left(\frac{m_1' + m_2'}{\sqrt{s}}\right)^2 \tag{3.76}$$

$$\Leftrightarrow \quad x_2 < \left(\frac{m_1' + m_2'}{\sqrt{s}}\right)^2 x_1. \tag{3.77}$$

The transformation can therefore not be performed for all $(x_1, x_2)-$combinations which lie in the intersection of Eq. (3.77) and Eq. (3.71). The situation is depicted in Fig. 3.1.

Obviously a corresponding "forbidden" region also exists in the case $x_2 > x_1$, that can be determined by replacing x_1 and x_2 in the above inequalities. In cases, where the original event lies in this region, there is, as described above, no other choice but to introduce a boost by transforming x_1 and x_2 differently. In cases where the linear transformation is possible (these cases typically make up a large majority as long as the mass changes are reasonable), the approach chosen to determine the constant of the linear transformation a consists of requesting

that the distance to threshold is constant under the transformation, i.e.

$$\frac{\sqrt{\hat{s}'}}{m'_{\text{fs}}} = \frac{\sqrt{\hat{s}}}{m_{\text{fs}}} \tag{3.78}$$

$$\Leftrightarrow \frac{\sqrt{x'_1 x'_2 s}}{m'_{\text{fs}}} = \frac{\sqrt{x_1 x_2 s}}{m_{\text{fs}}} \tag{3.79}$$

$$\Leftrightarrow \frac{\sqrt{a^2 x_1 x_2 s}}{m'_{\text{fs}}} = \frac{\sqrt{x_1 x_2 s}}{m_{\text{fs}}} \tag{3.80}$$

$$\Rightarrow a = \frac{m'_{\text{fs}}}{m_{\text{fs}}}, \tag{3.81}$$

where m_{fs} is the final state mass. In the case of s-channel production, m_{fs} corresponds to the invariant mass of the mediator. For t- and u- channel production m_{fs} is the sum of the masses of the produced particles.
If a is too large, i.e. $ax_1 > 1$ or $ax_2 > 1$ or in other words $a > a_{\max}(x_1, x_2)$, the maximal $a = a_{\max} - \epsilon$ is chosen.

In cases where

$$(ax_1 > 1 \text{ or } ax_2 > 1) \text{ and } a_{\max}\sqrt{\hat{s}} < m'_{\text{fs}} \tag{3.82}$$

a boost has to be introduced as there is not enough phase space left for the new final state to be produced on-shell even at rest. It is clear that for points in the forbidden region, a boost-less transformation is no longer a viable option. Instead x_1 and x_2 must be transformed differently. A possible transformation would be

$$x'_1 = 1 - \epsilon, \tag{3.83}$$

$$x'_2 = \left(\frac{m'_{\text{fs}}}{\sqrt{s}}\right)^2 + \delta, \tag{3.84}$$

where ϵ and δ are introduced for numerical purposes and should be chosen such that both x'_1 and x'_2 are contained in the available region of the numerical implementation of the parton density function, that is used. In order for the new point (x'_1, x'_2) to be in the allowed region one requires that

$$\sqrt{x'_1 x'_2 s} > m'_{\text{fs}} \tag{3.85}$$

$$\Leftrightarrow \delta > \left(\frac{m'_{\text{fs}}}{\sqrt{s}}\right)^2 \left(\frac{1}{(1-\epsilon)^2} - 1\right). \tag{3.86}$$

As the new point is on the boundary of the allowed region this corresponds to producing the particles at threshold. The ansatz in Eq. (3.83) and Eq. (3.84) is

therefore the transformation that introduces the smallest boost possible.

In order to estimate the severity of the problem one can determine the relative size of the problematic region

$$R = \frac{2\int_{x_1^*}^1 \mathrm{d}x_1 \ \left(c' x_1 - \frac{c}{x_1}\right)}{\int_c^1 \mathrm{d}x_1 \ \left(1 - \frac{c}{x}\right)}, \tag{3.87}$$

where x_1^* is the x_1-coordinate of the intersection between the boundary of the originally available phase space and the forbidden region. The coefficients $c^{(\prime)}$ are given by

$$c^{(\prime)} = \frac{\left(m_1^{(\prime)} + m_2^{(\prime)}\right)^2}{s} =: \frac{m_{\mathrm{fs}}^{(\prime)2}}{s}. \tag{3.88}$$

Hence

$$c' x_1^* = \frac{c}{x_1^*} \Rightarrow x_1^* = \sqrt{\frac{c}{c'}} = \frac{m_{\mathrm{fs}}}{m'_{\mathrm{fs}}}. \tag{3.89}$$

Solving the integrals in Eq. (3.87) and inserting Eq. (3.89) yields

$$R = \frac{c' - c(1 - \ln\frac{c}{c'})}{1 - c(1 - \ln(c))} \tag{3.90}$$

$$= \frac{\frac{m_{\mathrm{fs}}'^2}{m_{\mathrm{fs}}^2} - \left(1 - \ln\left(\frac{m_{\mathrm{fs}}^2}{m_{\mathrm{fs}}'^2}\right)\right)}{\frac{s}{m_{\mathrm{fs}}^2} - \left(1 - \ln\left(\frac{m_{\mathrm{fs}}^2}{s}\right)\right)} \tag{3.91}$$

$$= \frac{\frac{m_{\mathrm{fs}}'^2}{m_{\mathrm{fs}}^2} - \left(1 + \ln\left(\frac{m_{\mathrm{fs}}'^2}{m_{\mathrm{fs}}^2}\right)\right)}{\frac{s}{m_{\mathrm{fs}}^2} - \left(1 + \ln\left(\frac{s}{m_{\mathrm{fs}}^2}\right)\right)}, \tag{3.92}$$

for $m'_{\mathrm{fs}} > m_{\mathrm{fs}}$.

Examples for values of R in practice are shown in Fig. 3.2. Each curve belongs to a different starting point of a parameter scan in a supersymmetric model. In the considered process pairs of squarks with mass $m_{\tilde{q}}$ are produced, that ultimately decay into neutralinos. The final state mass in this case is given as $m_{\mathrm{fs}} = 2m_{\tilde{q}}$. One can clearly see that if the mass changes stay within reasonable bounds, R is around or below the 1% mark. In the worst case, the problematic region makes up about 4.7% of the total available phase space. This large value corresponds to more than a tripling of the squark mass.

Obviously physical events are not distributed uniformly in the x_1-x_2-plane and large values for x_1 and x_2 are suppressed by the PDFs. One can therefore interpret

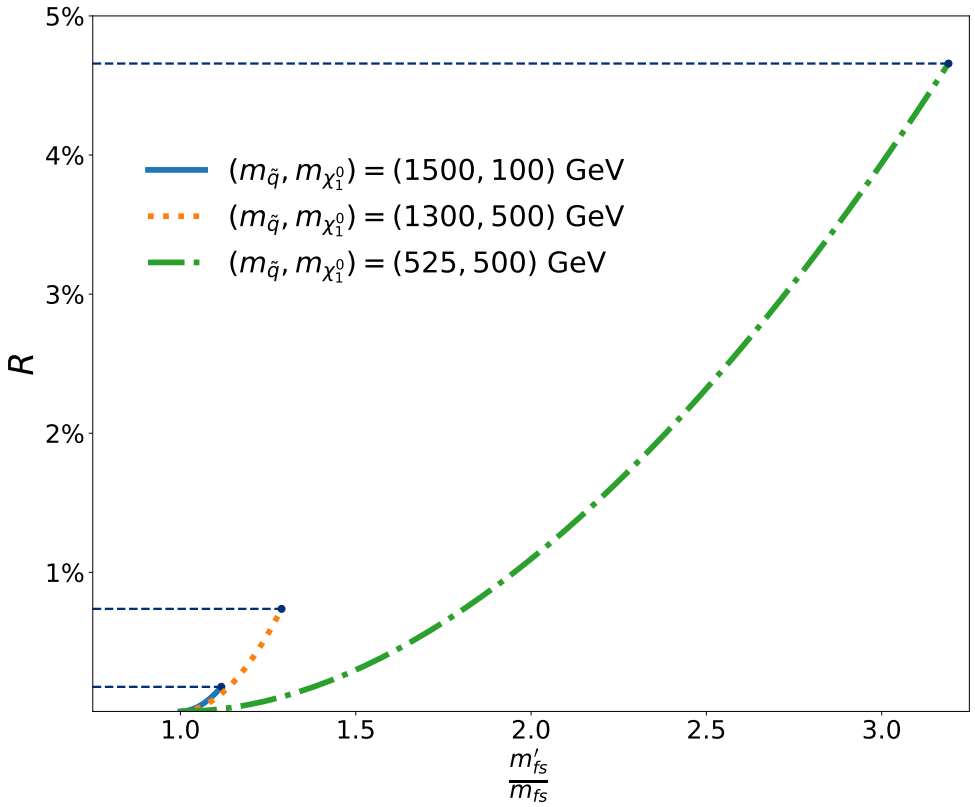

Figure 3.2: Relative size of the region where a linear transformation is kinematically impossible vs. $\frac{m'_{\text{fs}}}{m_{\text{fs}}}$ for different starting points in terms of squark and neutralino masses of the parameter scan from Ch. 4.4. Since the considered process is pair production the final state mass is given as $m^{(\prime)} = 2m_{\tilde{q}}^{(\prime)}$. The maximum of R is reached for transforming the squark mass from 525 GeV to 1675 GeV (green dash-dotted curve). In this case the relative size of the problematic region is $\approx 4.7\%$. In practice however there will be a smaller percentage of events, that need ancillary treatment since the problematic region corresponds to a situation in which one of the initial partons is strongly boosted, which is suppressed by the PDFs.

R as the upper limit for the percentage of events that cannot be transformed using the simple linear transformation.

3.2.1.2 Bijektive Transformations

As the transformations described in the previous chapter are not complete, i.e. there does not exist a valid transformation $t(x_1, x_2)$ for every point (x_1, x_2), one needs to think about other transformations that compensate for this shortcoming. As described above, the available phase space in the x_1-x_2-plane is bounded by

the function

$$x_2(x_1) = \frac{m_{\text{fs}}^2}{s}\frac{1}{x_1}. \tag{3.93}$$

As the final state mass increases (decreases) the available phase space shrinks (grows). In order to guarantee that there is a valid transformed phase space point for each original phase space point, one can demand that the distance to the boundary of the available phase space stays constant under the transformation, i.e.

$$\frac{\left|\binom{x_1}{x_2} - \binom{1}{1}\right|}{\left|\binom{a}{b} - \binom{1}{1}\right|} \stackrel{!}{=} \frac{\left|\binom{x_1'}{x_2'} - \binom{1}{1}\right|}{\left|\binom{a'}{b'} - \binom{1}{1}\right|}. \tag{3.94}$$

Here (a, b) and (a', b') are the intersection of the line g going through $(1, 1)$, (x_1, x_2) and (x_1', x_2'). This line is given by

$$g(x) = 1 - \frac{1 - x_2}{1 - x_1}(1 - x). \tag{3.95}$$

A sketch of this approach is shown in Fig. 3.3. Using that all points lie on g, Eq. (3.94) takes the form

$$(1 - x_1')^2 + (1 - g(x_1'))^2 = \frac{(1 - a')^2 + (1 - g(a'))^2}{(1 - a)^2 + (1 - g(a))^2}\left[(1 - x_1)^2 + (1 - g(x_1))^2\right]. \tag{3.96}$$

Inserting g into the left-hand side yields

$$(1 - x_1')^2 + (1 - g(x_1'))^2 = (1 - x_1')^2\left(1 + \left(\frac{1 - x_2}{1 - x_1}\right)^2\right) \tag{3.97}$$

$$= (1 - x_1')^2\frac{(1 - x_1)^2 + (1 - x_2)^2}{(1 - x_1)^2}. \tag{3.98}$$

The intersections $(a^{(\prime)}, b^{(\prime)})$ are given by finding the intersection between g and the phase space boundaries, i.e.

$$\frac{c^{(\prime)}}{a^{(\prime)}} = 1 - \frac{1 - x_2}{1 - x_1}(1 - a^{(\prime)}) \tag{3.99}$$

$$\Rightarrow a^{(\prime)} = \frac{x_1 - x_2 + u^{(\prime)}}{2(1 - x_2)}, \tag{3.100}$$

where $u^{(\prime)}$ is a symmetric function of $x_1^{(\prime)}$ and $x_2^{(\prime)}$

$$u^{(\prime)} = \sqrt{(x_1 - x_2)^2 + 4c^{(\prime)}(1 - x_1)(1 - x_2)}. \tag{3.101}$$

The solution to Eq. (3.99) with a negative sign of $u^{(\prime)}$ corresponds to the unphysical intersection for $x_1^{(\prime)}, x_2^{(\prime)} < 0$ and can thus be ignored. Finding $b^{(\prime)}$ can then easily be done by inserting Eq. (3.100) into g:

$$b^{(\prime)} = g(a^{(\prime)}) = \frac{x_2 - x_1 + u^{(\prime)}}{2(1 - x_1)}. \tag{3.102}$$

The first factor on the right-hand side of Eq. (3.96) can thus be written as

$$(1 - a^{(\prime)})^2 + (1 - b^{(\prime)})^2 = \frac{(1 - x_1)^2 + (1 - x_2)^2}{4(1 - x_1)^2(1 - x_2)^2} (2 - x_1 - x_2 - u^{(\prime)})^2 \tag{3.103}$$

$$\Rightarrow \frac{(1 - a')^2 + (1 - g(a'))^2}{(1 - a)^2 + (1 - g(a))^2} = \frac{(2 - x_1 - x_2 - u')^2}{(2 - x_1 - x_2 - u)^2}. \tag{3.104}$$

Therefore the transformation is given by

$$(1 - x_1')^2 \frac{(1 - x_1)^2 + (1 - x_2)^2}{(1 - x_1)^2} = \frac{(2 - x_1 - x_2 - u')^2}{(2 - x_1 - x_2 - u)^2} \left[(1 - x_1)^2 + (1 - g(x_1))^2\right] \tag{3.105}$$

$$\Leftrightarrow \frac{(1 - x_1')^2}{(1 - x_1)^2} = \frac{(2 - x_1 - x_2 - u')^2}{(2 - x_1 - x_2 - u)^2} \tag{3.106}$$

$$\Leftrightarrow \frac{1 - x_1'}{1 - x_1} = \frac{2 - x_1 - x_2 - u'}{2 - x_1 - x_2 - u} \tag{3.107}$$

$$\Leftrightarrow x_1' = 1 - (1 - x_1)\frac{2 - x_1 - x_2 - u'}{2 - x_1 - x_2 - u}. \tag{3.108}$$

Introducing a function $v(x_1, x_2)$ with

$$v(x_1, x_2) = \frac{2 - x_1 - x_2 - u'}{2 - x_1 - x_2 - u}, \tag{3.109}$$

and remembering that $x_2' = g(x_1')$ the transformation takes its final form:

$$x_1' = 1 - (1 - x_1)v(x_1, x_2), \tag{3.110}$$

$$x_2' = 1 - (1 - x_2)v(x_1, x_2). \tag{3.111}$$

The final piece of the transformation is the Jacobian:

$$\frac{\partial x_1'}{\partial x_1} = v - (1 - x_1)\frac{\partial v}{\partial x_1}, \tag{3.112}$$

$$\frac{\partial x_2'}{\partial x_2} = v - (1 - x_2)\frac{\partial v}{\partial x_2}, \tag{3.113}$$

$$\frac{\partial x_1'}{\partial x_2} = -(1 - x_1)\frac{\partial v}{\partial x_2}, \tag{3.114}$$

$$\frac{\partial x_2'}{\partial x_1} = -(1 - x_2)\frac{\partial v}{\partial x_1}. \tag{3.115}$$

And therefore

$$\frac{\partial x_1'}{\partial x_1}\frac{\partial x_2'}{\partial x_2} = \left[v - (1 - x_1)\frac{\partial v}{\partial x_1}\right]\left[v - (1 - x_2)\frac{\partial v}{\partial x_2}\right] \tag{3.116}$$

$$= v^2 + (1 - x_1)(1 - x_2)\frac{\partial v}{\partial x_1}\frac{\partial v}{\partial x_2} - v\left((1 - x_1)\frac{\partial v}{\partial x_1} + (1 - x_2)\frac{\partial v}{\partial x_2}\right), \tag{3.117}$$

$$\frac{\partial x_1'}{\partial x_2}\frac{\partial x_2'}{\partial x_1} = (1 - x_1)\frac{\partial v}{\partial x_2}(1 - x_2)\frac{\partial v}{\partial x_1} \tag{3.118}$$

$$= (1 - x_1)(1 - x_2)\frac{\partial v}{\partial x_1}\frac{\partial v}{\partial x_2}. \tag{3.119}$$

The Jacobian is then

$$\Rightarrow J = v^2 - v\left((1 - x_1)\frac{\partial v}{\partial x_1} + (1 - x_2)\frac{\partial v}{\partial x_2}\right). \tag{3.120}$$

The second term can be shown to vanish in a rather lengthy but simple series of steps, which can be found in Appendix B. Hence the Jacobian can we written in the following simple form:

$$J = v^2. \tag{3.121}$$

In summary, the full transformation is given by

$$x_1' = 1 - (1 - x_1)v(x_1, x_2), \tag{3.122}$$

$$x_2' = g(x_1') = 1 - (1 - x_2)v(x_1, x_2), \tag{3.123}$$

$$J = v^2(x_1, x_2). \tag{3.124}$$

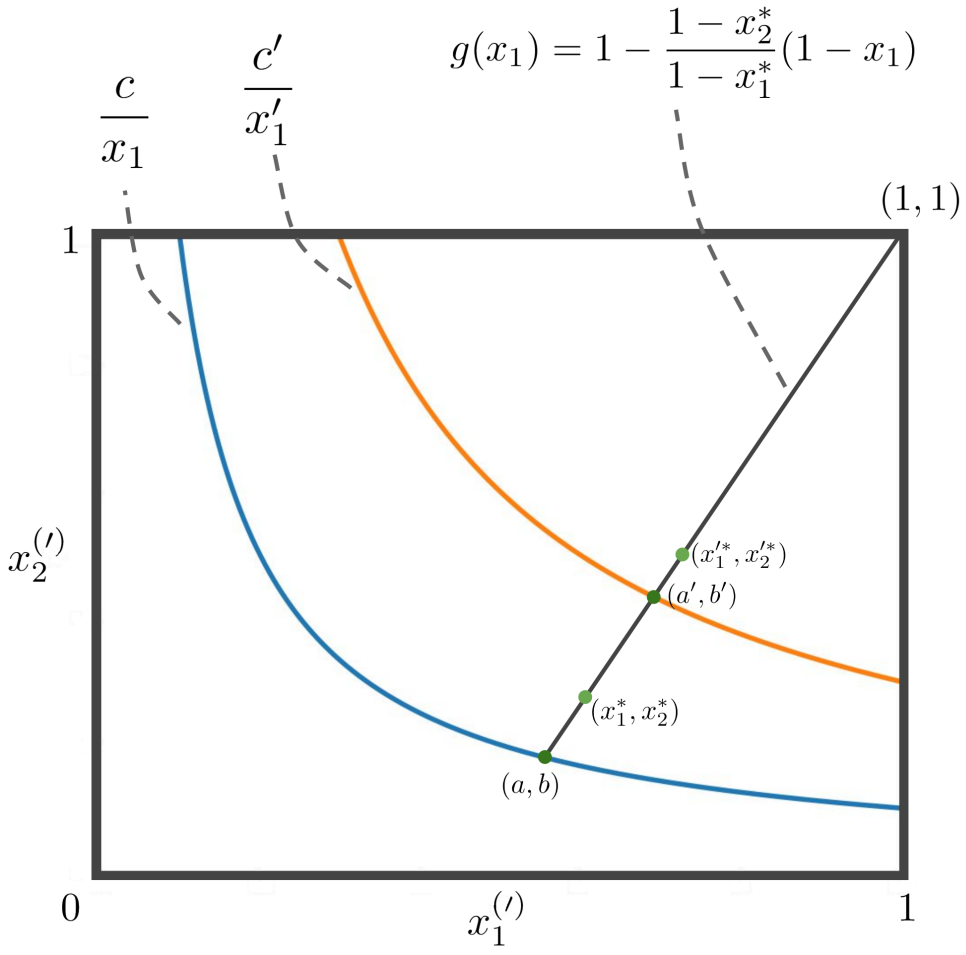

Figure 3.3: A bijective transformation from the original allowed phase space (area above the blue line) to the phase space for larger final state mass $m'_{\text{fs}} > m_{\text{fs}}$ (area above the orange line). The relative distance of a point to the boundary of the allowed phase space boundary is kept constant under the transformation. Note that the notation here deviates slightly from the notation in the text. The points $(x_1^{(\prime)}, x_2^{(\prime)})$ in the text are called $(x_1^{(\prime *)}, x_2^{(\prime *)})$ here.

3.2.1.3 In Practice

While the transformation from Ch. 3.2.1.2 avoids the problems described above for the boost invariant transformation, the linear transformation has the advantage of better reproducing the Breit-Wigners of resonances without the need for additional reweighting. In general, while the bijective transformation is mathematically superior, the transformation from section 3.2.1.1 better reproduces physical distributions at the price of producing unphysical events (e.g. $x_i > 1$) under the described circumstances. Therefore, in practice, mixing both approaches appears to be a natural choice. The proposed combination here is to use the linear transformation in as many cases as possible and to use the bijective transformation in cases where the former fails. This means

$$x_i' = t(x_i) = \begin{cases} ax_i, & \text{if } 0 < ax_1 < 1, 0 < ax_2 < 1 \\ 1 - (1 - x_i)v(x_1, x_2), & \text{else.} \end{cases} \tag{3.125}$$

The scaling factor a is the ratio of the new and old final state masses

$$a = \frac{m_{\text{fs}}'}{m_{\text{fs}}}. \tag{3.126}$$

For the production of a heavy s-channel mediator this corresponds to the ratio of the new and old off-shell masses M and M', i.e.

$$a = \frac{M'}{M}, \tag{3.127}$$

where M' is defined such that the "off-shellness" of the mediator is kept constant:

$$\frac{M' - m'}{\Gamma'} = \frac{M - m}{\Gamma} \tag{3.128}$$

$$\Leftrightarrow M' = m' + \frac{\Gamma'}{\Gamma}(M - m), \tag{3.129}$$

where m and m' are the respective on-shell masses. This way the old and the new mass are on the same position of the Breit-Wigner distribution.
For two final state particles in $u-$ or $t-$channel production the scaling factor becomes

$$a = \frac{m_1' + m_2'}{m_1 + m_2}. \tag{3.130}$$

The calculation of the Jacobian must then also be performed on an event by event basis using either Eq. (3.65) or Eq. (3.124) depending on the applied transformation.

3.2.2 Momentum Conservation

As outlined in Ch. 3.1, once a transformation has been performed, momentum conservation in the center-of-mass frame is employed in order to determine the final state momenta. This procedure includes, but is not limited to, the hard process. In fact it is an essential tool for the determination of the momenta of decay products of final state particles or of parton shower emissions. The fundamental idea is to utilize the fact that the original event provides a solution to the momentum conservation equations that can be built upon in order to find a new solution for the modified momentum conservation equations from the transformed event.

3.2.2.1 2-Particle Final States

Consider the collision of two partons with momenta k_1 and k_2 resulting in the production of two different particles with momenta $p_1 = (E_1, \vec{p}_1)$ and $p_2 = (E_2, \vec{p}_2)$. In their center-of-mass frame momentum conservation implies

$$\sqrt{\hat{s}} = E_1 + E_2, \tag{3.131}$$

$$\vec{k}_1 + \vec{k}_2 = \vec{p}_1 + \vec{p}_2 = \vec{0}. \tag{3.132}$$

In the present case k_1 and k_2 are given whereas p_1 and p_2 are to be determined.[2] Including the two on-shell conditions for the final state particles, one has to solve a system of six equations for eight variables. As this cannot be done uniquely, additional assumptions have to be made. If mass contributions to the squared matrix element are negligible, the direction of the final state particles in their center-of-mass frame is independent of the mass of the particles. One can then treat the directions of the final state particles as given, which reduces the number of variables to 4, namely the energies E_1 and E_2 and norms r_1 and r_2 of the three-momenta of $\vec{p}_1$ and $\vec{p}_2$. Using the on-shell conditions, Eq. (3.131) and Eq. (3.132) can be written as

$$\sqrt{\hat{s}} = \sqrt{r_1^2 + m_1^2} + \sqrt{r_2^2 + m_2^2}, \tag{3.133}$$

$$r_1\vec{e}_1 + r_2\vec{e}_2 = \vec{0}, \tag{3.134}$$

[2]Note that the problem here is formulated in a way that best describes the hard process, i.e. the scattering of two partons scattering and producing a 2-particle final state. The logic however is equivalent for example in the case of decays with $\sqrt{\hat{s}}$ corresponding to the mass of the decaying particle.

with $\vec{e}_i = \frac{\vec{p}_i}{r_i}$ being the unit vector in the direction of $\vec{p}_i$. Equation (3.134) implies

$$r_1 = r_2 =: r \tag{3.135}$$

such that the problem can be reduced to one equation for r:

$$\sqrt{\hat{s}} = \sqrt{r^2 + m_1^2} + \sqrt{r^2 + m_2^2}. \tag{3.136}$$

The solution can be expressed using the Källén function λ and reads

$$r = \frac{\lambda^{\frac{1}{2}}(\hat{s}, m_1^2, m_2^2)}{2\sqrt{\hat{s}}} = \frac{\sqrt{\hat{s}^2 + m_1^4 + m_2^4 - 2\hat{s}m_1^2 - 2\hat{s}m_2^2 - 2m_1^2m_2^2}}{2\sqrt{\hat{s}}}. \tag{3.137}$$

The new final state momenta in the center-of-mass frame can thus be expressed as

$$p_i' = \left(\sqrt{r'^2 + m_i'^2},\, r'\vec{e}_i\right), \tag{3.138}$$

where r' is given by Eq. (3.137) where the masses and center-of-mass energy are replaced with the new masses and center-of-mass energy. Finally the momenta can be boosted to the new lab frame defined by the new boost vector according to Eq. (3.40):

$$p_{i,\text{lab}}' = \Lambda(-\vec{b}')p_i'. \tag{3.139}$$

3.2.2.2 3-Particle Final States

Now consider the collision of two partons with momenta k_1 and k_2 resulting in the production of three different particles with momenta $p_i = (E_i, \vec{p}_i)$, $i = 1, \ldots, 3$. As in the previous chapter, momentum conservation in the center-of-mass frame implies

$$\sqrt{\hat{s}} = \sum_{i=1}^{3} E_i, \tag{3.140}$$

$$\vec{k}_1 + \vec{k}_2 = \sum_{i=1}^{3} \vec{p}_i = \vec{0}. \tag{3.141}$$

Here k_1 and k_2 can be viewed as given whereas the p_i are to be determined. Including the three on-shell conditions for the final state particles, one, in this instance, has to solve a system of seven equations for 12 unknowns. If one again

assumes that the directions of the final state particles are given and are constant under the transformation, the number of unknowns is reduced to 6, namely the energies E_i and norms r_i of the three-momenta $\vec{p}_i$. Using the on-shell conditions, Eq. (3.140) and Eq. (3.141) the problem can be rewritten as

$$\sqrt{\hat{s}} = \sum_{i=1}^{3} \sqrt{r_i^2 + m_i^2}, \tag{3.142}$$

$$\sum_{i=1}^{3} r_i \vec{e}_i = \vec{0}, \tag{3.143}$$

with $\vec{e}_i = \frac{\vec{p}_i}{r_i}$, again, being the unit vectors in the direction of the final state momenta.
Equation (3.143) can on the one hand be interpreted as a system of three equations for the three variables r_i and on the other hand as a statement of linear dependence between the unit vectors $\vec{e}_i$.
The concrete problem to be solved is, given a solution to Eq. (3.142) and Eq. (3.143), find a solution to

$$\sqrt{\hat{s}'} = \sum_{i=1}^{3} \sqrt{r_i'^2 + m_i'^2}, \tag{3.144}$$

$$\sum_{i=1}^{3} r_i' \vec{e}_i = \vec{0}. \tag{3.145}$$

Since Eq. (3.145) is a statement of linear dependence of the unit vectors, all allowed solutions lie in the null space of the matrix M whose columns are given by the unit vectors:

$$\text{null}(M) = \left\{ \vec{r} \in \mathbb{R}^3 \;\middle|\; M\vec{r} = \vec{0} \right\}, \quad M = (\vec{e}_1, \vec{e}_2, \vec{e}_3)\,. \tag{3.146}$$

To this end, it is useful to determine the dimensionality of the null space, often referred to as *nullity*. Given the rank-nullity theorem for matrices,

$$\dim \text{null}(M) + \dim \text{col}(M) = n = 3, \tag{3.147}$$

where $\text{col}(M)$ is the column space of M and $n = 3$ is the number of columns of M. There are three possibilities for the dimensionality of $\text{null}(M)$ as the dimension of the column space is either 3, 2 or 1. The case $\dim \text{col}(M) = 3$ is excluded for Eq. (3.143) explicitly states that the vectors are linearly dependent or in other words three-momentum is conserved in the original event. The case

$\dim \mathrm{col}(M) = 1$ is only possible if all three $\vec{e}_i$ are collinear or, since they are unit vectors, equal up to a sign. This is obviously not a physical solution, which leaves the case $\dim \mathrm{col}(M) = 2$ or $\dim \mathrm{null}(M) = 3 - 2 = 1$. One can therefore parameterize the solution set as

$$\left\{ \vec{r}' = \eta \vec{r} \in \mathbb{R}^3_+ \;\middle|\; \eta \in \mathbb{R}_+ \right\}. \tag{3.148}$$

Then the problem can be reduced to determining η using Eq. (3.144):

$$\sqrt{\hat{s}'} = \sum_{i=1}^{3} \sqrt{r_i'^2 + m_i'^2} \tag{3.149}$$

$$= \sqrt{(\eta r_1)^2 + m_1'^2} + \sqrt{(\eta r_2)^2 + m_2'^2} + \sqrt{(\eta r_3)^2 + m_3'^2} \tag{3.150}$$

$$= \sqrt{r_1^2 \eta^2 + m_1'^2} + \sqrt{r_2^2 \eta^2 + m_2'^2} + \sqrt{r_3^2 \eta^2 + m_3'^2}. \tag{3.151}$$

Due to the shape of the right-hand side, this equation can easily be solved numerically using for example Brent's method.[3]

Once a solution is found one can proceed as described in the previous chapter in order to determine the new lab frame final state momenta.

3.2.2.3 Multi-Particle Final States

The procedure from the previous chapter can easily be generalized to n final state particles. Let $k = (\sqrt{\hat{s}}, \vec{0})$ be the total initial state momentum in the center-of-mass frame and $p_i = (E_i, \vec{p_i})$ for $i = 1, \ldots, n$ the momenta of the final state particles in the same frame. Then the corresponding momentum conservation equations read

$$\sqrt{\hat{s}} = \sum_{i=1}^{n} \sqrt{r_i^2 + m_i^2}, \tag{3.152}$$

$$\vec{0} = \sum_{i=1}^{n} r_i \vec{e_i}, \tag{3.153}$$

with $r_i = |\vec{p_i}|$ and $\vec{e_i} = \frac{\vec{p_i}}{r_i}$. Assuming the $\vec{e_i}$ are given, i.e. the angles of all particles are known and constant under the transformation, the problem is to find new r_i'

[3] Brent's method takes as input an interval that contains the desired root of the function. One can easily choose $[0, \sqrt{s}]$ as the starting interval, as Brent's method typically converges within 10 to 20 steps in the typical cases here.

such that

$$\sqrt{\hat{s}'} = \sum_{i=1}^{n} \sqrt{r_i'^2 + m_i'^2}, \tag{3.154}$$

$$\vec{0} = \sum_{i=1}^{n} r_i' \vec{e_i}. \tag{3.155}$$

For $n > 3$, determining the dimension of the null space of the matrix M implied by Eq. (3.155),

$$M = (\vec{e}_1, \ldots, \vec{e}_n)\,, \tag{3.156}$$

is more complicated. The cases $\dim \mathrm{null}(M) = 0$ and $\dim \mathrm{null}(M) = n - 1$ can be excluded by equivalent arguments to those given in the previous chapter. In principal all other nullities are possible. A particularly compelling subspace[4] of the null space however is the one of the previous chapter:

$$\mathcal{S} = \left\{ \vec{r}' = \eta \vec{r} \in \mathbb{R}_+^n \;\middle|\; \eta \in \mathbb{R}_+ \right\}. \tag{3.157}$$

The attractiveness of this solution lies in the fact that even in cases where multiple (a priori arbitrary) solutions to Eq. (3.154) and Eq. (3.155) are possible, choosing an element from $\mathcal{S}$ fixes the ordering of the final state momenta such that if in the original event

$$|\vec{p}_1| > |\vec{p}_2| > \ldots > |\vec{p}_n| \tag{3.158}$$

in the center-of-mass frame, then also

$$|\vec{p}\,'_1| > |\vec{p}\,'_2| > \ldots > |\vec{p}\,'_n|\,. \tag{3.159}$$

In this case, similarly to the 3-particle final state case, the final equation to be solved becomes,

$$\sqrt{\hat{s}'} = \sum_{i=1}^{n} \sqrt{r_i'^2 + m_i'^2} \tag{3.160}$$

$$= \sum_{i=1}^{n} \sqrt{r_i^2 \eta^2 + m_i'^2}. \tag{3.161}$$

[4]Technically the given set of vectors don't form a vector space as no element has an additive inverse in the set. The term "subspace" is therefore only accurate up to this restriction.

Note that for n massless final state particles the right-hand side is linear in η. This is the case when a massive particle decays into massless particles and potentially QCD or QED radiation from the parton shower. Note however that the described approach is based on the fact that both the original and new initial state is massive and that their masses are known. For this reason it cannot simply be applied to parton shower branchings, i.e. the transformation of the parton shower emissions, or merged jet production, i.e. the transformation of the parton, that is included in the hard process, and its emissions. A workaround for the former and a solution for the latter are discussed in Ch. 3.2.4.

3.2.3 Structure of HepMC Eventfiles

In order to address the complications from the previous chapter, namely the eventuality that one or more masses of particles involved in the process are unknown, one first needs to understand the structure and the available information that is contained in event files once a parton shower algorithm was executed. Since the idea of the method described in Ch. 3.1 is to employ momentum conservation to propagate the transformation of the momenta of the hard process through the full event, a crucial bit of information is where in the event momentum is actually conserved. Fig. 3.4 depicts a (particularly small) event for the production of a top pair at the LHC as produced by MadGraph5_aMC@NLO [86] and subsequently passed on to Pythia8 [91] for the simulation of the parton shower and decays. In Fig. 3.4 the labels of the edges denote the ID of the corresponding particle as defined in the "Monte Carlo particle numbering scheme" (PDG ID) [95], a unique ID number within the event (barcode) and status code. Starting at the top, one can see two initial state protons (PDG ID 2212) each splitting into an up quark (PDG ID 2) and a corresponding diquark (PDG ID 2101). The up quarks both emit gluons as part of the initial state parton shower, that then ultimately scatter at the hard vertex "V3" to produce the top quark pair (PDG IDs 6 and -6). The top and anti-top eventually decay into a W boson (PDG IDs 24 and -24) and a (anti-)bottom quark (PDG IDs 5 and -5). Finally the W bosons both decay leptonically.

There are however multiple copies with differing momenta of nearly all involved particles. The top quark for example undergoes three momentum changes at the vertices "V6", "V10" and "V15" before it decays. These momenta are connected by boosts that are the result of the top quark recoiling against parton shower emissions. Consequently, although globally momentum is conserved between the initial protons and the stable final state particles, there are many (unphysical)

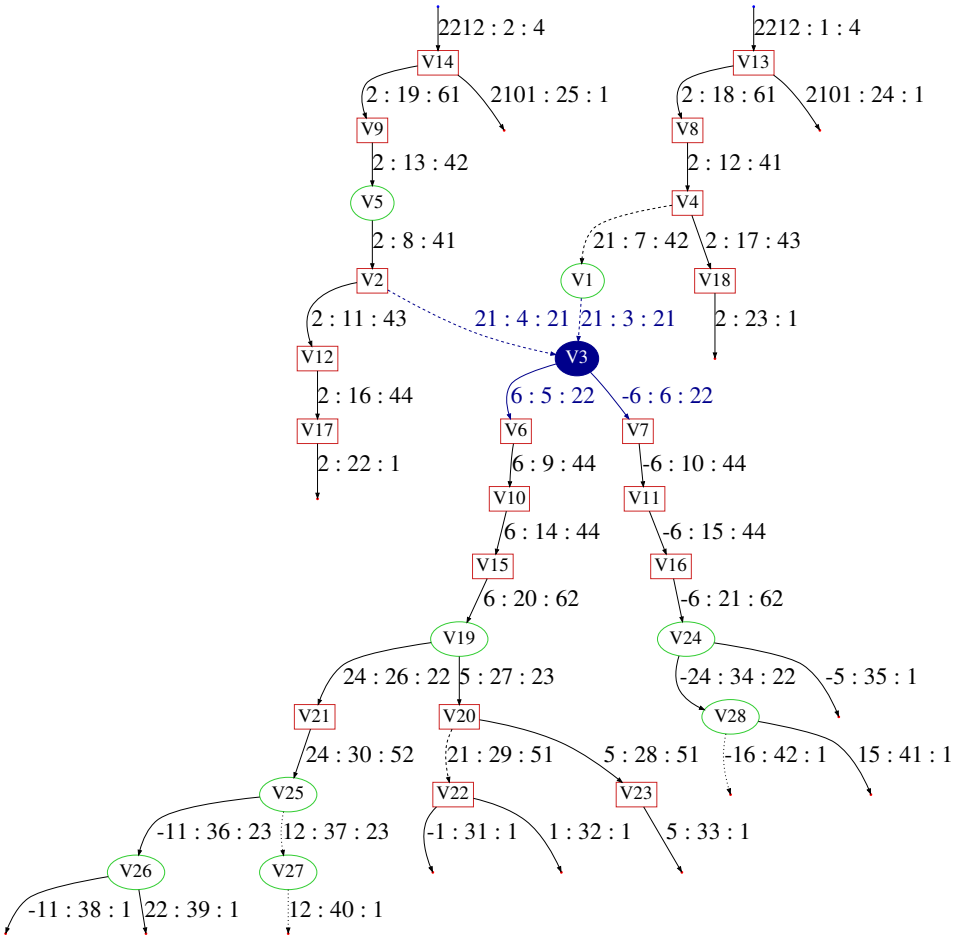

Figure 3.4: A depiction of a Monte Carlo event for the production of a top pair at the LHC. The hard process was generated using MadGraph5_aMC@NLO [86] and is highlighted in blue. All other vertices and particles were produced by Pythia8 [91]. The labels of the vertices correspond to their unique event identifier or barcode. The labels of the edges denote the ID of the corresponding particle as defined in the "Monte Carlo particle numbering scheme" (PDG ID) [95], a unique ID number within the event (barcode) and status code. Particles with a status code of 1 are stable final state particles. Green and round vertices indicate momentum conservation at the vertex and correspondingly red and rectangular vertices indicate a lack thereof. Momentum is conserved at the hard vertex ("V3"). Due to the nature of the final state parton shower, momentum is not conserved at every vertex. This makes the propagation of the transformation through the event non-trivial. Note that this event only has 42 particles and is therefore unusually small. Typical event sizes range from about 200 to about 400 particles for this process.

vertices in an event where momentum is not conserved locally. Nonetheless it is crucial to identify classes of vertices or subgraphs where momentum is conserved. To begin with one can consider the hard vertex. Since the hard process itself is

independent of the higher order effects of the parton shower, momentum is always conserved between the initial and final state of the hard process and all momenta live in the LHC lab frame. Additionally the total momentum of the last copies of the top pair is equal to the hard final state momentum and so momentum is conserved between the initial state of the hard process and the boosted top pair (barcodes 20 and 21). Note that the event shown in Fig. 3.4 is based on parton showers without emissions from the hard final state, which is also a premise of the algorithm described in this work. This is due to the fact that final state emissions impair the momentum conservation described above. For example if a hard final state particle emits a gluon that then showers, there is no momentum conservation between the emitting hard final state particle on the one hand and the gluon leafs as well as the boosted hard final state particle on the other hand. It is therefore no longer possible to assume that the boosted hard final state particle is in the LHC lab frame.
One can also see that momentum is always conserved at decay vertices (e.g. "V19") but not at emission vertices (e.g. "V20"). Moreover all decaying particles live in the LHC lab frame which means that momentum is conserved between a decaying particle and all of its stable descendants. Since momentum is not conserved at emission vertices and emitting particles can live in an arbitrary reference frame, the question arises of how parton shower emissions are to be treated in this framework. Given for example the original and transformed bottom quark in the event in Fig. 3.4, how are the momenta of the final down (PDG ID 1, barcode 31), anti-down (PDG ID -1, barcode 32) and bottom quark (barcode 33) to be determined? A possible approach is described in Ch. 3.2.4.

3.2.4 Decays and Jet Formation

If there were no parton shower emissions, the propagation of the transformation could be done straightforwardly by simply using the methods described in Ch. 3.2.2. The parton shower adds complexity in two ways. First by adding QCD or QED radiation to the event that additionally needs to be transformed and second through boosting hard particles that recoil against this radiation. The latter can be dealt with by directly considering the decay into the boosted copies of the hard particles following the ideas of Ch. 3.2.2. Handling the former however is more intricate. As discussed, emissions from hard final state particles spoil momentum conservation in decay chains and must therefore be excluded at the generation level. Thus all emissions are either part of the initial state radiation or the product of radiation from the end of the decay chain, most importantly

from (anti-)quarks and gluons that ultimately produce jets. Consider for example the decay of a top quark into a W boson and a bottom quark as depicted at vertex "V19" of Fig. 3.4. One possible approach for the transformation is to use the methods of Ch. 3.2.2.1 to determine new momenta for the initial decay products (barcodes 26 and 27) and to continue from there. Unfortunately the QCD emissions of the bottom quark cause a violation of momentum conservation in this subgraph, since it recoils against other subgraphs. Thus the momentum of the initial bottom quark (barcode 27) is different from the sum of the momenta of the stable emitted particles (barcodes 31 and 32) and the recoiled bottom quark (barcode 33). Since a reverse engineering of the parton shower emissions would counteract the purpose of this algorithm, there is no straightforward way to propagate the change in momentum of the initial bottom quark.
The workaround proposed here is to, in a first step, treat the entire subgraph as one particle, that can roughly be thought of as the b-jet induced by the bottom quark. Then, in a second step, to perform the transformation of a multi-particle final state decay with the b-jet as the decaying particle and the constituents of the b-jet as the decay products. The internal representation of the decay of the top quark from Fig. 3.4 is depicted in Fig. 3.5. Only the last copy of the W boson enters the decay and the transformation of the bottom quark is done in the described two step process. The main complication with this approach is the

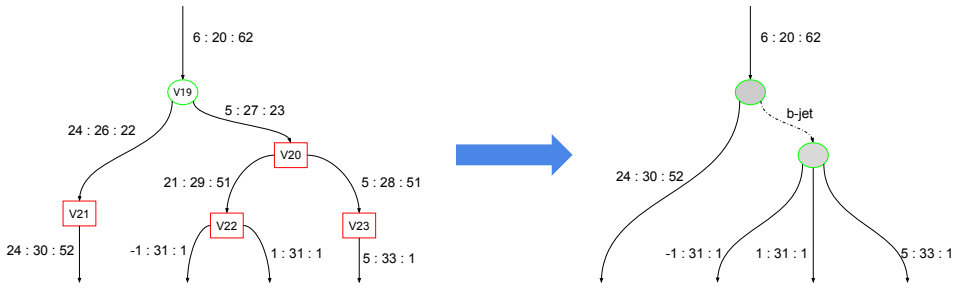

Figure 3.5: Left: The subgraph corresponding to the top decay from Fig. 3.4. Right: Internal representation of the subgraph that is used for the transformation of the decay products. Only the last copy of the W boson is left and an artificial b-jet was introduced in an intermediate step. The momentum of the b-jet is given by the sum of the (anti-)down quarks and the momentum of the last copy of the bottom quark.

reliance of the methods from Ch. 3.2.2 on the knowledge of all masses involved in the process. The mass of the artificial b-jet however can a priori be arbitrary as long as momentum is conserved at the internal top decay vertex. Since the masses, and consequently also momenta, of particles that are the sources of par-

ton showers are changed during the kinematical transformations, the jet masses must generally be changed accordingly. This is due to the fact that after a transformation of the source particle of a jet, there might not be enough energy left to produce jets with the original mass. By re-setting jet masses however, one effectively introduces additional transformations, that need to be accompanied by corresponding reweighting factors in order to exactly reproduce for example jet mass distributions. Since this effect is expected to be small though and the derivation of the reweighting factor is non-trivial, it is not considered in the present work. The proposed procedure of setting new jet masses is depicted in Fig. 3.6 for pure QCD jets and Fig. 3.7 for jets including QED radiation. The basic idea is to keep the ratio of the kinematical proportion of the jet mass and the total available energy constant. This guarantees that the new jet mass is kinematically allowed and takes up just as much of the available energy as before the transformation. Consider, for example, the (rest-frame) decay of the top

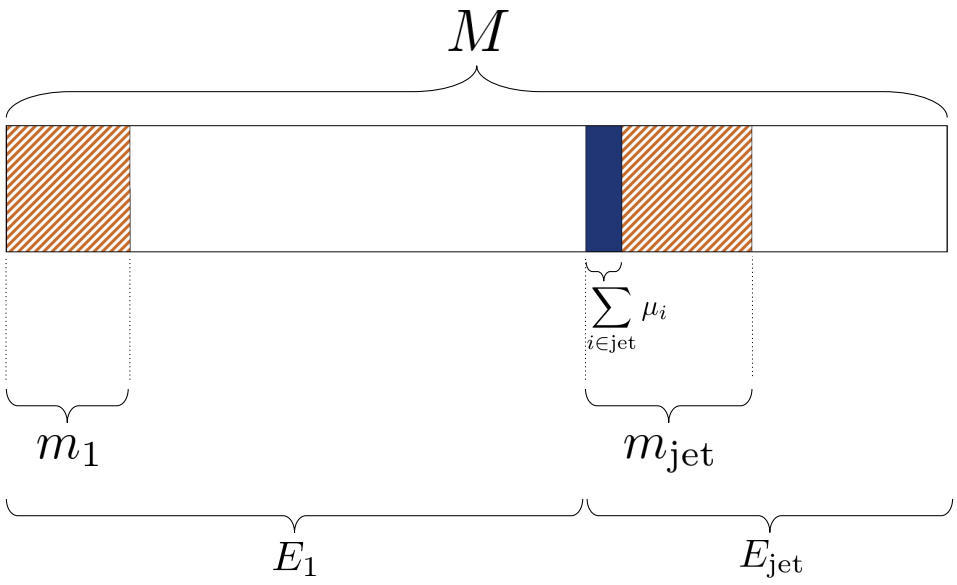

Figure 3.6: Depiction of the allocation of energy between a jet and a sibling particle. Consider a particle with (on- or off-shell) mass M, that, in its center-of-mass frame, decays into a jet j and an additional particle p_1. The total energy of the decay is given by M and is shared by the jet (E_jet) and p_1 (E_1). The energy of the jet is separated into the total jet mass m_jet and jet momentum, while the jet mass itself is again separated into the on-shell masses μ_i of its constituents and a kinematical mass given by $m_\text{jet,kin} = m_\text{jet} - \sum_{i\in\text{jet}} \mu_i$. In order to guarantee that the new jet mass is kinematically allowed for arbitrary M and m_1, one can keep the proportion, that $m_\text{jet,kin}$ takes up, constant.

quark from Fig. 3.5 into a bottom quark and a W boson. If one were to decrease

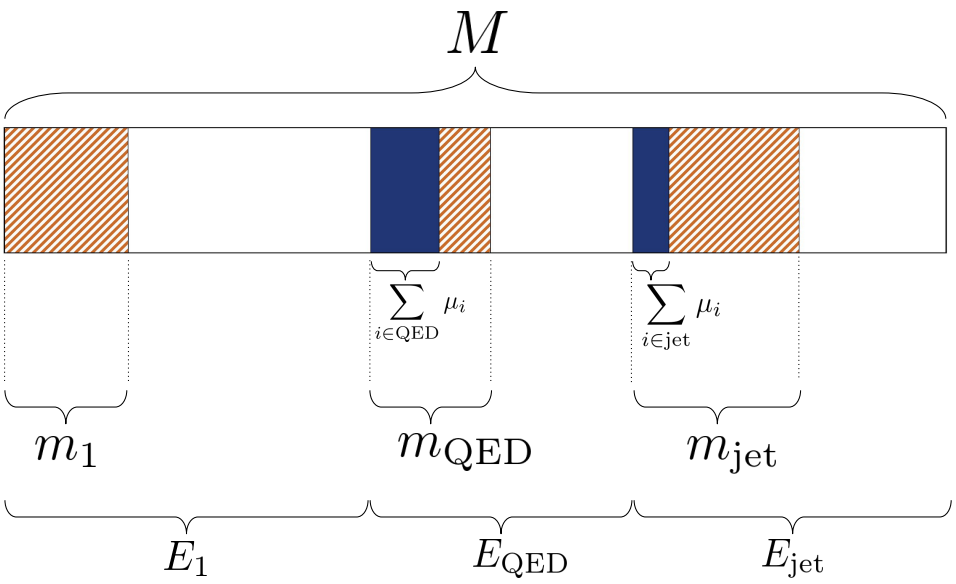

Figure 3.7: Depiction of the allocation of energy between a QCD jet, a QED jet and a sibling particle. Consider a particle with (on- or off-shell) mass M, that, in its center-of-mass frame, decays into a jet j and an additional particle p_1, that subsequently emits QED radiation. The total energy of the decay is given by M and is shared by the QCD jet (E_{jet}), the QED radiation (E_{QED}) and p_1 (E_1). The energies of the QCD jet and the QED radiation are separated into their total masses m_{jet} and m_{QED} and their momenta, while the QCD and QED jet masses themselves are again separated into the on-shell masses μ_i of their constituents and kinematical masses given by $m_{\mathrm{jet,kin}} = m_{\mathrm{jet}} - \sum_{i\in\mathrm{jet}} \mu_i$ and $m_{\mathrm{QED,kin}} = m_{\mathrm{QED}} - \sum_{i\in\mathrm{QED}} \mu_i$. In order to guarantee that the new QED and QCD jet masses are kinematically allowed for arbitrary M and m_1, one can keep the proportion, that $m_{\mathrm{jet,kin}}$ and $m_{\mathrm{QED,kin}}$ take up, constant.

the mass of the top quark from m_t to $m_t' < m_t$ as part of a parameter scan, the new top quark mass could be smaller than the original (b-)jet mass m_{jet}. Such a mass change therefore requires the adjustment of the jet mass. As described above, one possible approach is to keep the relative share of kinematical jet mass to top mass constant. The total phase space available for the jet mass in the decay is given by

$$m_t - m_W - \sum_{i \in \text{jet}} \mu_i, \tag{3.162}$$

where μ_i are the (often negligible) on-shell masses of the partonic constituents of the jet. On the other hand the mass of the jet is bounded below by exactly this sum of constituent on-shell masses $\sum_{i\in\text{jet}} \mu_i$, i.e.

$$\sum_{i \in \text{jet}} \mu_i < m_{\text{jet}} < m_t - m_W. \tag{3.163}$$

The idea is therefore to keep the relative share of the kinematical part of the jet mass

$$m_{\text{jet,kin}} = m_{\text{jet}} - \sum_{i \in \text{jet}} \mu_i \tag{3.164}$$

in the rest-frame of the decaying particle constant. With M being the on-shell mass of the decaying particle, and m_1 being the mass of the remaining decay product (the W in the case of the top-decay), the requirement reads:

$$\frac{m'_{\text{jet,kin}}}{M' - m_1' - \sum_{i\in\text{jet}} \mu_i} = \frac{m'_{\text{jet}} - \sum_{i\in\text{jet}} \mu_i}{M' - m_1' - \sum_{i\in\text{jet}} \mu_i} \overset{!}{=} \frac{m_{\text{jet}} - \sum_{i\in\text{jet}} \mu_i}{M - m_1 - \sum_{i\in\text{jet}} \mu_i}. \tag{3.165}$$

And thus the transformed jet mass is given by

$$m'_{\text{jet}} = \sum_{i \in \text{jet}} \mu_i + m_{\text{jet}} \frac{M' - m_1' - \sum_{i\in\text{jet}} \mu_i}{M - m_1 - \sum_{i\in\text{jet}} \mu_i}. \tag{3.166}$$

Similarly if, for example, after the original decay QED radiation is emitted from the remaining decay product, this radiation can be treated as a QED jet, whose mass must also be determined. Only in this case the energy is shared by three (pseudo-)particles, namely the two jets and the remaining decay product. The determination of the masses can be done analogously to Eq. (3.166), i.e.

$$\frac{m'_J - \sum_{i\in J} \mu_i}{M' - m_1' - \sum_{i\in\text{jet}} \mu_i - \sum_{i\in\text{QED}} \mu_i} \overset{!}{=} \frac{m_{\text{jet}} - \sum_{i\in\text{jet}} \mu_i}{M - m_1 - \sum_{i\in\text{jet}} \mu_i - \sum_{i\in\text{QED}} \mu_i} \tag{3.167}$$

and therefore

$$m'_J = \sum_{i \in J} \mu_i + m_J \frac{M' - m'_1 - \sum_{i \in \text{jet}} \mu_i - \sum_{i \in \text{QED}} \mu_i}{M - m_1 - \sum_{i \in \text{jet}} \mu_i - \sum_{i \in \text{QED}} \mu_i}, \tag{3.168}$$

where $J \in \{\text{jet}, \text{QED}\}$. Once the jet masses are set, the resulting four-momentum can first be used for the transformation of the jets and then be used as the input for a $1 \to n$ decay with its constituents as the final state. Note that an implicit assumption that is made here, is that the number of emitted partons does not depend on the energy scale of the jet production process. This is in reality clearly not correct. Generally the more energy the parton shower has the more branchings it will produce. The error introduced by making this assumption can however be assumed to be small enough in order to not render the algorithm futile. Thus the assumption is maintained.

Another caveat emerges if one is interested in parton shower merging, i.e. the addition of n extra partons in the hard final state for the purpose of combining them with the parton shower emissions. In merged events, these extra partons are treated differently from the usual hard final state particles by programs like Pythia8 [91] that abstain from saving a copy of these particles in the LHC lab frame. Rather the parton shower uses the initial state radiation to recoil against and thus momentum is exchanged between the two. Consider a MC Event with one additional parton as depicted in Fig. 3.8. A transformed version of the extra parton could therefore certainly be found by using the methods of Ch. 3.2.2.2. Unfortunately the momentum of the extra parton does not suffice for the calculation of the momenta of its descendants, i.e. the leafs of the corresponding subgraph. The methods described above for the transformation of jet masses no longer work in this case, since the available phase space after the transformation is unknown, due to a lack of momentum conservation in the relevant subgraph. One could therefore think about applying a boost to the extra parton and take the result as the new jet. The required boost vector would in this case be deduced from the boost between the total momentum of the old descendants and the old extra parton. Unfortunately the total momentum of the old descendants and the momentum of the old extra parton are not connected by a boost. This can easily be understood by noticing that the extra parton is on-shell and therefore (nearly) massless whereas the invariant mass of its descendants, which essentially correspond to the jet, is generally finite. This complication is in indeed not trivially solvable. In this work an approach is presented that is compatible with the transformation from Ch. 3.2.1.1 and produces sound results in the context of the

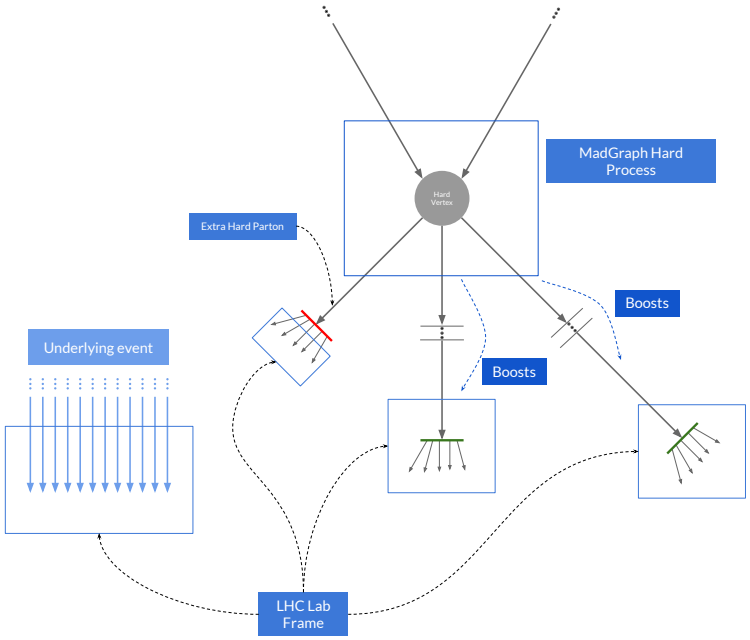

Figure 3.8: Sketch of a MC Event with parton shower as produced by Pythia8. Green lines mean momentum conservation, red lines mean no momentum conservation. Together the momentum from the underlying event / initial state radiation, the jet leafs and the descendants of the two hard final state particles make up the momenta of the two colliding protons.

processes described in Ch. 4. No assertion about the validity of this approach is made beyond this use case.

Consider now the process depicted in Fig. 3.8, i.e.

$$p\ p\ \rightarrow\ a_1\ a_2\ b \tag{3.169}$$

where a_1 and a_2 are the regular hard final state particles and b is the extra parton either from matrix element generation or a parton shower. Subsequently at least b is the source of a parton shower, namely

$$b \rightarrow q_1, \ldots, q_m, \tag{3.170}$$

where m is the number of partons produced in the parton shower and q_k are the corresponding partons. Note that the notation here is merely figurative. In fact, as already discussed, the momentum of the left and right hand side are different:

$$p(b) \neq \sum_k p(q_k) =: p_J. \tag{3.171}$$

The goal of the approach is to find a good approximation for p_J as it were produced by a parton shower origination from a process with the new final state masses. The first step is to generate the transformed extra parton at the hard vertex in a $2 \to 2+1$ decay following the instructions in Ch. 3.2.2. The first assumption made here is that the p_T of transformed extra partons are a good proxy for the jet p_T, thus

$$p_T\left(b'\right) \coloneqq p_T\left(p'_J\right). \tag{3.172}$$

Here b' is the extra parton after the transformation. Secondly the assumption is made that the longitudinal momentum of the jet does not change significantly under the transformation, i.e.

$$p_z(p'_J) = p_z(p_J). \tag{3.173}$$

The only component missing now is the jet mass. The idea for setting the jet mass here follows the already described process of setting jet masses. The crucial difference is the unknown available phase space that is required. Therefore assuming that the invariant mass to energy ratio of the jet does not change drastically, one can make the ansatz

$$\frac{m'_J - \sum_i \mu_i}{\sqrt{m'^2_j + r'^2_j} - \sum_i \mu_i} = \text{const.} \tag{3.174}$$

Solving for the new jet mass yields

$$m'_j = \begin{cases} \frac{bc}{\sqrt{1-c^2}}, & \text{if } \sum_i \mu_i = 0 \\ \frac{a}{1+c}\left(1 + \sqrt{1-(1+c)[(1-c) - \frac{b^2c^2}{(1-c)a^2}]}\right), & \text{if } \sum_i \mu_i > 0 \end{cases} \tag{3.175}$$

where

$$a = \sum_i \mu_i,\ b = r'_j,\ c = \frac{m_j - \sum_i \mu_i}{E_j - \sum_i \mu_i}. \tag{3.176}$$

A possible evolution of this approach could make use of the difference between extra partons that are below or above the merging scale. Partons generated by the event generator for the hard event could then be treated differently from partons generated by the parton shower.

3.3 Reweighting

The idea of reweighting Monte Carlo events in order to scan the parameter space of new physics models was put forward in [73]. Reweighting constitutes the second important element of the reusing algorithm. While kinematical transformations are necessary to ensure that transformed events are kinematically allowed and their kinematical distributions approach the true one, reweighting is necessary to fix imperfections of the transformations. The following chapter will describe the reweighting factors for the transformation of the hard process (Ch. 3.3.1) and briefly sketch out other reweighting factors that, in most cases, make up only sub-dominant contributions (Ch. 3.3.2).

3.3.1 Hard Process Reweighting Factors

The total weight factor for the hard process was already derived in Eq. (3.21) and is given by

$$w_{ab} = f_a(x_1) f_b(x_2) \frac{1}{2\hat{s}} \Phi \, \overline{|M_{ab}|^2}. \tag{3.177}$$

This chapter will give a brief overview of each individual factor in this equation and also mention which factors give the dominant contributions under the transformations introduced in Ch. 3.2.1.

Flux Factor

Since the partonic flux factor is given by

$$\frac{1}{2\hat{s}} = \frac{1}{2x_1 x_2 s}, \tag{3.178}$$

the corresponding new event weight is given by the ratio of the new and the old flux:

$$w_{\text{Flux}} = \frac{1/\hat{s}'}{1/\hat{s}} = \frac{\hat{s}}{\hat{s}'}. \tag{3.179}$$

Consider, for example, the boost invariant transformation from Ch. 3.2.1.1. Then

$$x_1' = a x_1, \;\; x_2' = a x_2 \Rightarrow \hat{s}' = a^2 \hat{s}, \tag{3.180}$$

where

$$a = \frac{m'_{\text{final state}}}{m_{\text{final state}}} \tag{3.181}$$

is a constant. The reweighting factor is in this case therefore simply given by the constant

$$w_{\text{Flux}} = \left(\frac{m_{\text{final state}}}{m'_{\text{final state}}}\right)^2 \tag{3.182}$$

and can be ignored. This is however no longer true once the bijective transformation from Ch. 3.2.1.2 is used.

Phase space

Since the scope of this work is largely limited to tree level processes, the most relevant final state configuration consists of two particles. The corresponding phase space integral, as discussed in Ch. 2.2, is given by

$$\mathrm{d}\Phi_2 = \frac{\mathrm{d}\cos\theta\mathrm{d}\phi}{16\pi^2}\frac{\lambda^{\frac{1}{2}}(\hat{s}, m_3^2, m_4^2)}{2\hat{s}}, \tag{3.183}$$

where m_3 and m_4 are the masses of the final state particles and $\lambda(\cdot)$ is the Källén function. The phase space reweighting factor is in this case thus given by

$$w_{\text{PS}} = \frac{\Phi'}{\Phi} = \frac{\lambda^{\frac{1}{2}}(\hat{s}', m_3'^2, m_4'^2)}{2\hat{s}'} \Bigg/ \frac{\lambda^{\frac{1}{2}}(\hat{s}, m_3^2, m_4^2)}{2\hat{s}} \tag{3.184}$$

$$= \frac{\lambda^{\frac{1}{2}}(\hat{s}', m_3'^2, m_4'^2)}{\lambda^{\frac{1}{2}}(\hat{s}, m_3^2, m_4^2)}\frac{2\hat{s}}{2\hat{s}'} \tag{3.185}$$

$$= \frac{\hat{s}}{\hat{s}'}\sqrt{\frac{\lambda(\hat{s}', m_3'^2, m_4'^2)}{\lambda(\hat{s}, m_3^2, m_4^2)}}. \tag{3.186}$$

One can easily see that the right hand side is invariant under the boost invariant transformation. Therefore, similarly to the flux factor reweighting, phase space reweighting is only relevant if the bijective transformation is applied.

Parton Density Functions

The parton density functions are the most important factors in Eq. (3.177). As discussed briefly in Ch. 2.2, the parton density functions $f_i(x_j)$ represent the probability of finding a parton of type i inside the proton at momentum fraction x_j at a given factorization scale. As such they have a strong influence on the kinematical distributions of the momenta of final state particles. For processes in which the final state angular distributions are independent of the particle masses

the PDFs even account for the dominant contribution (see for example Ch. 4). The effect of a change in x_j and subsequently in the PDFs can easily be accounted for by reweighting each event by

$$w_{\mathrm{PDF},ab} = \frac{f_a(x_1')f_b(x_2')}{f_a(x_1)f_b(x_2)}, \tag{3.187}$$

where the x_j' are determined by the transformation in Ch. 3.2.1. Note that in practice it is crucial to use the exact same PDF set and factorization scale for the calculation of the reweighting factor that were used for the generation of the events. Depending on the desired accuracy, choosing a different PDF set can lead to discrepancies in the kinematical distributions that might lead to unreliable results if one wants to study whether the given parameter point of the model is excluded by LHC data or not.
Given the functional form of the PDFs, this factor is relevant both in cases where the boost invariant transformation or the bijective transformation is applied. In many cases the PDF reweighting factor turns out to be the principal component of Eq. (3.177) and in some cases, depending on the desired accuracy of the algorithm, solely considering this factor can even be sufficient.

Matrix Element
Including the matrix element in the reweighting process is particularly interesting under certain conditions. The most important situations arise when either the angular distributions of the final state momenta in the center-of-mass frame of the process significantly depend on the particle masses or the phase space point after the transformation is vastly different from the original phase space point. The transformation proposed in Ch. 3.2 keeps the directions of the momenta in the center-of-mass frames constant which is only a suitable approach if the angular distributions for the considered parameter points in the center-of-mass frame are equal or at least similar. The second case strongly depends on the specific transformation that is chosen. An ideal transformation would actually leave the value of the matrix element invariant as in this case the reweighting factor would be one. Since the ideal transformation is unknown though, the question whether matrix element reweighting is necessary must be answered based on the observation of the performance of the chosen transformation for the considered processes. Analytically the matrix element reweighting factor is given by

$$w_{\mathrm{ME},ab} = \frac{\overline{|M_{ab}'|^2}}{\overline{|M_{ab}|^2}}. \tag{3.188}$$

3.3.2 Reweighting Factors beyond the Hard Process

Beyond the reweighting factors of the hard event, a few other factors can (and sometimes should) be considered, the most important ones being

- the Jacobian,
- jet mass transformation weights,
- weights for detector simulation,
- and decay matrix element weights / branching ratios.

Note that, given the results of Ch. 3.2, the Jacobian is a constant under the boost invariant transformation and thus is only relevant if the bijective transformation is used. However, since its computation takes virtually no time, there is no reason not to include the Jacobian even for cases where is can be expected to only make up a subdominant contribution.
The second factor arises if heavy final state particles decay as part of the parton shower. The given algorithm relies on the narrow width approximation being valid and consequently each individual on-shell decay can be factorised. In this case, the widths for individual decays are given as analytical functions and therefore can be computed very quickly. For the example of SUSY, most spectrum generators already add this functionality by default and for new physics models in the FeynRules format MadGraph5_aMC@NLO [86] will automatically calculate these. With the branching ratios of the new (BR') and original (BR) parameter point calculated one can simply reweight each event by the change in the branching ratio. Explicitly for the example of particle X decaying to particle Y and Z the reweighting factor is given by

$$w_{\mathrm{BR}} = \frac{BR'(X \to YZ)}{BR(X \to YZ)} \,. \tag{3.189}$$

Another factor comes from the transformation of the jet masses as described in Ch. 3.2.4. Since every transformation that is performed implies a reweighting factor only leaving the jet masses unchanged could bypass this effect. In many cases however this is, as discussed, kinematically impossible. The additional reweighting factor that would have to be included is the ratio of the probabilities for the new and the old jet mass given the momenta of the particles that precede the production of the jet. Determining these probabilities is however similarly computationally expensive as re-running the parton shower on the respective part

of the process and is thus omitted in this work. The error introduced by neglecting this factor turns out to be appropriately small as can be seen for example in Ch. 4. One of the most expensive parts of the event generation and processing tool chain is the detector simulation. While the results presented in Ch. 4 were produced by using the full detector simulation as offered by Delphes [77], it should be mentioned that depending on the desired accuracy other solutions have been proposed in the literature. For instance instead of performing the full detector simulation, the momenta of detector level particles can be smeared by a simple prescription and then used as detector measurements [96].

Chapter 4

Applications

While up until this point the theoretical foundation of the new algorithm was discussed, the following chapter will present a set of use cases. In a real world application the presented algorithm can develop its full potential in so-called parameter scans. Many BSM models predict additional new particles. One of the interesting phenomenological versions of the MSSM, the pMSSM-19, for example has 19 free parameter, 15 of which are masses [97]. The parameter space, that needs to be studied, therefore has $d = 15$ dimensions, if all free couplings are fixed. In principal every possible combination of masses (and couplings) could be realized in nature. In cases where the dimension of the parameter space is large, the goal of parameter scans is to select a $\tilde{d} < d$-dimensional subspace of the parameter space and to fix all remaining parameters to a fixed value. Then theoretical predictions can be made for a large number of points in the $\tilde{d}$ dimensional parameter space and compared to experimental data.
Theoretical predictions typically involve heavy use of Monte Carlo event generators like MadGraph5_aMC@NLO [86] or Pythia 8 [91]. The larger the parameter space the more computationally intense the process becomes. The algorithm described in the present work promises to reduce the computational complexity by reusing Monte Carlo events from one point in the parameter space to generate events for a parameter point with different masses. In Ch. 4.1 the result of the algorithm will be displayed for one of the simplest possible cases. A single additional boson acts as an s-channel mediator while all couplings are fixed. The results shown are the kinematical distributions of the additional mediator as well as of the final state particles before and after transformation and reweighting from a given origin to a target mass configuration. Monte Carlo events for the origin as well es the target parameter point are generated using standard event generators and then compared to the resulting distributions of the new approach.

The slightly more complicated case of lepton pair production is shown for a model with a fourth generation of quarks in Ch. 4.2 and in the context of a simple supersymmetric model in Ch. 4.3. Finally a parameter scan for an experimental search conducted by the ATLAS corporation for squarks in final states is reproduced with the new algorithm and CheckMATE2 [72] in Ch. 4.4.

4.1 Production of Heavy s-channel Mediators

A first, relatively simple, process to look at, with respect to the transformation and reweighting algorithm described in Ch. 3, is the production of a heavy, color-neutral spin 1 boson, that is typically referred to as Z'. From an experimental point of view a Z' boson adds to the Drell-Yann process and produces an additional Breit-Wigner peak at its mass $M_{Z'}$ [37].
From a theoretical perspective a wide range of models, from those postulating extra dimensions to E_6 Grand Unified Theories, can predict such a particle [37]. Generally, if the Z' is the spin 1 mediator of an additional $U(1)$ gauge symmetry, its couplings to the fermions of the SM in the weak basis can be parameterized as follows [98]:

$$\sum_k \left(ig^k_{L,\nu}\ \bar{\nu}_{L,k}\gamma^\mu \nu_{L,k} + \sum_{D\in\{L,R\}} \left(ig^k_{D,l}\ \bar{l}_{D,k}\gamma^\mu l_{D,k} + ig^k_{D,u}\ \bar{u}_{D,k}\gamma^\mu u_{D,k} + ig^k_{D,d}\ \bar{d}_{D,k}\gamma^\mu d_{D,k} \right) \right) Z'_\mu. \tag{4.1}$$

Here k is a generation index and $g^k_{L,\nu}$, $g^k_{D,l}$, $g^k_{D,u}$ and $g^k_{D,d}$ are coupling constants describing how strongly neutrinos, leptons, and up- and down-type quarks couple to the new Z'. Similarly to the generation of the CKM matrix in the SM, applying unitary transformations to the fermion fields yields the physical mass basis of Eq. (4.1) and produces mixing matrices $\epsilon^{ij}_{D,f}$ for $D \in \{L, R\}$ and $f \in \{\nu, l, u, d\}$. Therefore, theoretically, the generation dependence of the couplings given in Eq. (4.1) can lead to tree-level flavor changing neutral currents (FCNCs), which are strongly experimentally constrained [37]. Below only universal, i.e. generation independent, couplings are assumed in which case no FCNCs can occur. This means the mixing matrices are diagonal and proportional to the unit matrix:

$$\epsilon^{jk}_{D,f} = ig_x\ c_{D,f}\ \delta^{jk}, \tag{4.2}$$

Table 4.1: Parameters used for the generation of the MC events with MadGraph5_aMC@NLO [86].

	No. of events	PDF	μ_f	μ_r	$M_{Z'}$	$\Gamma_{Z'}$
old	$5 \cdot 10^5$	CT14lo	91.188 GeV	91.188 GeV	500 GeV	21.59 GeV
new	$5 \cdot 10^5$	CT14lo	91.188 GeV	91.188 GeV	1000 GeV	21.59 GeV

where g_x is the coupling constant of the new $U(1)$ symmetry and $c_{R,\nu} = 0$ for models without right-handed neutrinos. The values used for the below simulation are:

$$c_{D,f} = \begin{pmatrix} -0.267 & 0.5 & 0.344 & -0.422 \\ 0.233 & 0 & 0.077811 & -0.156 \end{pmatrix}. \tag{4.3}$$

Concerning the algorithm from Ch. 3, there is now merely one parameter that can be changed, namely the mass $M_{Z'}$ of the new Z' boson. This means that the transformation can be specifically chosen such that the Breit-Wigner of the new Z' is reproduced as closely as possible, therefore minimizing the influence of the reweighting procedure and, as a consequence, the additional statistical error that is introduced.
Consider the process

$$pp \to Z' + X \to \mu^+\mu^- + X \tag{4.4}$$

for two different Z' masses $M_{Z'}$ and $M'_{Z'}$. The parameters that were chosen here are given in Table 4.1. The first question to ask is whether the invariant mass distribution of the Z' is reproduced correctly. Fig. 4.1 shows the distributions for the new parameter point taken directly from MadGraph5_aMCNLO and the distributions of the Z' mass of the transformed events with and without reweighting. One can see that without reweighting the distribution is reproduced already quite well. While the peak is at the correct position, the shape is still slightly different close to the peak. This is due to the fact that for this process the transformation is essentially given by the boost invariant transformation since the problematic region according to Eq. (3.87) only makes up $\approx 0.24\%$ of the phase space. Clearly physical events are not distributed uniformly in phase space. However since the boost invariant transformation fails if at least one of the x_i of Ch. 3.3.1 becomes large, this region is further suppressed by PDF effects. This domination of the boost invariant transformation explains the difference in the

shapes between the true and the transformed distribution for $M_{Z'}$, since

$$\begin{aligned} M'^2_{Z'} &= p'^2_{Z'} && (4.5)\\ &= (p'_1 + p'_2)^2 && (4.6)\\ &= (x'_1 + x'_2, 0, 0, x'_1 - x'_2)^2 \frac{s}{4} && (4.7)\\ &= a^2(x_1 + x_2, 0, 0, x_1 - x_2)^2 \frac{s}{4} && (4.8)\\ &= a^2 p^2_{Z'} && (4.9)\\ &= a^2 M^2_{Z'}. && (4.10) \end{aligned}$$

Therefore the transformation leaves the shape of the Breit-Wigner invariant and merely shifts the peak to the correct position. The true shape of the Breit-Wigner however depends on the mass of the Z', hence the differences in the true curve and the curve without reweighting. Reweighting the events with the ratio of the matrix elements at the new and the old parameter point then fixes the shape and the distributions align perfectly. Note that no other reweighting factors are needed at this point. The Jacobian for the chosen transformation is essentially a constant and all other factors are kinematical factors that are irrelevant to the invariant mass distribution.

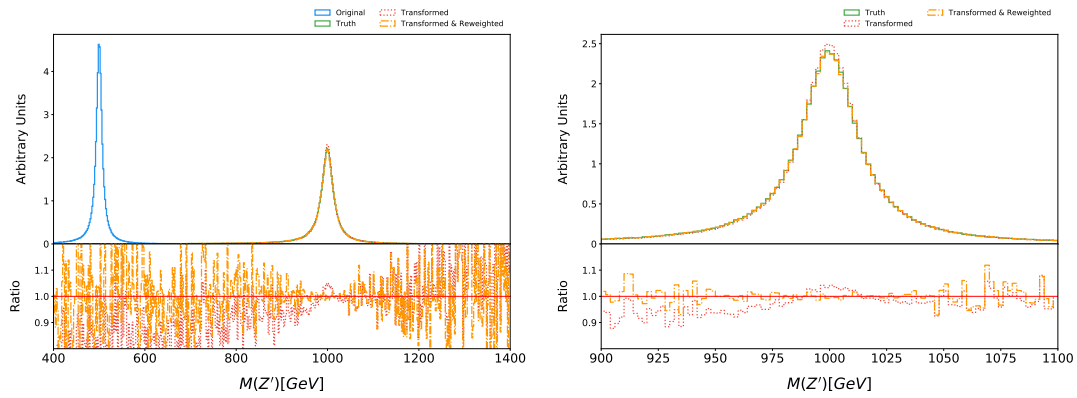

Figure 4.1: Invariant mass of the Z' boson before and after the transformation and reweighting. The transformation shifts the curve from its 500 GeV central point (blue) to the new central point at 1000 GeV (green). One can see however that the shape ôf the Breit-Wigner distribution also depends on the mass and therefore the transformation alone is not sufficient (red). Reweighting the events with all required weights then fixes the discrepancies (orange).

The next step is then to look at the angular distributions of the muons. Fig. 4.2 shows the energies as well as transverse and longitudinal momenta of the muon. Now the PDFs become the dominant reweighting factors. This is due to the

fact the the angles were kept constant in the rest frame of the Z' as part of the transformation. This implies that the dominant contribution of the angular distributions comes from the boost of the lab frame with respect to the Z' rest frame. This boost is in turn largely determined by the values of the PDFs for the new and old values of x_i. Similarly to the invariant mass distributions of the

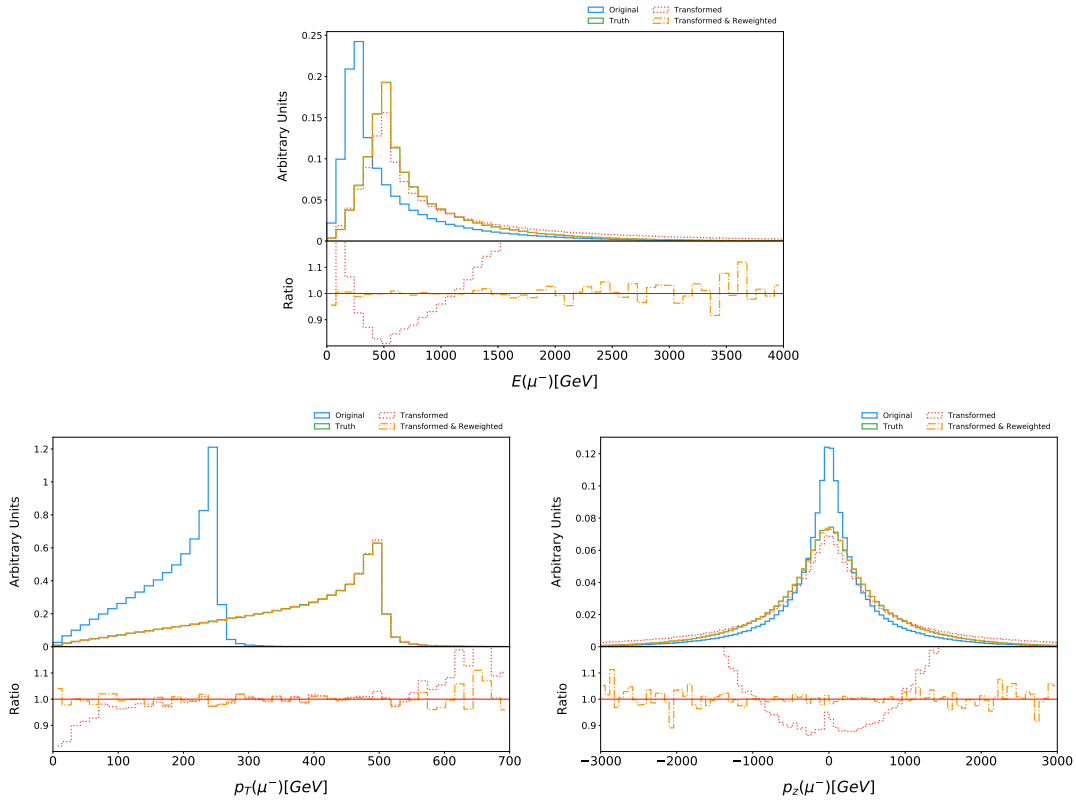

Figure 4.2: Momentum distributions of the final state μ^- for change in Z' mass from 500 GeV (blue) to 1000 GeV (green). One can clearly see the transformation shifting the distributions to nearly the right energy scale but leads to wrong shapes (red). Reweighting then fixes the shapes (orange).

Z', one can clearly see the transformation shifting the distributions to nearly the right energy scale. The shapes however differ to a similar extend. Reweighting then fixes the shapes.

4.2 Production of Heavy Fermion Pairs

Since the previous chapter described how the transformation and reweighting works for mass changes of s-channel mediators, the natural next step is to investigate the mass changes for t- and u-channel production. Just as in the previous chapter, a simple extension of the SM is chosen for this purpose, by adding a

Table 4.2: Parameters used for the generation of the MC events with MadGraph5_aMC@NLO [86]

	No. of events	PDF	μ_f	μ_r	$m_{t'}$
old	$1 \cdot 10^6$	CT14lo	91.188 GeV	91.188 GeV	400 GeV
new	$1 \cdot 10^6$	CT14lo	91.188 GeV	91.188 GeV	700 GeV

fourth generation of quarks (t', b'). Although a fourth generation model is essentially excluded by a series of experiments [99] [100], due to its simplicity, it serves as an excellent example for the application of the reusing algorithm from Ch. 3, not only for heavy t- and u-channel final states, but also the presented decay and jet procedures. While in the previous chapter possible decays and emissions of the final state muons were ignored, the generation of the hard process in MadGraph5_aMC@NLO [86] here is supplemented by a parton shower and decays using Pythia8 [91]. There are therefore two important versions for each particle involved in the decay chains. First the particles that are the direct products of the decaying particle. If for example the t' decays into a b' and a W, there will be one version each of the b' and W that have momenta whose sum exactly equals the momentum of the decaying t'. For the second version of each the b' and W, this is not necessarily any longer the case. The reason is the fact that both, the b' and the W, can, and in many cases will, emit gluons or photons respectively and therefore lose momentum. The algorithm, that is used to deal with this kind of situation, is described in Ch. 3.2.4.

Concretely consider the production of a $t'\bar{t}'$ pair, i.e. $pp \to t'\bar{t}' + X$, with subsequent decays into (anti-)b' and (anti-)top quarks. The top quarks then further decay into bottom quarks and W bosons, that then finally decay leptonically. The only parameter that is changed for the purpose of this algorithm is the mass of the t' while all other parameters like the b' mass or the coupling constants and decay widths are kept constant. The parameters for the event generation for both the original and target parameter point are summarized in Table 4.2. The transformation of the hard process, that was used here, is the one of Ch. 3.2.1.3. The results for the t' are shown in Fig. 4.3 in the case of the versions before gluon emissions and in Fig. 4.4 of the versions after parton shower emissions. Displayed are the distributions of all components of the four-momentum of the t'. Both for the full event generation original and new ("Truth") parameter point as well as for different sets of weights. One can see that the transformation alone ("Transformation") is able to shift the threshold energy to the right position but

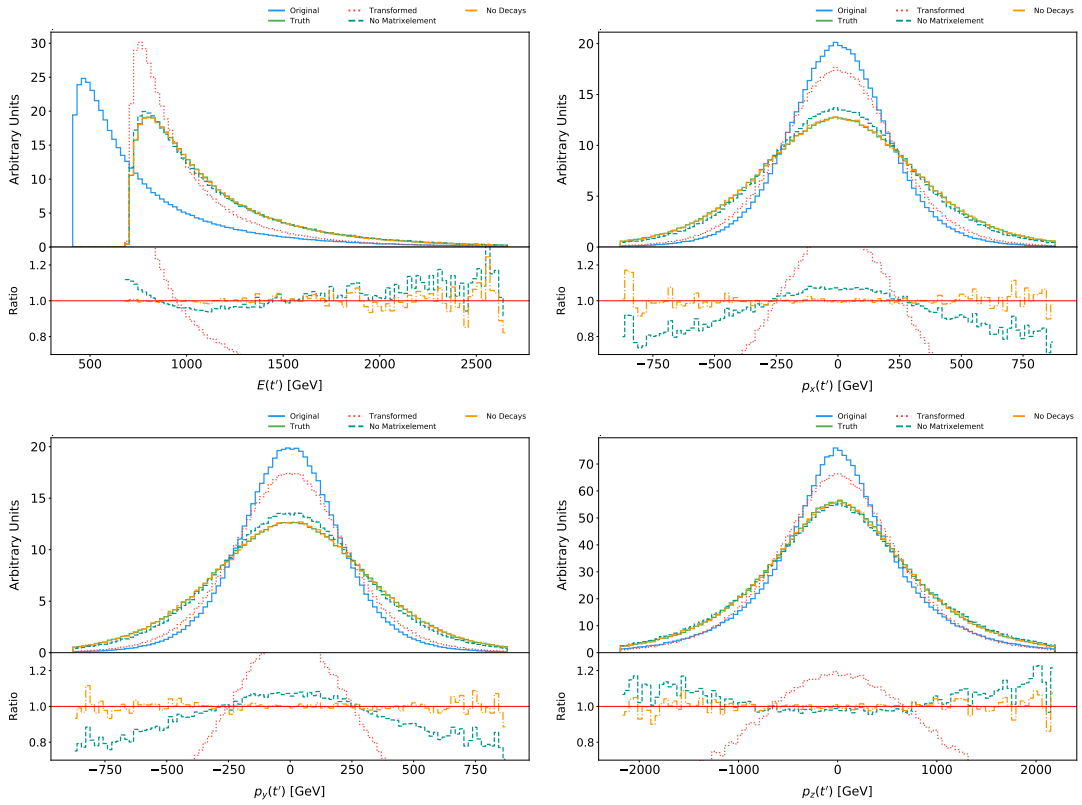

Figure 4.3: Impact of the transformation and reweighting on the momentum distributions before parton showering of the t'. The energy distributions show that without reweighting (red dotted line) only the mass is reproduced correctly while the shape does not nearly resemble the target distribution (solid green line). Adding PDF-, flux- and phase space reweighting improves the predictions significantly (dashed green line). A perfect reproduction however is only possible if matrix element reweighting is used (dash-dotted orange line).

is not able to produce the correct shape. This, of course, is to be expected as the threshold energy is given simply by the mass of the t'. Adding more weights then solves this problem for all components. While adding all weights listed in Ch. 3.3.1 except the production matrix element ("No Matrixelement"), i.e. the Jacobian, PDF-, flux- and phase space weights, shows a significant improvement, only adding the matrix element weight produces perfect distributions ("No Decays"). One should however consider that the calculation of the matrix element weights, depending on the process, can be computationally expensive. In practice, depending on the use case, one can therefore trade accuracy for performance by neglecting the matrix element weight.

Corresponding results for the b' are shown in Fig. 4.5 and Fig. 4.6. For the b' the sole transformation already does a much better job. This is due to the fact that the mass of the b' is not changed. The effects of the weights are extremely

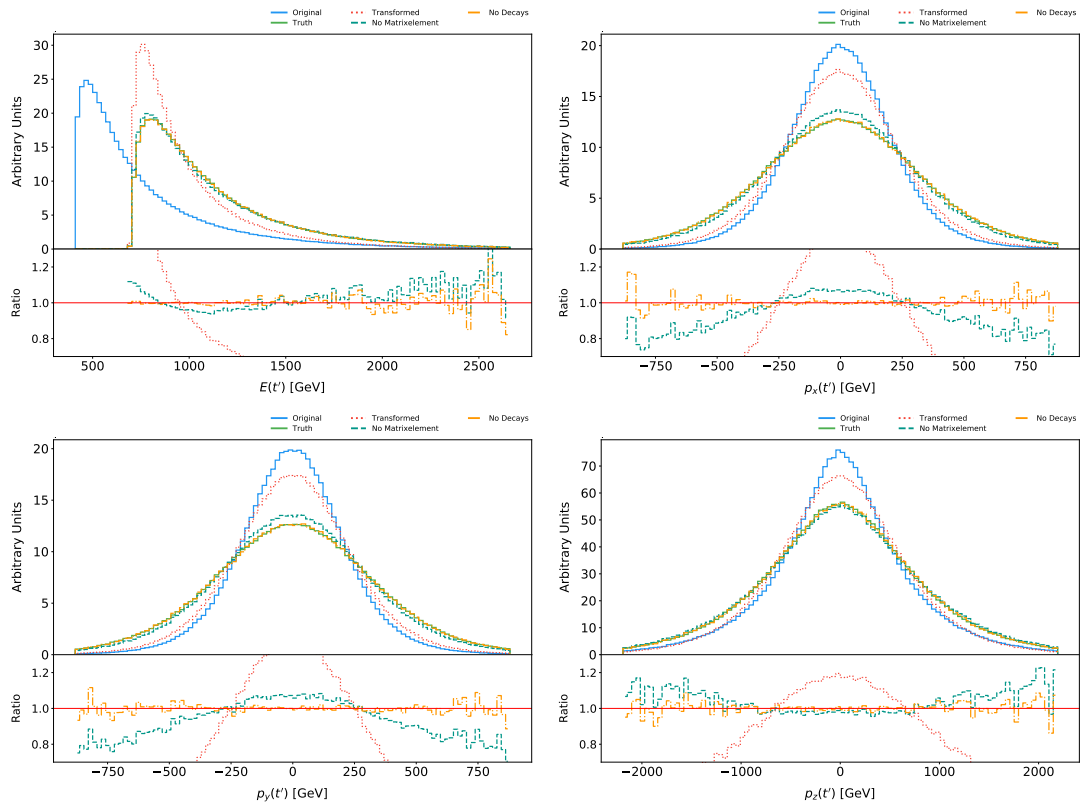

Figure 4.4: Impact of the transformation and reweighting on the momentum distributions after parton showering of the t'. The energy distributions show that without reweighting (red dotted line) only the mass is reproduced correctly while the shape does not nearly resemble the target distribution (solid green line). Adding PDF-, flux- and phase space reweighting improves the predictions significantly (dashed green line). A perfect reproduction however is only possible if matrix element reweighting is used (dash-dotted orange line).

similar to the t' case.

Finally this process allows for a study of jet distributions (Fig. 4.7) and distributions of particles that are the result of a multi-step decay chain, in this case leptons and neutrinos in Fig. 4.8. In both cases it is no longer sufficient to just use the production matrix element in order to produce perfect distributions. Instead one would need to also include decay matrix elements as well as weights that are the results of the jet algorithm described in Ch. 3.2.4. For many use cases however neglecting these effects will presumably be sufficient.

4.3 Squark Pair Production

The next step is to study a process that contains both s- and non-s-channel diagrams. Since the practice test of the presented algorithm in Ch. 4.4 considers

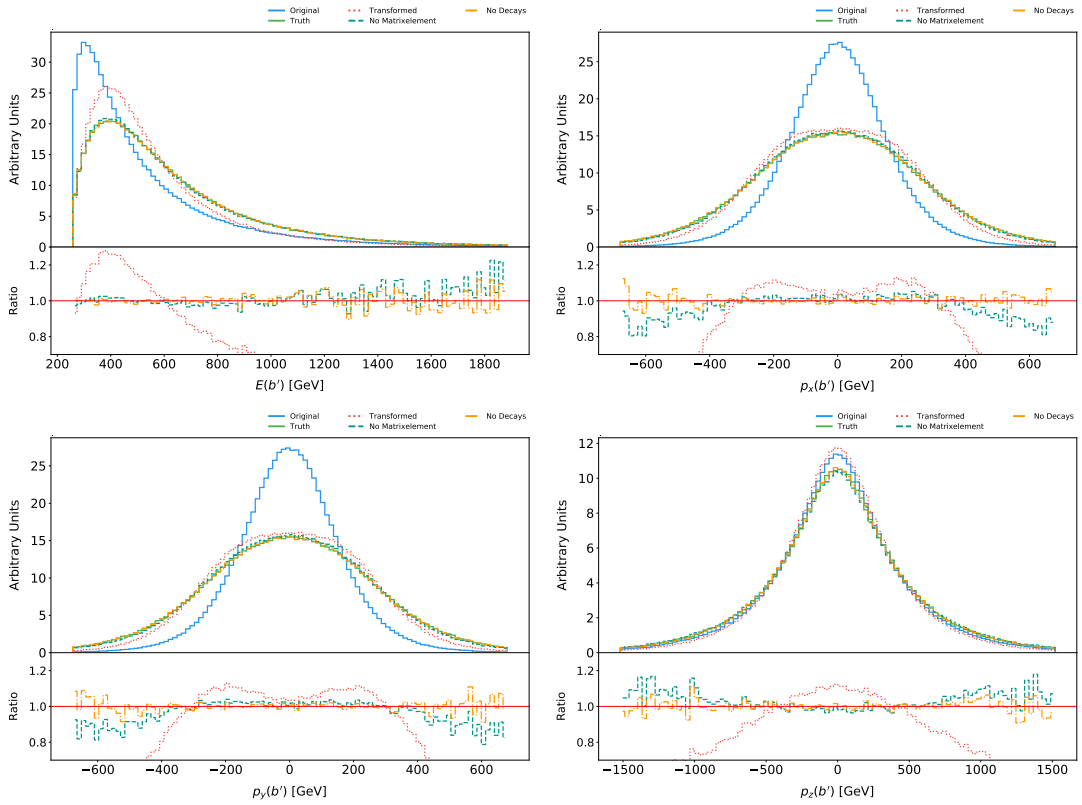

Figure 4.5: Impact of the transformation and reweighting on the momentum distributions before parton shower emissions of the b' decay product of the t'. The energy distributions show that without reweighting (red dotted line) only the mass is reproduced correctly while the shape does not nearly resemble the target distribution (solid green line). Adding PDF-, flux- and phase space reweighting improves the predictions significantly (dashed green line). A perfect reproduction however is only possible if matrix element reweighting is used (dash-dotted orange line).

the production of squark pairs in the Minimal Supersymmetric Standard Model (MSSM), it makes sense to look at the distributions of the involved particles first. The MSSM is, as the name suggests, an extension of the SM that is based on adding an additional symmetry called *supersymmetry* (SUSY) to the SM. This supersymmetry is a space-time symmetry that introduces relations between fermions and bosons such that its generator Q transforms fermionic fields into bosonic fields and vice-versa [34], i.e.

$$Q\,|\text{fermion}\rangle = |\text{boson}\rangle\,, \quad Q\,|\text{boson}\rangle = |\text{fermion}\rangle\,. \tag{4.11}$$

The transformed states then only differ regarding their spins and share all other quantum numbers and properties with the original state. The attractiveness of

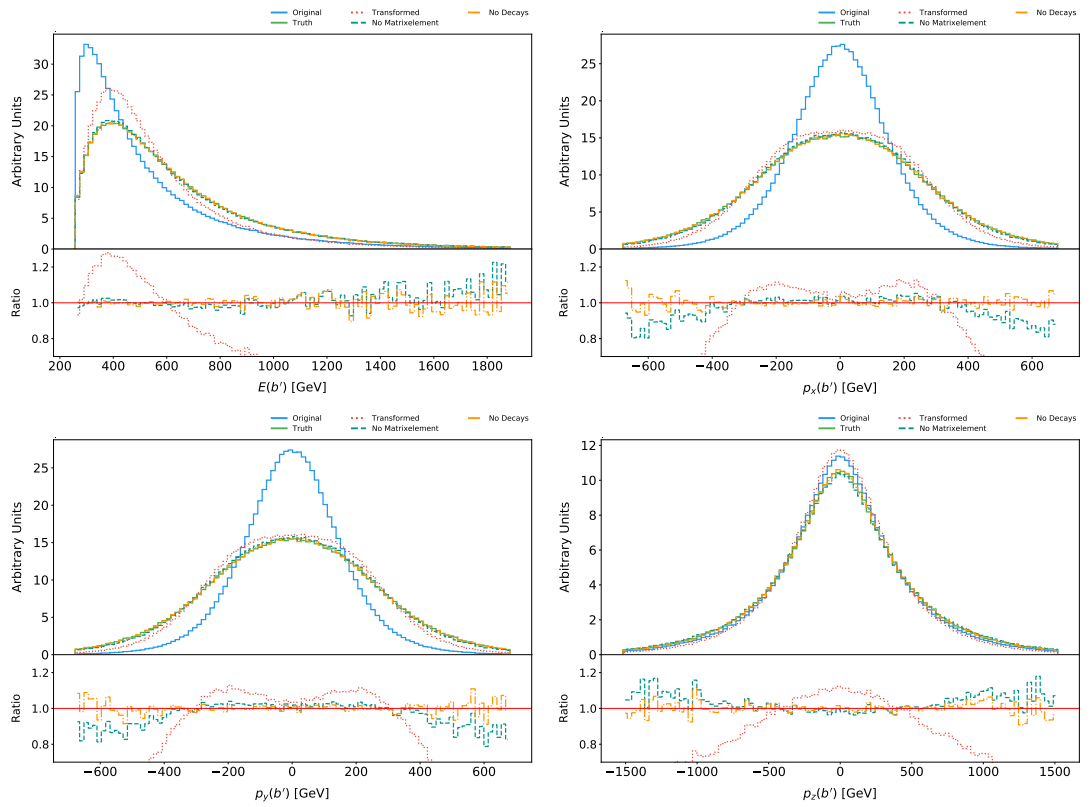

Figure 4.6: Impact of the transformation and reweighting on the momentum distributions after parton shower emissions of the b' decay product of the t'. The energy distributions show that without reweighting (red dotted line) only the mass is reproduced correctly while the shape does not nearly resemble the target distribution (solid green line). Adding PDF-, flux- and phase space reweighting improves the predictions significantly (dashed green line). A perfect reproduction however is only possible if matrix element reweighting is used (dash-dotted orange line).

SUSY lies in the number of potential problems of the SM it can solve. Many supersymmetric models, for example, predict a stable neutral particle that can serve as a candidate for dark matter [101]. Models with unbroken[1] or softly broken supersymmetry also offer an elegant solution to the hierarchy problem [34]. The MSSM is the supersymmetric model with the smallest number of new particles. More concretely it introduces a partner particle (*sparticle*) $\tilde{p}$ for each particle p in the SM. The bosonic spin-0 partners of the Standard Model fermions are called sfermions, so the partner of a given right-handed quark $\tilde{q}_R$ for example is called a *squark*. Partners of SM gauge bosons are called *gauginos*, e.g. the partner of the gluon $\tilde{g}$ is called *gluino*. Other SUSY particles, that are relevant here, are the

[1] In models with an unbroken supersymmetry the masses of the SUSY partners are the same as their original counterparts. Since none of these particles have been observed yet, SUSY must be broken in nature, that way allowing for large sparticle masses.

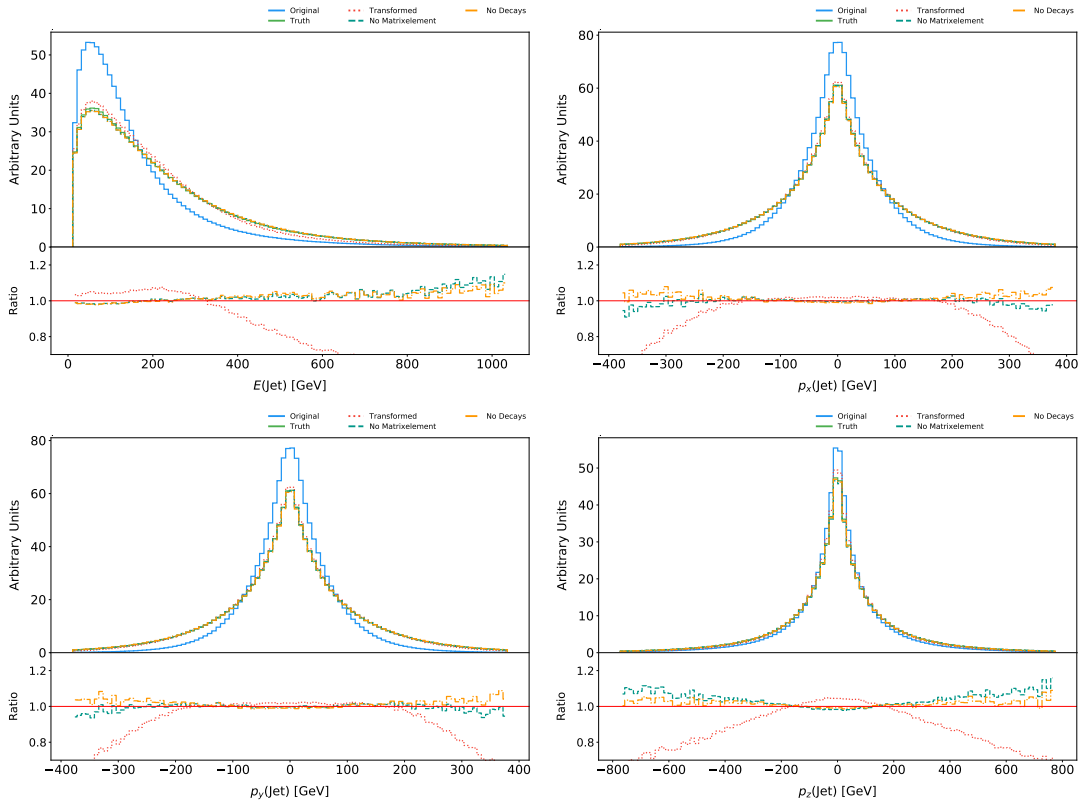

Figure 4.7: Impact of the transformation and reweighting on the jet distributions in t' pair production. The energy distributions show that without reweighting (red dotted line) only the mass is reproduced correctly while the shape does not nearly resemble the target distribution (solid green line). Adding PDF-, flux- and phase space reweighting improves the predictions significantly (dashed green line). For a perfect reproduction of the target distribution however adding matrix element reweighting (dash-dotted orange line) is not sufficient in this case. Rather additional reweighting factors from decays and jet handling must be applied in order to fix the distributions.

so-called neutralinos $\tilde{\chi}^0_{1,2,3,4}$. They are the four neutral mass eigenstates of the mixing of higgsinos and weak gauginos, i.e. the SUSY counterparts of the Higgs and the electroweak gauge bosons [34]. If the lightest neutralino $\tilde{\chi}^0_1$ is stable, for example in models with conserved R-Parity, and its mass is the smallest amongst all stable SUSY particles, it is also called the LSP ("Lightest Supersymmetric Particle"). In that case all supersymmetric particles eventually decay into this neutralino. This makes the neutralino a popular candidate for weakly interacting massive particle (WIMP) dark matter [101].
In the following the production of squark pairs with subsequent decays into jets and neutralinos, i.e.

$$pp \to \tilde{q}\bar{\tilde{q}} + X, \quad \tilde{q} \to q\tilde{\chi}^0_1, \tag{4.12}$$

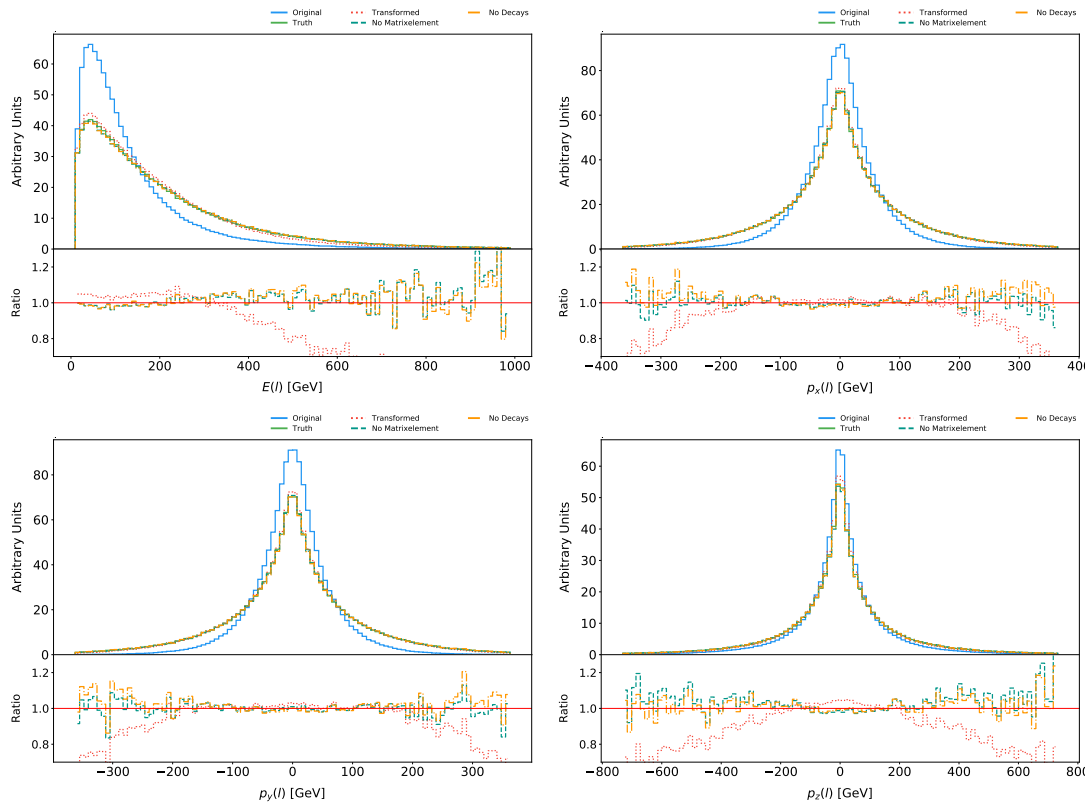

Figure 4.8: Impact of the transformation and reweighting on the lepton distributions in t' pair production with subsequent decays. The energy distributions show that without reweighting (red dotted line) only the mass is reproduced correctly while the shape does not nearly resemble the target distribution (solid green line). Adding PDF-, flux- and phase space reweighting improves the predictions significantly (dashed green line). For a perfect reproduction of the target distribution however adding matrix element reweighting (dash-dotted orange line) is not sufficient in this case. Rather additional reweighting factors from decays and jet handling must be applied in order to fix the distributions

with $q \in \{d_L, d_R, u_L, u_R, c_L, c_R, s_L, s_R\}$ is considered. The squarks are all given equal masses $m_{\tilde{q}}$ so that the parameters that were transformed are $m_{\tilde{q}}$ and $m_{\tilde{\chi}_0^1}$. Numerical values for the transformation can be found in Table 4.3. The results for the squarks are shown in Fig. 4.9 and the results for the neutralino in Fig. 4.10. Results for the jets are shown in Fig. 4.11. Similarly to the t' distributions from the previous chapter, one can see that the transformed and unweighted distributions ("Transformed") of the $\tilde{q}$ momenta components merely reproduce the squark masses. This is in accordance with the expectation that at least those reweighting factors must be included, that make up the leading contributions to the kinematical distributions. Adding the Jacobian, PDF, flux and phase space reweighting factors then consequently drastically improves the prediction ("No

Table 4.3: Parameters used for the generation of the MC events with MadGraph5_aMC@NLO [86].

	No. of events	PDF	μ_f	μ_r	$m_{\tilde{q}}$	$m_{\tilde{\chi}_1^0}$
old	$1 \cdot 10^6$	CT14lo	91.188 GeV	91.188 GeV	700 GeV	400 GeV
new	$1 \cdot 10^6$	CT14lo	91.188 GeV	91.188 GeV	900 GeV	600 GeV

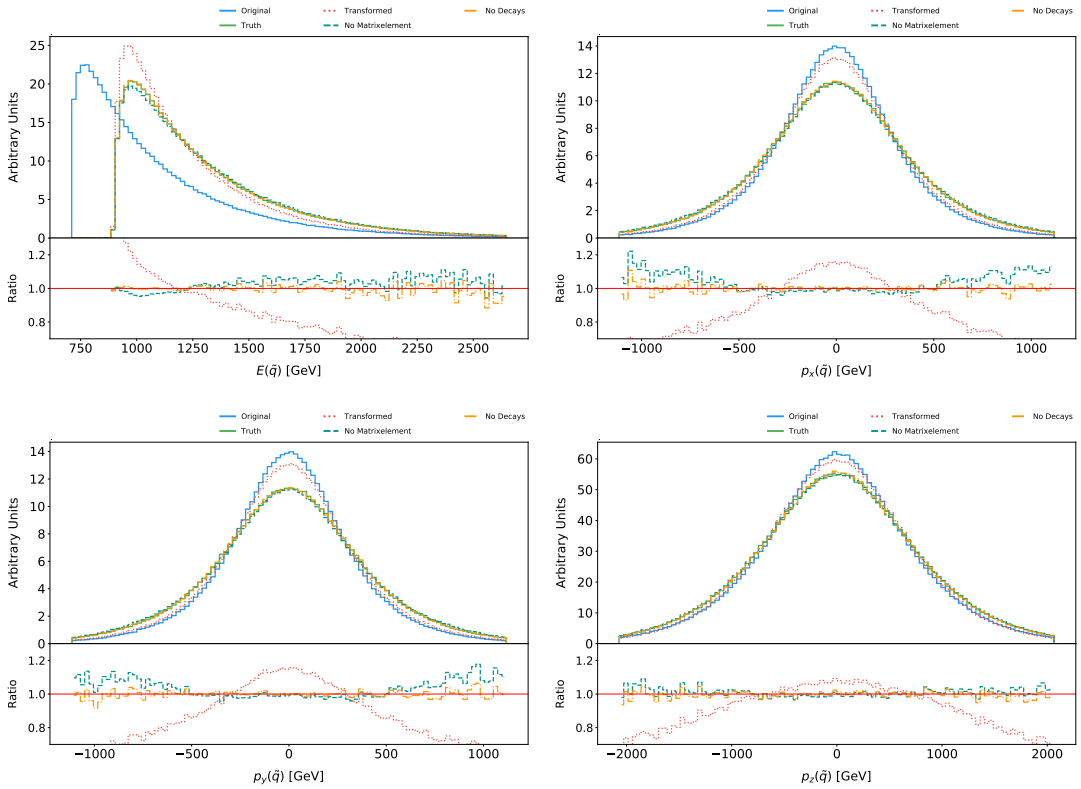

Figure 4.9: Impact of the transformation and reweighting on the momentum distributions of $\tilde{q}$ after parton shower emissions. The energy distributions show that without reweighting ("Transformed") only the mass is reproduced correctly while the shape does not nearly resemble the target distribution ("Truth"). Adding PDF-, flux- and phase space reweighting improves the predictions significantly ("No Matrixelement"). A perfect reproduction however is only possible if matrix element reweighting is used ("No Decays").

Matrixelement"). Adding the matrix element weight on top fixes the shapes of the distributions entirely ("No Decays"). It can be assumed that in practice in scans over multiple parameters of some BSM models, the number of events is noticeably smaller and therefore the difference between the prediction with and without the matrix element weight cannot be resolved. In that case the relatively expensive calculations of the matrix element weights can be omitted. The jet

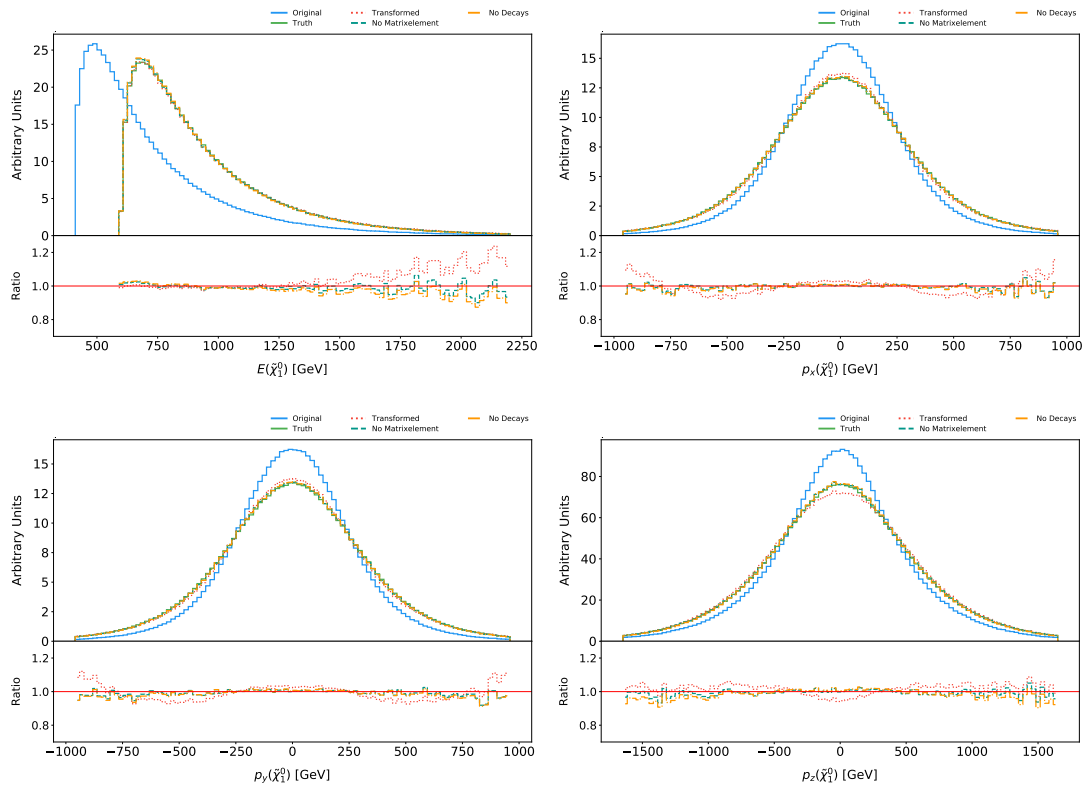

Figure 4.10: Impact of the transformation and reweighting on the neutralino momentum distributions after parton shower emissions. The energy distributions show that without reweighting ("Transformed") the mass is reproduced correctly while the shape does diverges from the target distribution ("Truth") at high energies. Adding PDF-, flux- and phase space reweighting improves the predictions significantly ("No Matrixelement"). For a perfect reproduction of the target distribution however adding matrix element reweighting (dash-dotted orange line) is not sufficient in this case. Rather additional reweighting factors from decays and jet handling must be applied in order to fix the distributions.

and neutralino distributions strongly resemble the lepton distributions from the previous chapter. While once again the inclusion of all hard process weight factors except the matrix element produces nearly optimal results, the inclusion of the production matrix element does not improve the prediction. This can again be reduced to the fact that for perfect predictions one also needs to reweight using the decay matrix elements and account for the transformations applied during the jet handling algorithm.

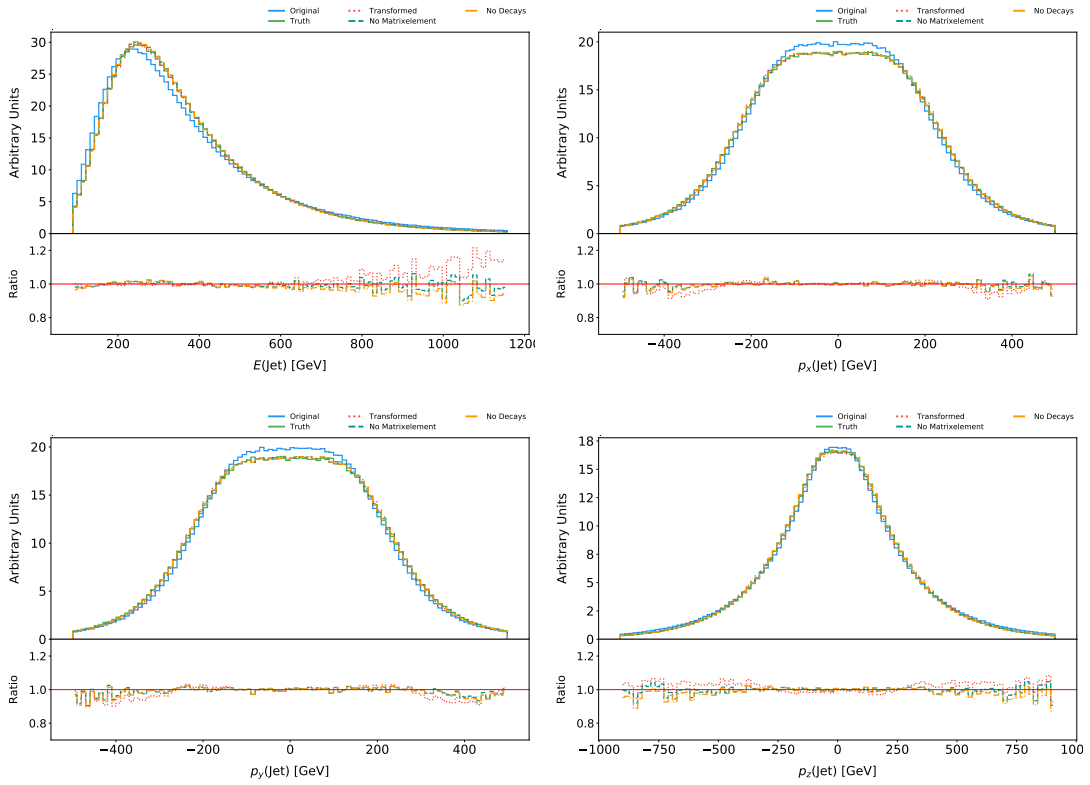

Figure 4.11: Impact of the transformation and reweighting on the jet distributions in squark pair production. The energy distributions show that without reweighting ("Transformed") the mass is reproduced correctly while the shape diverges from the target distribution ("Truth") at high energies. Adding PDF-, flux- and phase space reweighting improves the predictions significantly ("No Matrixelement"). For a perfect reproduction of the target distribution however adding matrix element reweighting ("No Decays") is not sufficient in this case. Rather additional reweighting factors from decays and jet handling must be applied in order to fix the distributions.

4.4 A Reproduction of ATLAS Limits

Up until this point all applications were based on simple processes and only considered the transformation from a given parameter point to one target parameter point. In practice however particularly interesting use cases for the proposed algorithm are scans over, potentially multidimensional, parameter spaces of BSM models, that can determine which parts of the parameter spaces can be excluded by experimental observations, e.g. direct LHC searches. The goal here is to better display when the approximations used by the transformation and reweighting algorithm break down in a real world scenario.

Typically comparisons between model predictions and experimental searches are

implemented using software packages like CheckMATE2 [72]. The idea behind these programs is to mimic the experimental searches as closely as possible using Monte Carlo events instead of physically measured ones. This then allows one to analyze the difference between predictions of the BSM model and the experiment by counting events that fall into *signal regions*, that are defined in the experimental searches [72]. The result of both the experimental searches and the theoretical studies consists, among others, of so called *exclusion limits* that separate regions of the parameter space, that are excluded by measurements, from regions that are still in agreement with the considered experimental searches. This is therefore a way to set limits on the (mass) parameters of the BSM model.
Based on the results of Ch. 4.3 the goal in this chapter is to demonstrate in how far the algorithm described here is able to reproduce the limits of a search conducted by the ATLAS collaboration for squarks in final states [102] as produced by the corresponding CheckMATE2 implementation. The proposed transformation and reweighting approach (new approach) is directly compared against the full MC event generation tool chain (benchmark).
The focus here will be on the process

$$pp \to \tilde{q}\bar{\tilde{q}} \to jj\tilde{\chi}_1^0\tilde{\chi}_1^0 \tag{4.13}$$

within the Minimal Supersymmetric Standard Model (MSSM). The squarks directly decay into a quark and a neutralino that constitutes the (stable) LSP. The masses of all other SUSY particles are set such that they decouple from the theory and can be ignored. The masses of the squarks are set to be degenerate over the first two generations, while the third generation is decoupled. A corresponding set of 10000 MC events was generated for each parameter point using MadGraph5_aMCNLO [86]. Subsequent parton showering of the events was done using Pythia 8 [91]. For the parton density functions the LHAPDF implementation of NNPDF2.3LO [103] was used. Additionally Pythia 8 was used for CKKW-L merging [104] with up to two additional jets, where the merging scale parameter was set to a quarter of the squark mass. Parton shower merging is important for the correct reproduction of the hard region of the jet distributions. While the parton shower reproduces the soft and collinear behavior of QCD emissions, it is not able to predict the behavior of hard jets that is typically dominated by fixed order effects. Thus up to two additional hard jets are produced at leading order using MadGraph5_aMCNLO and then merged using Pythia 8. Since the search in [102] is focused on jet and missing transverse energy signatures in the detector, it is crucial for the MC events to get both the jet and LSP

distributions right, making parton shower merging a vital ingredient of the MC chain. The merging procedure itself is implemented in Pythia 8 by reweighting the events relatively to the sample without any additional emissions. These additional merging weights must be considered in the reweighting factor of Ch. 3.3.1.

All weights from Ch. 3.3.1 except the matrix element weight were applied in

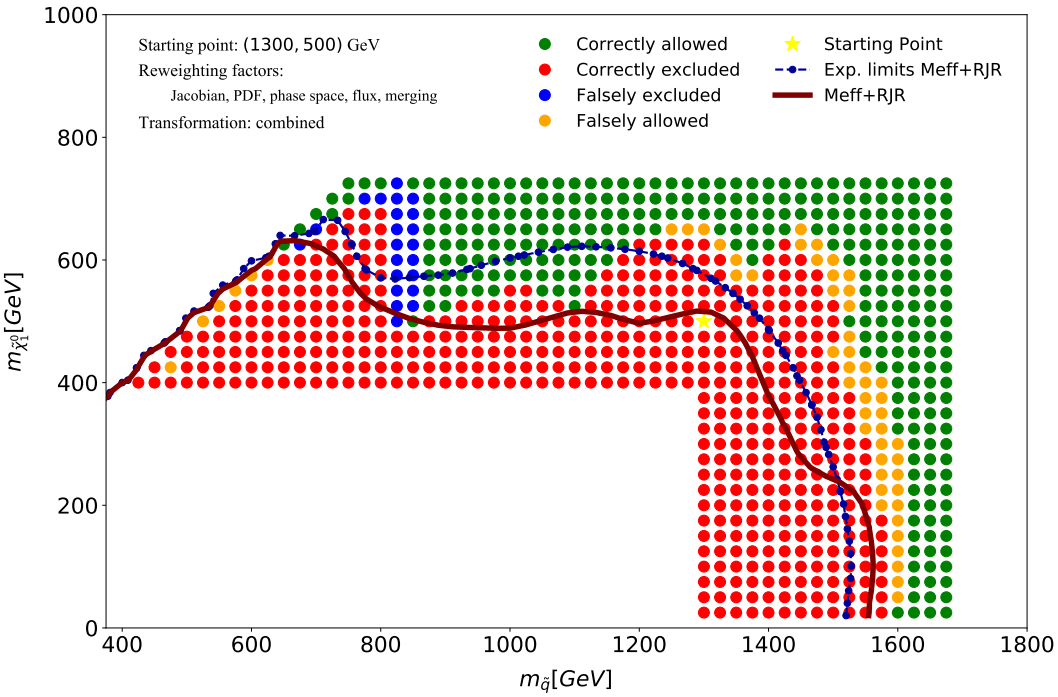

Figure 4.12: Limits on $m_{\tilde{q}}$ and $m_{\tilde{\chi}_1^0}$ in the MSSM with degenerate squark masses and decoupled gluinos. A comparison is shown between CheckMATE2 [72] results with events generated using the usual MC event generator tool chain (benchmark) and the proposed transformation and reweighting algorithm (new approach). Parameter points in green (red) are allowed (excluded) in both approaches while blue (orange) points are excluded (allowed) in the benchmark case and allowed (excluded) in the new approach. The starting point for the new approach at $m_{\tilde{q}}, m_{\tilde{\chi}_1^0} = (1300, 500)\,\text{GeV}$ is marked as a yellow star. Additionally the best fit expected and observed curves from the original ATLAS search are shown for comparison. One can see that the new approach reproduces the benchmark to a high degree even though no matrix element weights were included in the reweighting factor.

the new approach. Leaving out the matrix element significantly improves the speed of the algorithm and is the preferred procedure in many cases where the matrix element contributions are sub-leading compared to, for example, the PDF reweighting factor. As discussed above, a weight from parton shower merging was additionally applied in the reweighting procedure. The results for three different starting points of the parameter scan can be seen in Fig. 4.12 - 4.14. If the start-

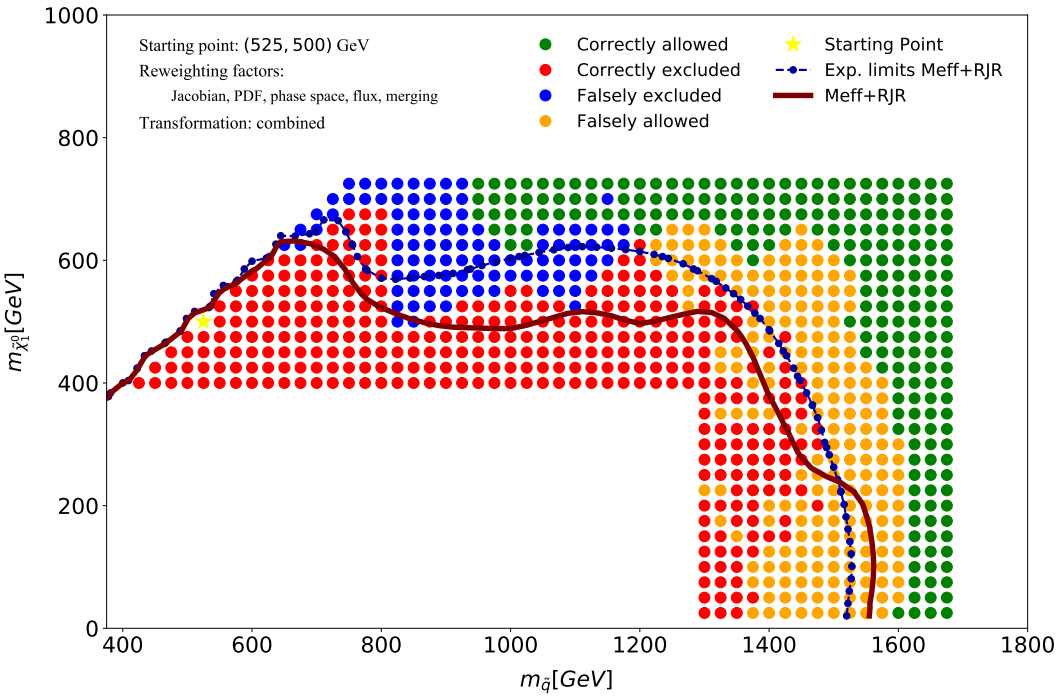

Figure 4.13: Limits on $m_{\tilde{q}}$ and $m_{\tilde{\chi}_1^0}$ in the MSSM with degenerate squark masses and decoupled gluinos. A comparison is shown between CheckMATE2 [72] results with events generated using the usual MC event generator tool chain (benchmark) and the proposed transformation and reweighting algorithm (new approach). Parameter points in green (red) are allowed (excluded) in both approaches while blue (orange) points are excluded (allowed) in the benchmark case and allowed (excluded) in the new approach. The starting point for the new approach at $m_{\tilde{q}}, m_{\tilde{\chi}_1^0} = (525, 500)\,\text{GeV}$ is marked as a yellow star. Additionally the best fit expected and observed curves from the original ATLAS search are shown for comparison. One can see that choosing the starting point in the suppressed region, where the masses of the squark and the neutralino are very close, implies larger uncertainties than in cases with central starting points.

ing point is chosen appropriately, the new approach agrees with the benchmark extremely well (see Fig. 4.12). Any differences between the benchmark and the new approach can be reduced to either statistical uncertainties (particularly in the suppressed region, where the squark and neutralino masses are close), due to the relatively low number of events used, or inaccuracies of the new approach, such as the missing matrix element weight or, more importantly, imperfections in the way the algorithm handles jet distributions. Since the ATLAS search is extremely sensitive to jet distributions, even small effects cause differences in CheckMATE2 results. This problem is emphasized when the starting point is chosen poorly (see Fig. 4.13). In this case the production of jets is strongly suppressed at the starting point due to the proximity of the squark and the LSP

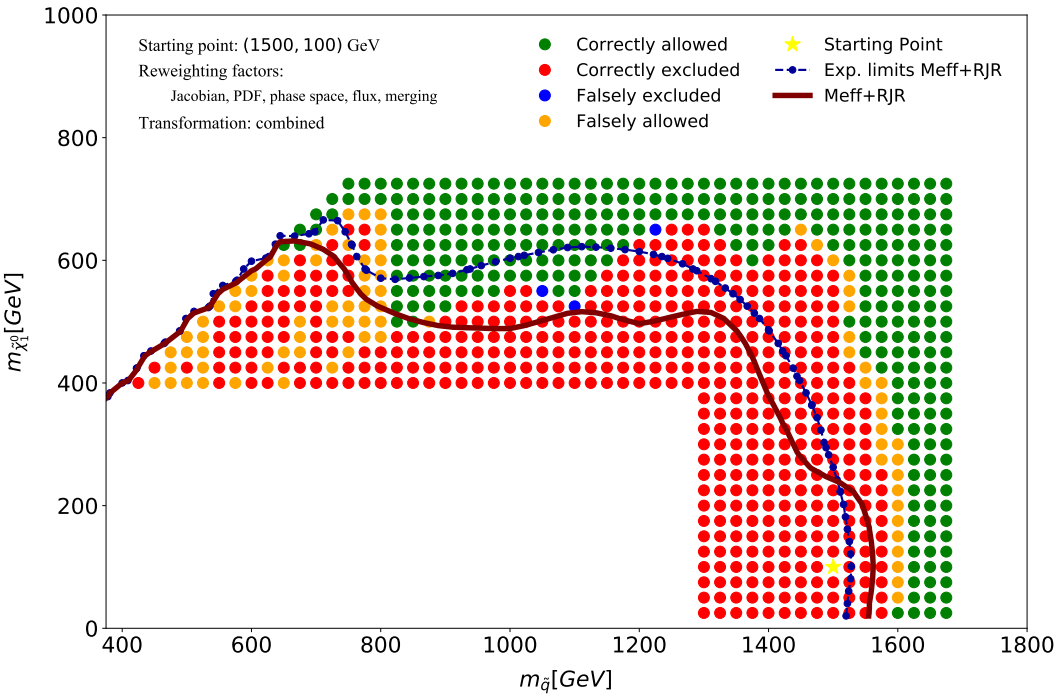

Figure 4.14: Limits on $m_{\tilde{q}}$ and $m_{\tilde{\chi}_1^0}$ in the MSSM with degenerate squark masses and decoupled gluinos. A comparison is shown between CheckMATE2 [72] results with events generated using the usual MC event generator tool chain (benchmark) and the proposed transformation and reweighting algorithm (new approach). Parameter points in green (red) are allowed (excluded) in both approaches while blue (orange) points are excluded (allowed) in the benchmark case and allowed (excluded) in the new approach. The starting point for the new approach at $m_{\tilde{q}}, m_{\tilde{\chi}_1^0} = (1500, 100)\,\text{GeV}$ is marked as a yellow star. Additionally the best fit expected and observed curves from the original ATLAS search are shown for comparison. One can see that the new approach produces extremely accurate results for squark masses above 800 GeV. In the small squark mass region however, increased statistical uncertainties caused by the reweighting cause the new approach to be less reliable.

masses. In this case the jets predicted by the new approach no longer follow the behaviour of the benchmark jets in the bulk of the parameter space, particularly around the exclusion limit. On the contrary the region where jet production is suppressed is reproduced better than in the previous case, since the jet distributions in this region are close to the ones at the starting point. Finally Fig. 4.14 shows that choosing the parameter point far away from kinematically demanding regions can lead to unreliable results. Transformations for large mass differences typically involve large reweighting factors and therefore larger statistical uncertainties. This in turn then leads to the "sprinkle" effect for squark masses below 800 GeV.

Overall the new approach, if applied carefully, offers an accurate alternative to the benchmark. The main reason however to use the new approach is the significant decrease in required CPU time. For the production of the data used for Fig. 4.12 - 4.14 the total time saving factor was of the order of ≈ 10. This factor however includes the reading and writing times of the event files. Since the current implementation of the new approach only produces output events for one target parameter point, the original event has to be read for each target point individually. These reading times are a dominant contribution to the overall event generation and evaluation chain and were almost identical in the benchmark case and the new approach. It is therefore safe to say that an implementation of the new approach into a library like CheckMATE2, where the entire generation and evaluation process happens inside the RAM, will enable an additional drastic increase in performance advantages of the new approach over full MC simulations.

Chapter 5

Conclusion

While the LHC has long been running, the nature of any physics beyond the Standard Model is still unclear. New ideas and models need to be developed in order to both explain the lack of observations at the LHC and the already known incompleteness of the Standard Model itself (dark matter, neutrino masses, etc.). Comparing experimental data and theoretical predictions however can, in many cases, be challenging as many-dimensional parameter spaces make global fits computationally demanding. In this work a new method was introduced, that could be used to drastically increase the sampling speed of parameter scans for the LHC. The combination of momentum transformations and Monte Carlo reweighting, appears to be a promising approach to reduce the number of model parameter points that need to be fully simulated.

This new method was shown to be successful in predicting the kinematical distributions of all momenta involved in several processes and it was shown, that upon correctly choosing a starting point, parameter scans can be performed without having to rerun the usual Monte Carlo toolchain for each model parameter point. It is however crucial to bear in mind the most significant caveats, that the new algorithm has: Most importantly and by construction the algorithm can't simply be used for any process and any parameter point combination. The starting parameter point must contain all information needed in order to reproduce the physics of the target parameter point. If for example a new decay channel opens up at the target parameter point that was not accessible at the original point, no Monte Carlo events will be available for transformation that contain the corresponding decay. Therefore choosing the starting parameter point is essential for producing usable results.

Another caveat is the treatment of parton showers. On the one hand the introduced methods lack support for certain parton shower features like hadronization

or parton emissions inside the hard event, which limit their applicability to processes in which neither plays a significant role. On the other hand the treatment of jets turns out to be rather delicate. Determining jet masses or taking into account parton shower merging can merely be done on the basis of heuristics and are the biggest source for deviations between full simulation and the described approach.
It is however theoretically possible to combine the transformation of events and reweighting with parton shower algorithms only in particular cases. Then the treatment of QCD or QED radiation can be left to the parton shower while everything else is processed by the new algorithm. Corresponding studies are left for future work.

Appendix A

Boosts between to momenta

Here a short reminder of the relevant formalism and the construction of boosts between two given momenta is given. A Lorentz boost of a momentum $p = (E, \vec{p})$ in a given direction $\vec{n}$ with $|\vec{n}| = 1$ and is given by

$$E' = \gamma \left(E - \beta \vec{n} \cdot \vec{p}\right) \tag{A.1}$$

$$\vec{p}' = \vec{p} + \left[(\gamma - 1)(\vec{n} \cdot \vec{p}) - \gamma \beta E\right] \vec{n}, \tag{A.2}$$

where $\gamma = (1 - \beta^2)^{-\frac{1}{2}}$. A boost depends on three parameters: The direction of the boost as given by $\vec{n}$ and the size of the boost as given by β. The vector $\vec{\beta} = \beta \vec{n}$ is often called the "boost vector" and can be used to define the boost. Thus given two distinct momenta $p_1 = (E_1, \vec{p}_1)$ and $p_2 = (E_2, \vec{p}_2)$ the boost from p_1 to p_2 is given by

$$E_2 = \gamma \left(E_1 - \beta \vec{n} \cdot \vec{p_1}\right) \tag{A.3}$$

$$\vec{p}_2 = \vec{p}_1 + \left[(\gamma - 1)(\vec{n} \cdot \vec{p_1}) - \gamma \beta E_1\right] \vec{n}, \tag{A.4}$$

where $\vec{n}$ and β are to be determined. This can be achieved by noting that Eq. (A.4) implies that $\vec{p}_2 - \vec{p}_1$ and $\vec{n}$ are collinear and that the size of the vector $\vec{p}_2 - \vec{p}_1$ is given by the factor in front of $\vec{n}$. Hence

$$\vec{p}_2 - \vec{p}_1 = \lambda \vec{n}, \quad \lambda = (\gamma - 1)(\vec{n} \cdot \vec{p_1}) - \gamma \beta E_1 \tag{A.5}$$

and therefore

$$\vec{n} = \frac{\vec{p}_2 - \vec{p}_1}{|\vec{p}_2 - \vec{p}_1|}. \tag{A.6}$$

Eq. (A.3) can then be used to determine β. As γ is quadratic in β, solving Eq. (A.3) in general yields two distinct solutions β_+ and β_-:

$$\beta_\pm = \frac{(\vec{n}\cdot\vec{p}_1)E_1 \pm E_2\sqrt{(\vec{n}\cdot\vec{p}_1)^2 + (E_2^2 - E_1^2)}}{(\vec{n}\cdot\vec{p}_1)^2 + E_2^2} \tag{A.7}$$

The physical solution must fulfill Eq. (A.4), which can be simplified to one equation by considering the norms of both sides of the equation:

$$|\vec{p}_2 - \vec{p}_1| = (\gamma - 1)(\vec{n}\cdot\vec{p_1}) - \gamma\beta E_1. \tag{A.8}$$

Appendix B

Jacobian of the bijective transformation

The Jacobian of the bijective transformation introduced in Ch. 3.2.1.2 takes the form

$$\Rightarrow J = v^2 - v\left((1-x_1)\frac{\partial v}{\partial x_1} + (1-x_2)\frac{\partial v}{\partial x_2}\right). \tag{B.1}$$

The notation can be somewhat simplified by introducing new variables a and b as

$$a = 1 - x_1, \quad b = 1 - x_2. \tag{B.2}$$

Then the second term of Eq. (B.1) becomes

$$v\left((1-x_1)\frac{\partial v}{\partial x_1} + (1-x_2)\frac{\partial v}{\partial x_2}\right) = v\left(a\frac{\partial v}{\partial a}\frac{\partial a}{\partial x_1} + b\frac{\partial v}{\partial b}\frac{\partial b}{\partial x_2}\right) \tag{B.3}$$

$$= -v\left(a\frac{\partial v}{\partial a} + b\frac{\partial v}{\partial b}\right). \tag{B.4}$$

It is therefore sufficient to show that

$$a\frac{\partial v}{\partial a} + b\frac{\partial v}{\partial b} = 0. \tag{B.5}$$

In order to prove Eq. (B.5) consider the functions $u^{(\prime)}$ and v that were defined in Ch. 3.2.1.2 as

$$u^{(\prime)} = \sqrt{(x_1 - x_2)^2 + 4c^{(\prime)}(1-x_1)(1-x_2)}, \tag{B.6}$$

$$v(x_1, x_2) = \frac{2 - x_1 - x_2 - u'}{2 - x_1 - x_2 - u}. \tag{B.7}$$

In terms of a and b they read

$$u^{(\prime)}(a, b) = \sqrt{(a-b)^2 + 4c^{(\prime)}ab} \tag{B.8}$$

$$= \sqrt{a^2 + b^2 + (4c^{(\prime)} - 2)ab} \tag{B.9}$$

$$= \sqrt{a^2 + b^2 + 2\tilde{c}^{(\prime)}ab}, \tag{B.10}$$

and

$$v(a, b) = \frac{a + b - u}{a + b - u'}, \tag{B.11}$$

where

$$\tilde{c}^{(\prime)} = 2c^{(\prime)} - 1. \tag{B.12}$$

In order to show that Eq. (B.5) holds, consider the partial derivatives of v with respect to a and b:

$$\partial_a v = \frac{(1 - \partial_a u')(a + b - u) - (1 - \partial_a u)(a + b - u')}{(a + b - u)^2} \tag{B.13}$$

Bringing the denominator to the other side, this reads

$$(a + b - u)^2 \partial_a v = -u + u' + (a + b)\left(\partial_a u - \partial_a u'\right) + u\partial_a u' - u'\partial_a u. \tag{B.14}$$

Since v is symmetric in a and b the partial derivative with respect to b is given by

$$(a + b - u)^2 \partial_b v = -u + u' + (a + b)\left(\partial_b u - \partial_b u'\right) + u\partial_b u' - u'\partial_b u. \tag{B.15}$$

The partial derivatives of $u^{(\prime)}$ are

$$\partial_a u^{(\prime)} = \frac{1}{2u^{(\prime)}}(2a + 2\tilde{c}^{(\prime)}b) \tag{B.16}$$

$$= \frac{1}{u^{(\prime)}}(a + \tilde{c}^{(\prime)}b) \tag{B.17}$$

and

$$\partial_b u^{(\prime)} = \frac{1}{2u^{(\prime)}}(2b + 2\tilde{c}^{(\prime)}a) \tag{B.18}$$

$$= \frac{1}{u^{(\prime)}}(b + \tilde{c}^{(\prime)}a). \tag{B.19}$$

Hence

$$\partial_a u - \partial_a u' = \frac{a + \tilde{c}b}{u} - \frac{a + \tilde{c}'b}{u'} = \frac{a(u' - u) + b(\tilde{c}u' - \tilde{c}'u)}{uu'}, \tag{B.20}$$

$$\partial_b u - \partial_b u' = \frac{b + \tilde{c}a}{u} - \frac{b + \tilde{c}'a}{u'} = \frac{b(u' - u) + a(\tilde{c}u' - \tilde{c}'u)}{uu'} \tag{B.21}$$

as well as

$$u\partial_a u' - u'\partial_a u = u\frac{a + \tilde{c}'b}{u'} - u'\frac{a + \tilde{c}b}{u} = \frac{a(u^2 - u'^2) + b(\tilde{c}'u^2 - \tilde{c}u'^2)}{uu'}, \tag{B.22}$$

$$u\partial_b u' - u'\partial_b u = u\frac{b + \tilde{c}'a}{u'} - u'\frac{b + \tilde{c}a}{u} = \frac{b(u^2 - u'^2) + a(\tilde{c}'u^2 - \tilde{c}u'^2)}{uu'}. \tag{B.23}$$

Inserting these identities into Eq. (B.14) and multiplying both sides of the equation by uu' results in

$$\begin{aligned} uu'(a + b - u)^2\partial_a v = &- u^2u' + uu'^2 \\ &+ a^2(u' - u) + b^2(\tilde{c}u' - \tilde{c}'u') \\ &+ ab(\tilde{c}u' - \tilde{c}'u) + ab(u' - u) \\ &+ a(u^2 - u'^2) + b(\tilde{c}'u^2 - \tilde{c}^2u'^2). \end{aligned} \tag{B.24}$$

Since $u^{(\prime)}$ is a square root, sorting the terms by the order of $u^{(\prime)}$ has the potential to easier identify terms that can cancel each other out. With $N \coloneqq uu'(a+b-u)^2$ this takes the following form

$$\begin{aligned} N\partial_a v = &- u^2u' + uu'^2 \\ &+ u^2(a + \tilde{c}'b) - u'^2(a + \tilde{c}b) \\ &- u(a^2 + \tilde{c}'b^2 + 2c'ab) + u'(a^2 + \tilde{c}b^2 + 2cab). \end{aligned} \tag{B.25}$$

The partial derivative of v with respect to b can, due to the symmetry of v, be found by replacing a by b and vice versa in the previous equation. The weighted sum of both is therefore given by

$$\begin{aligned} Na\,\partial_a v + Nb\,\partial_b v = &(-u^2u' + uu'^2)(a + b) \\ &+ u^2(a^2 + b^2 + 2\tilde{c}'ab) - u'^2(a^2 + b^2 + 2\tilde{c}ab) \\ &- u(a^3 + b^3 + (4c' - 1)a^2b + (4c' - 1)ab^2) \\ &+ u'(a^3 + b^3 + (4c - 1)a^2b + (4cc - 1)ab^2). \end{aligned} \tag{B.26}$$

Now note that

$$(a^2 + b^2 + 2\tilde{c}^{(\prime)}ab) = u^{(\prime)2}. \tag{B.27}$$

Therefore the terms in the second line of Eq. (B.26) cancel each other out and one is left with

$$\begin{aligned} Na\,\partial_a v + Nb\,\partial_b v =&(-u^2u' + uu'^2)(a+b) \\ &- u(a^3 + b^3 + (4c' - 1)a^2b + (4c' - 1)ab^2) \\ &+ u'(a^3 + b^3 + (4c - 1)a^2b + (4cc - 1)ab^2) \qquad \text{(B.28)} \\ =&u'(a^3 + b^3 + (4c - 1)a^2b + (4cc - 1)ab^2 - u^2(a+b)) \\ &- u(a^3 + b^3 + (4c' - 1)a^2b + (4c' - 1)ab^2 - u'^2(a+b)). \qquad \text{(B.29)} \end{aligned}$$

Now since

$$\begin{aligned} u^{(\prime)2}(a+b) &= (a^2 + b^2 + (4c^{(\prime)} - 2)ab))(a+b) && \text{(B.30)} \\ &= a^3 + b^3 + (4c^{(\prime)} - 1)a^2b + (4c^{(\prime)} - 1)ab^2, && \text{(B.31)} \end{aligned}$$

Eq. (B.29) reads

$$Na\,\partial_a v + Nb\,\partial_b v = u' \cdot 0 - u \cdot 0 = 0, \tag{B.32}$$

which proves the conjecture.

Bibliography

[1] G Apollinari et al. *High-Luminosity Large Hadron Collider (HL-LHC): Preliminary Design Report*. CERN Yellow Reports: Monographs. Geneva: CERN, 2015. DOI: 10.5170/CERN-2015-005. URL: http://cds.cern.ch/record/2116337.

[2] David d'Enterria. "CMS physics highlights in the LHC Run 1". In: *PoS* Bormio2015 (2015), p. 027. DOI: 10.22323/1.238.0027. arXiv: 1504.06519 [hep-ex].

[3] Georges Aad et al. "Observation of a new particle in the search for the Standard Model Higgs boson with the ATLAS detector at the LHC". In: *Phys. Lett.* B716 (2012), pp. 1–29. DOI: 10.1016/j.physletb.2012.08.020. arXiv: 1207.7214 [hep-ex].

[4] Serguei Chatrchyan et al. "Observation of a New Boson at a Mass of 125 GeV with the CMS Experiment at the LHC". In: *Phys. Lett.* B716 (2012), pp. 30–61. DOI: 10.1016/j.physletb.2012.08.021. arXiv: 1207.7235 [hep-ex].

[5] John Ellis, Mary K. Gaillard, and Dimitri V. Nanopoulos. "A Historical Profile of the Higgs Boson". In: *The standard theory of particle physics: Essays to celebrate CERN's 60th anniversary*. Ed. by Luciano Maiani and Luigi Rolandi. 2016, pp. 255–274. DOI: 10.1142/9789814733519_0014. arXiv: 1504.07217 [hep-ph].

[6] Peter Ware Higgs. "Broken symmetries, massless particles and gauge fields". In: *Phys. Lett.* 12 (1964), pp. 132–133.

[7] François Englert and Robert Brout. "Broken symmetry and the mass of gauge vector mesons". In: *Physical Review Letters* 13.9 (1964), p. 321.

[8] M. Tanabashi et al. "Review of Particle Physics". In: *Phys. Rev. D* 98 (3 Aug. 2018), p. 127. DOI: 10.1103/PhysRevD.98.030001. URL: https://link.aps.org/doi/10.1103/PhysRevD.98.030001.

[9] S. W. Herb et al. "Observation of a Dimuon Resonance at 9.5-GeV in 400-GeV Proton-Nucleus Collisions". In: *Phys. Rev. Lett.* 39 (1977), pp. 252–255. DOI: 10.1103/PhysRevLett.39.252.

[10] G. Arnison et al. “Experimental Observation of Isolated Large Transverse Energy Electrons with Associated Missing Energy at s**(1/2) = 540-GeV”. In: *Phys. Lett.* 122B (1983). [,611(1983)], pp. 103–116. DOI: 10.1016/0370-2693(83)91177-2.

[11] G. Arnison et al. “Experimental Observation of Lepton Pairs of Invariant Mass Around 95-GeV/c**2 at the CERN SPS Collider”. In: *Phys. Lett.* 126B (1983), pp. 398–410. DOI: 10.1016/0370-2693(83)90188-0.

[12] F. Abe et al. “Observation of top quark production in $\bar{p}p$ collisions”. In: *Phys. Rev. Lett.* 74 (1995), pp. 2626–2631. DOI: 10.1103/PhysRevLett.74.2626. arXiv: hep-ex/9503002 [hep-ex].

[13] K. Kodama et al. “Observation of tau neutrino interactions”. In: *Phys. Lett.* B504 (2001), pp. 218–224. DOI: 10.1016/S0370-2693(01)00307-0. arXiv: hep-ex/0012035 [hep-ex].

[14] *Standard Model Summary Plots Summer 2019*. Tech. rep. ATL-PHYS-PUB-2019-024. Geneva: CERN, July 2019. URL: http://cds.cern.ch/record/2682186.

[15] Saranya Samik Ghosh. “Highlights from the Compact Muon Solenoid (CMS) Experiment”. In: *Universe* 5.1 (2019), p. 28. DOI: 10.3390/universe5010028. arXiv: 1901.05340 [hep-ex].

[16] Michael Rammensee. “SUSY searches: Recent results from ATLAS and CMS”. In: *J. Phys. Conf. Ser.* 631.1 (2015), p. 012072. DOI: 10.1088/1742-6596/631/1/012072.

[17] P. J. E. Peebles and Bharat Ratra. “The Cosmological Constant and Dark Energy”. In: *Rev. Mod. Phys.* 75 (2003). [,592(2002)], pp. 559–606. DOI: 10.1103/RevModPhys.75.559. arXiv: astro-ph/0207347 [astro-ph].

[18] Gianfranco Bertone, Dan Hooper, and Joseph Silk. “Particle dark matter: Evidence, candidates and constraints”. In: *Phys. Rept.* 405 (2005), pp. 279–390. DOI: 10.1016/j.physrep.2004.08.031. arXiv: hep-ph/0404175 [hep-ph].

[19] Morad Aaboud et al. “Constraints on mediator-based dark matter and scalar dark energy models using $\sqrt{s} = 13$ TeV pp collision data collected by the ATLAS detector”. In: *JHEP* 05 (2019), p. 142. DOI: 10.1007/JHEP05(2019)142. arXiv: 1903.01400 [hep-ex].

[20] Adish Vartak. *Dark matter search in CMS. Dark matter searches at the CMS experiment*. Tech. rep. CMS-CR-2017-147. Geneva: CERN, June 2017. URL: https://cds.cern.ch/record/2271096.

[21] Austin Joyce et al. “Beyond the Cosmological Standard Model”. In: *Phys. Rept.* 568 (2015), pp. 1–98. DOI: 10.1016/j.physrep.2014.12.002. arXiv: 1407.0059 [astro-ph.CO].

[22] Y. Fukuda et al. “Evidence for Oscillation of Atmospheric Neutrinos”. In: *Phys. Rev. Lett.* 81 (8 Aug. 1998), pp. 1562–1567. DOI: 10.1103/PhysRevLett.81.1562. URL: https://link.aps.org/doi/10.1103/PhysRevLett.81.1562.

[23] Q. R. Ahmad et al. “Direct Evidence for Neutrino Flavor Transformation from Neutral-Current Interactions in the Sudbury Neutrino Observatory”. In: *Phys. Rev. Lett.* 89 (1 June 2002), p. 011301. DOI: 10.1103/PhysRevLett.89.011301. URL: https://link.aps.org/doi/10.1103/PhysRevLett.89.011301.

[24] Patrick Huet and Eric Sather. “Electroweak baryogenesis and standard model CP violation”. In: *Phys. Rev. D* 51 (2 Jan. 1995), pp. 379–394. DOI: 10.1103/PhysRevD.51.379. URL: https://link.aps.org/doi/10.1103/PhysRevD.51.379.

[25] George W. S. Hou. “Source of CP Violation for the Baryon Asymmetry of the Universe”. In: *Int. J. Mod. Phys.* D20 (2011), pp. 1521–1532. DOI: 10.1142/S0218271811019694. arXiv: 1101.2161 [hep-ph].

[26] Don Colladay and V. Alan Kostelecky. “CPT violation and the standard model”. In: *Phys. Rev.* D55 (1997), pp. 6760–6774. DOI: 10.1103/PhysRevD.55.6760. arXiv: hep-ph/9703464 [hep-ph].

[27] Helge Kragh. *Physics and the Totalitarian Principle*. 2019. arXiv: 1907.04623 [physics.hist-ph].

[28] R. D. Peccei and Helen R. Quinn. “CP Conservation in the Presence of Pseudoparticles”. In: *Phys. Rev. Lett.* 38 (25 June 1977), pp. 1440–1443. DOI: 10.1103/PhysRevLett.38.1440. URL: https://link.aps.org/doi/10.1103/PhysRevLett.38.1440.

[29] Thomas Mannel. “Theory and Phenomenology of CP Violation”. In: *Nuclear Physics B - Proceedings Supplements* 167 (2007). Proceedings of the 7th International Conference on Hyperons, Charm and Beauty Hadrons, pp. 170–174. ISSN: 0920-5632. DOI: https://doi.org/10.1016/j.nuclphysbps.2006.12.083. URL: http://www.sciencedirect.com/science/article/pii/S0920563206010711.

[30] Hai-Yang Cheng. “The strong CP problem revisited”. In: *Physics Reports* 158.1 (1988), pp. 1–89.

[31] Leanne D Duffy and Karl van Bibber. “Axions as dark matter particles”. In: *New Journal of Physics* 11.10 (Oct. 2009), p. 105008. DOI: 10.1088/1367-2630/11/10/105008. URL: https://doi.org/10.1088%2F1367-2630%2F11%2F10%2F105008.

[32] N. Du et al. “Search for Invisible Axion Dark Matter with the Axion Dark Matter Experiment”. In: *Phys. Rev. Lett.* 120 (15 Apr. 2018), p. 151301.

DOI: 10.1103/PhysRevLett.120.151301. URL: https://link.aps.org/doi/10.1103/PhysRevLett.120.151301.

[33] Pavel Fileviez Pérez, Clara Murgui, and Alexis D. Plascencia. "Axion Dark Matter, Proton Decay and Unification". In: *JHEP* 01 (2020), p. 091. DOI: 10.1007/JHEP01(2020)091.

[34] Stephen P. Martin. "A Supersymmetry primer". In: (1997). [Adv. Ser. Direct. High Energy Phys.18,1(1998)], pp. 1–98. DOI: 10.1142/9789812839657_0001,10.1142/9789814307505_0001. arXiv: hep-ph/9709356 [hep-ph].

[35] Gian Francesco Giudice. "Naturally Speaking: The Naturalness Criterion and Physics at the LHC". In: *Perspectives on LHC Physics* (June 2008), pp. 155–178. DOI: 10.1142/9789812779762_0010. URL: http://dx.doi.org/10.1142/9789812779762_0010.

[36] Sabine Hossenfelder. "Screams for explanation: finetuning and naturalness in the foundations of physics". In: *Synthese* (2019), pp. 1–19.

[37] Thomas G. Rizzo. "Z' phenomenology and the LHC". In: *Proceedings of Theoretical Advanced Study Institute in Elementary Particle Physics : Exploring New Frontiers Using Colliders and Neutrinos (TASI 2006): Boulder, Colorado, June 4-30, 2006*. 2006, pp. 537–575. arXiv: hep-ph/0610104 [hep-ph]. URL: http://www-public.slac.stanford.edu/sciDoc/docMeta.aspx?slacPubNumber=slac-pub-12129.

[38] Rudolf Haag, Jan T Łopuszański, and Martin Sohnius. "All possible generators of supersymmetries of the S-matrix". In: *Nuclear Physics B* 88.2 (1975), pp. 257–274.

[39] Philip Bechtle et al. "Killing the cMSSM softly". In: *Eur. Phys. J.* C76.2 (2016), p. 96. DOI: 10.1140/epjc/s10052-015-3864-0. arXiv: 1508.05951 [hep-ph].

[40] M. Shifman. "Musings on the Current Status of HEP". In: *Mod. Phys. Lett.* A35.07 (2020), p. 2030003. DOI: 10.1142/S0217732320300037. arXiv: 2001.00101 [physics.hist-ph].

[41] Manuel Drees and Fazlollah Hajkarim. "Neutralino Dark Matter in Scenarios with Early Matter Domination". In: *JHEP* 12 (2018), p. 042. DOI: 10.1007/JHEP12(2018)042. arXiv: 1808.05706 [hep-ph].

[42] Howard E. Haber. "The Status of the minimal supersymmetric standard model and beyond". In: *Nucl. Phys. Proc. Suppl.* 62 (1998). [,469(1997)], pp. 469–484. DOI: 10.1016/S0920-5632(97)00688-9. arXiv: hep-ph/9709450 [hep-ph].

[43] Jan H Oort et al. "The force exerted by the stellar system in the direction perpendicular to the galactic plane and some related problems". In: *Bulletin of the Astronomical Institutes of the Netherlands* 6 (1932), p. 249.

[44] Fritz Zwicky. "Die rotverschiebung von extragalaktischen nebeln". In: *Helvetica physica acta* 6 (1933), pp. 110–127.

[45] Fritz Zwicky. "On the Masses of Nebulae and of Clusters of Nebulae". In: *The Astrophysical Journal* 86 (1937), p. 217.

[46] N. Aghanim et al. "Planck 2018 results. VI. Cosmological parameters". In: (2018). arXiv: 1807.06209 [astro-ph.CO].

[47] Richard Massey, Thomas Kitching, and Johan Richard. "The dark matter of gravitational lensing". In: *Rept. Prog. Phys.* 73 (2010), p. 086901. DOI: 10.1088/0034-4885/73/8/086901. arXiv: 1001.1739 [astro-ph.CO].

[48] Moritz Habermehl, Mikael Berggren, and Jenny List. "WIMP Dark Matter at the International Linear Collider". In: (2020). arXiv: 2001.03011 [hep-ex].

[49] M Bashkanov and D P Watts. "A new possibility for light-quark dark matter". In: *Journal of Physics G: Nuclear and Particle Physics* 47.3 (Feb. 2020), 03LT01. DOI: 10.1088/1361-6471/ab67e8. URL: https://doi.org/10.1088%2F1361-6471%2Fab67e8.

[50] Douglas Clowe, Anthony Gonzalez, and Maxim Markevitch. "Weak-Lensing Mass Reconstruction of the Interacting Cluster 1E 0657-558: Direct Evidence for the Existence of Dark Matter". In: *The Astrophysical Journal* 604.2 (Apr. 2004), pp. 596–603. DOI: 10.1086/381970. URL: https://doi.org/10.1086%2F381970.

[51] Chiara Mastropietro and Andreas Burkert. "Simulating the Bullet Cluster". In: *Mon. Not. Roy. Astron. Soc.* 389 (2008), pp. 967–988. DOI: 10.1111/j.1365-2966.2008.13626.x. arXiv: 0711.0967 [astro-ph].

[52] Vincent R. Bouillot et al. "Probing dark energy models with extreme pairwise velocities of galaxy clusters from the DEUS-FUR simulations". In: *Mon. Not. Roy. Astron. Soc.* 450 (2015), pp. 145–159. DOI: 10.1093/mnras/stv558. arXiv: 1405.6679 [astro-ph.CO].

[53] Robert Thompson, Romeel Davé, and Kentaro Nagamine. "The rise and fall of a challenger: the Bullet Cluster in Λ cold dark matter simulations". In: *Mon. Not. Roy. Astron. Soc.* 452.3 (2015), pp. 3030–3037. DOI: 10.1093/mnras/stv1433. arXiv: 1410.7438 [astro-ph.CO].

[54] Jounghun Lee and Eiichiro Komatsu. "BULLET CLUSTER: A CHALLENGE TO ΛCDM COSMOLOGY". In: *The Astrophysical Journal* 718.1 (June 2010), pp. 60–65. DOI: 10.1088/0004-637x/718/1/60. URL: https://doi.org/10.1088%2F0004-637x%2F718%2F1%2F60.

[55] O. Buchmueller et al. "Higgs and Supersymmetry". In: *Eur. Phys. J.* C72 (2012), p. 2020. DOI: 10.1140/epjc/s10052-012-2020-3. arXiv: 1112.3564 [hep-ph].

[56] *SUSY October 2019 Summary Plot Update*. Tech. rep. ATL-PHYS-PUB-2019-044. Geneva: CERN, Oct. 2019. URL: http://cds.cern.ch/record/2697155.

[57] Christopher T. Hill and Elizabeth H. Simmons. "Strong dynamics and electroweak symmetry breaking". In: *Phys. Rept.* 381 (2003). [Erratum: Phys. Rept.390,553(2004)], pp. 235–402. DOI: 10.1016/S0370-1573(03)00140-6. arXiv: hep-ph/0203079 [hep-ph].

[58] *Combined measurement of the total and differential cross sections in the $H \to \gamma\gamma$ and the $H \to ZZ^* \to 4\ell$ decay channels at $\sqrt{s}$ =13 TeV with the ATLAS detector*. Tech. rep. ATLAS-CONF-2019-032. Geneva: CERN, July 2019. URL: http://cds.cern.ch/record/2682844.

[59] *Top Working Group Summary Plots — Autumn 2018*. Tech. rep. ATL-PHYS-PUB-2018-034. Geneva: CERN, Nov. 2018. URL: http://cds.cern.ch/record/2647993.

[60] Alan Barr and Jesse Liu. "Analysing parameter space correlations of recent 13 TeV gluino and squark searches in the pMSSM". In: *Eur. Phys. J.* C77.3 (2017), p. 202. DOI: 10.1140/epjc/s10052-017-4752-6. arXiv: 1608.05379 [hep-ph].

[61] Philip Bechtle et al. "The Light and Heavy Higgs Interpretation of the MSSM". In: *Eur. Phys. J.* C77.2 (2017), p. 67. DOI: 10.1140/epjc/s10052-016-4584-9. arXiv: 1608.00638 [hep-ph].

[62] Howard Baer, Vernon Barger, and Michael Savoy. "Upper bounds on sparticle masses from naturalness or how to disprove weak scale supersymmetry". In: *Phys. Rev.* D93.3 (2016), p. 035016. DOI: 10.1103/PhysRevD.93.035016. arXiv: 1509.02929 [hep-ph].

[63] Gianfranco Bertone et al. "Global analysis of the pMSSM in light of the Fermi GeV excess: prospects for the LHC Run-II and astroparticle experiments". In: *JCAP* 1604.04 (2016), p. 037. DOI: 10.1088/1475-7516/2016/04/037. arXiv: 1507.07008 [hep-ph].

[64] K. J. de Vries et al. "The pMSSM10 after LHC Run 1". In: *Eur. Phys. J.* C75.9 (2015), p. 422. DOI: 10.1140/epjc/s10052-015-3599-y. arXiv: 1504.03260 [hep-ph].

[65] Sabine Kraml et al. "SModelS: a tool for interpreting simplified-model results from the LHC and its application to supersymmetry". In: *Eur. Phys. J.* C74 (2014), p. 2868. DOI: 10.1140/epjc/s10052-014-2868-5. arXiv: 1312.4175 [hep-ph].

[66] Philip Bechtle et al. "SCYNet: Testing supersymmetric models at the LHC with neural networks". In: (2017). arXiv: 1703.01309 [hep-ph].

[67] Sabine Kraml et al. "SModelS v1.0: a short user guide. " In: (2014). arXiv: 1412.1745 [hep-ph].

[68] Michele Papucci et al. "Fastlim: a fast LHC limit calculator". In: *Eur. Phys. J.* C74.11 (2014), p. 3163. DOI: 10.1140/epjc/s10052-014-3163-1. arXiv: 1402.0492 [hep-ph].

[69] D. Barducci et al. "XQCAT: eXtra Quark Combined Analysis Tool". In: *Comput. Phys. Commun.* 197 (2015), pp. 263–275. DOI: 10.1016/j.cpc.2015.08.016. arXiv: 1409.3116 [hep-ph].

[70] Manuel Drees et al. "CheckMATE: Confronting your Favourite New Physics Model with LHC Data". In: *Comput. Phys. Commun.* 187 (2015), pp. 227–265. DOI: 10.1016/j.cpc.2014.10.018. arXiv: 1312.2591 [hep-ph].

[71] Jong Soo Kim et al. "A framework to create customised LHC analyses within CheckMATE". In: *Comput. Phys. Commun.* 196 (2015), pp. 535–562. DOI: 10.1016/j.cpc.2015.06.002. arXiv: 1503.01123 [hep-ph].

[72] Daniel Dercks et al. "CheckMATE 2: From the model to the limit". In: (2016). arXiv: 1611.09856 [hep-ph].

[73] James S. Gainer et al. "Exploring Theory Space with Monte Carlo Reweighting". In: *JHEP* 10 (2014), p. 078. DOI: 10.1007/JHEP10(2014)078. arXiv: 1404.7129 [hep-ph].

[74] G. Peter Lepage. "A new algorithm for adaptive multidimensional integration". In: *Journal of Computational Physics* 27.2 (1978), pp. 192–203.

[75] Andy Buckley et al. "General-purpose events generators for LHC physics". In: *Phys. Rept.* 504 (2011), pp. 145–233. DOI: 10.1016/j.physrep.2011.03.005. arXiv: 1101.2599 [hep-ph].

[76] M. Tanabashi et al. "Review of Particle Physics". In: *Phys. Rev. D* 98 (3 Aug. 2018), pp. 546–556. DOI: 10.1103/PhysRevD.98.030001. URL: https://link.aps.org/doi/10.1103/PhysRevD.98.030001.

[77] The DELPHES 3 collaboration et al. "DELPHES 3: a modular framework for fast simulation of a generic collider experiment". In: *Journal of High Energy Physics* 2014.2 (Feb. 2014), p. 57. ISSN: 1029-8479. DOI: 10.1007/JHEP02(2014)057. URL: https://doi.org/10.1007/JHEP02(2014)057.

[78] Alexandre Deur, Stanley J. Brodsky, and Guy F. de Teramond. "The QCD Running Coupling". In: *Prog. Part. Nucl. Phys.* 90 (2016), pp. 1–74. DOI: 10.1016/j.ppnp.2016.04.003. arXiv: 1604.08082 [hep-ph].

[79] Jonathan M. Butterworth, Guenther Dissertori, and Gavin P. Salam. "Hard Processes in Proton-Proton Collisions at the Large Hadron Collider". In: *Ann. Rev. Nucl. Part. Sci.* 62 (2012), pp. 387–405. DOI: 10.1146/annurev-nucl-102711-094913. arXiv: 1202.0583 [hep-ex].

[80] G. Altarelli and G. Parisi. “Asymptotic freedom in parton language.” In: *Nucl. Phys. B126* (1977), pp. 298–318.

[81] Yuri L. Dokshitzer. “Calculation of the Structure Functions for Deep Inelastic Scattering and e+ e- Annihilation by Perturbation Theory in Quantum Chromodynamics.” In: *Sov. Phys. JETP* 46 (1977). [Zh. Eksp. Teor. Fiz.73,1216(1977)], pp. 641–653.

[82] V. N. Gribov and L. N. Lipatov. “Deep inelastic e p scattering in perturbation theory”. In: *Sov. J. Nucl. Phys.* 15 (1972). [Yad. Fiz.15,781(1972)], pp. 438–450.

[83] Karol Kovarik, Pavel M. Nadolsky, and Davison E. Soper. “Hadron structure in high-energy collisions”. In: (2019). arXiv: 1905.06957 [hep-ph].

[84] Hung-Liang Lai et al. “New parton distributions for collider physics”. In: *Phys. Rev.* D82 (2010), p. 074024. DOI: 10.1103/PhysRevD.82.074024. arXiv: 1007.2241 [hep-ph].

[85] Rabah Abdul Khalek et al. “A First Determination of Parton Distributions with Theoretical Uncertainties”. In: (2019). arXiv: 1905.04311 [hep-ph].

[86] J. Alwall et al. “The automated computation of tree-level and next-to-leading order differential cross sections, and their matching to parton shower simulations”. In: *JHEP* 07 (2014), p. 079. DOI: 10.1007/JHEP07(2014)079. arXiv: 1405.0301 [hep-ph].

[87] Johan Alwall et al. “A Standard format for Les Houches event files”. In: *Comput. Phys. Commun.* 176 (2007), pp. 300–304. DOI: 10.1016/j.cpc.2006.11.010. arXiv: hep-ph/0609017 [hep-ph].

[88] B. Webber. “Parton shower Monte Carlo event generators”. In: *Scholarpedia* 6.12 (2011). revision #128236, p. 10662. DOI: 10.4249/scholarpedia.10662.

[89] Michael H. Seymour and Marilyn Marx. “Monte Carlo Event Generators”. In: *Proceedings, 69th Scottish Universities Summer School in Physics : LHC Phenomenology (SUSSP69): St.Andrews, Scotland, August 19-September 1, 2012*. 2013, pp. 287–319. DOI: 10.1007/978-3-319-05362-2_8. arXiv: 1304.6677 [hep-ph].

[90] Michael E. Peskin and Daniel V. Schroeder. *An Introduction to quantum field theory*. Reading, USA: Addison-Wesley, 1995. ISBN: 9780201503975, 0201503972. URL: http://www.slac.stanford.edu/~mpeskin/QFT.html.

[91] Torbjörn Sjöstrand et al. “An Introduction to PYTHIA 8.2”. In: *Comput. Phys. Commun.* 191 (2015), pp. 159–177. DOI: 10.1016/j.cpc.2015.01.024. arXiv: 1410.3012 [hep-ph].

[92] Johannes Bellm et al. "Herwig 7.0/Herwig++ 3.0 release note". In: *Eur. Phys. J.* C76.4 (2016), p. 196. DOI: 10.1140/epjc/s10052-016-4018-8. arXiv: 1512.01178 [hep-ph].

[93] T. Gleisberg et al. "Event generation with SHERPA 1.1". In: *JHEP* 02 (2009), p. 007. DOI: 10.1088/1126-6708/2009/02/007. arXiv: 0811.4622 [hep-ph].

[94] Matt Dobbs and Jørgen Beck Hansen. "The HepMC C++ Monte Carlo event record for High Energy Physics Available via the following web-address: http://home.cern.ch/mdobbs/HepMC/." In: *Computer Physics Communications* 134.1 (2001), pp. 41–46. ISSN: 0010-4655. DOI: https://doi.org/10.1016/S0010-4655(00)00189-2. URL: http://www.sciencedirect.com/science/article/pii/S0010465500001892.

[95] M. Tanabashi et al. "Review of Particle Physics". In: *Phys. Rev. D* 98 (3 Aug. 2018), pp. 560–563. DOI: 10.1103/PhysRevD.98.030001. URL: https://link.aps.org/doi/10.1103/PhysRevD.98.030001.

[96] Csaba Balázs et al. "ColliderBit: a GAMBIT module for the calculation of high-energy collider observables and likelihoods". In: *The European Physical Journal C* 77.11 (2017), p. 795.

[97] Vardan Khachatryan et al. "Phenomenological MSSM interpretation of CMS searches in pp collisions at sqrt(s) = 7 and 8 TeV". In: *JHEP* 10 (2016), p. 129. DOI: 10.1007/JHEP10(2016)129. arXiv: 1606.03577 [hep-ex].

[98] M. Tanabashi et al. "Review of Particle Physics". In: *Phys. Rev. D* 98 (3 Aug. 2018), pp. 786–789. DOI: 10.1103/PhysRevD.98.030001. URL: https://link.aps.org/doi/10.1103/PhysRevD.98.030001.

[99] Abdelhak Djouadi and Alexander Lenz. "Sealing the fate of a fourth generation of fermions". In: *Phys. Lett.* B715 (2012), pp. 310–314. DOI: 10.1016/j.physletb.2012.07.060. arXiv: 1204.1252 [hep-ph].

[100] Otto Eberhardt et al. "Impact of a Higgs boson at a mass of 126 GeV on the standard model with three and four fermion generations". In: *Phys. Rev. Lett.* 109 (2012), p. 241802. DOI: 10.1103/PhysRevLett.109.241802. arXiv: 1209.1101 [hep-ph].

[101] M. Tanabashi et al. "Review of Particle Physics". In: *Phys. Rev. D* 98 (3 Aug. 2018), pp. 396–405. DOI: 10.1103/PhysRevD.98.030001. URL: https://link.aps.org/doi/10.1103/PhysRevD.98.030001.

[102] Morad Aaboud et al. "Search for squarks and gluinos in final states with jets and missing transverse momentum using 36 fb^{-1} of $\sqrt{s} = 13$ TeV pp collision data with the ATLAS detector". In: *Phys. Rev.* D97.11 (2018),

p. 112001. DOI: 10.1103/PhysRevD.97.112001. arXiv: 1712.02332 [hep-ex].

[103] Andy Buckley et al. "LHAPDF6: parton density access in the LHC precision era". In: *Eur. Phys. J.* C75 (2015), p. 132. DOI: 10.1140/epjc/s10052-015-3318-8. arXiv: 1412.7420 [hep-ph].

[104] Leif Lonnblad. "Correcting the color dipole cascade model with fixed order matrix elements". In: *JHEP* 05 (2002), p. 046. DOI: 10.1088/1126-6708/2002/05/046. arXiv: hep-ph/0112284 [hep-ph].

Eidesstattliche Erklärung

Ich, Frederic Poncza,

erkläre hiermit, dass diese Dissertation und die darin dargelegten Inhalte die eigenen sind und selbstständig, als Ergebnis der eigenen originären Forschung, generiert wurden.

Hiermit erkläre ich an Eides statt

1. Diese Arbeit wurde vollständig oder größtenteils in der Phase als Doktorand dieser Fakultät und Universität angefertigt;

2. Sofern irgendein Bestandteil dieser Dissertation zuvor für einen akademischen Abschluss oder eine andere Qualifikation an dieser oder einer anderen Institution verwendet wurde, wurde dies klar angezeigt;

3. Wenn immer andere eigene- oder Veröffentlichungen Dritter herangezogen wurden, wurden diese klar benannt;

4. Wenn aus anderen eigenen- oder Veröffentlichungen Dritter zitiert wurde, wurde stets die Quelle hierfür angegeben. Diese Dissertation ist vollständig meine eigene Arbeit, mit der Ausnahme solcher Zitate;

5. Alle wesentlichen Quellen von Unterstützung wurden benannt;

6. Wenn immer ein Teil dieser Dissertation auf der Zusammenarbeit mit anderen basiert, wurde von mir klar gekennzeichnet, was von anderen und was von mir selbst erarbeitet wurde;

7. Kein Teil dieser Arbeit wurde vor deren Einreichung veröffentlicht.

21.09.2020

_____

Frederic Poncza